

THE UNIVERSITY OF CALGARY

Effects of Holes on Interior Column-Slab Connections

BY

Corey Finnigan

A THESIS

**SUBMITTED TO THE FACULTY OF GRADUATE STUDIES
IN PARTIAL FULFILLMENT OF THE REQUIREMENTS FOR THE
DEGREE OF MASTER OF SCIENCE**

DEPARTMENT OF CIVIL ENGINEERING

CALGARY, ALBERTA

September, 1988

© Corey Finnigan 1988

THE UNIVERSITY OF CALGARY
FACULTY OF GRADUATE STUDIES

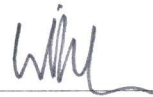
The undersigned certify that they have read, and recommend to the Faculty of Graduate Studies, a thesis entitled, "Effects of Holes on Interior Column-Slab Connections," submitted by Corey Finnigan in partial fulfillment of the requirements for the degree of Master of Science in Engineering.



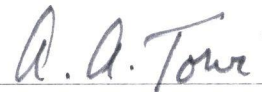
Supervisor, Dr. R.E. Loov
Department of Civil Engineering



Dr. A.E. McMullen
Department of Civil Engineering



Dr. W.H. Dilger
Department of Civil Engineering



Prof. A.A. Torvi
Department of Mechanical Engineering

Date

Oct 21, 1988

Abstract

This is a study of the punching shear strength of interior slab-column connections. The connections contain tension reinforcement only, no shear reinforcement. The study is directed toward the effect of vertical holes through the slab close to the column.

A review of past investigations into slab-column connections reveals that there are many equations for prediction of punching shear strength. Nearly all of the equations are based on results from laboratory tests of a simply supported specimen.

Using finite element analysis the suitability of the laboratory specimen is examined. The finite element analysis raises some question about shape and support conditions of the laboratory specimen. However the problems with the finite element model and the results it gave preclude rejecting the test specimen and its corresponding data.

One of the papers reviewed describes a logical model for predicting punching shear strength. This model, proposed by Rankin and Long in 1987 [24], is adapted to handle slabs that include holes. Three methods of reducing the critical section due to holes are investigated. The results show that the method currently used by the Canadian Design Code is more conservative than necessary. It is recommended that the method first proposed by R.E. Loov, called the 90 degree wedge method be adopted for use.

Acknowledgements

Not enough thanks can be given to Dr. R.E. Loov for his patience and guidance. Many others helped, standouts are Leslie Sharpe and her Suns and Al J. Cameron who regularly led me out of the wilderness.

Finally to C.M.L. Gribbon whose support made it all that much easier.

Contents

Abstract	iii
Acknowledgements	iv
List of Tables	viii
List of Figures	ix
List of Symbols	xi
1 Ultimate Shear Strength and Vertical Holes	1
1.1 Introduction	1
1.2 Problem	2
1.3 Assumptions Made for a Laboratory Specimen	2
1.4 Chapter Summary	4
2 Literature Review	6
2.1 Introduction	6
2.2 Slab-Column Connections With Vertical Holes	6
2.2.1 Experiments and Testing Done by Moe	6
2.2.2 Study by ASCE-ACI Committee 426	10
2.2.3 Experiments Carried Out by Mowrer and Vanderbilt	13
2.2.4 Thesis by Zaidi	14
2.2.5 Paper by Roll, Zaidi, Sabinis and Chaung (ACI SP-30)	17
2.2.6 Paper by Hawkins, Criswell and Roll (ACI SP-42)	19
2.2.7 Summary	20
2.3 Slab-Column Connections Without Vertical Holes	21
2.3.1 Punching Strength of Reinforced Concrete Slabs	21
2.3.2 Shear Strength of Continuous Plates	22
2.3.3 Shear Strength of Slabs: Basic Principle and Their Relation to Current Methods of Analysis	23
2.3.4 The Punching Strength of Slabs, A Flexural Approach Using Finite Elements	23
2.3.5 A Two Phase Approach to the Prediction of the Punching Strength of Slabs	24
2.3.6 Predicting the Punching Strength of Conventional Slab-Column Specimens	26

2.4	Discussion	30
3	Suitability of Laboratory Specimen	31
3.1	Introduction	31
3.2	Choice of Computer Program	32
3.2.1	Element STIF65	33
3.3	Design of Reinforcing Steel	36
3.4	Element Layering	36
3.5	Element Layouts	37
3.6	Run Times and Iterations	41
3.7	Analysis of Slabs With Holes	41
3.8	Data Recorded	44
3.9	Failure Criteria for the Model	44
3.10	Results	51
3.10.1	Load Deflection Curves	51
3.10.2	Position of the Line of Zero Flexural Stress	51
3.10.3	Deflections along Lines of Zero Flexural Stress	53
3.10.4	Deflections Along Various cross Sections	56
3.10.5	Flexural and Shear Cracking	56
3.10.6	Reactions at the Column	64
3.11	Analysis and Discussion of Finite Element Results	69
4	Examination of Prediction Equations	80
4.1	Introduction	80
4.2	Application of Rankin and Long's Model to Slabs with Holes	80
4.2.1	Flexural Punching Strength	81
4.2.2	Shear Punching Strength	83
4.3	Methods for Reduction of b	85
4.4	Comparison With Test Results	87
4.4.1	Results Using Adapted Equations	89
4.4.2	Results Using Code Equation	92
4.5	Summary	96
5	Summary and Conclusions	97
5.1	Restatement of Problem	97
5.2	Summary	97
5.3	Conclusions	98
	Bibliography	100
	Appendix A Design of Reinforcing Steel	105

List of Tables

3.1	Coordinates for Node Stacks at Column	65
4.1	Comparison of Various Methods for Hole Reduction, Using Adapted Prediction Equation	89
4.2	Comparison of Various Methods for Hole Reduction, Using Design Code Prediction Equation	91

List of Figures

1.1	Drop Panel and Column Capital	1
1.2	Slab-Column System, 4.5 m o/c	3
1.3	Points of Contraflexure, Deflected Slab	3
1.4	Simply Supported Slab	4
2.1	Hole Patterns for Moe's Tests	7
2.2	Moe's Case 2: $b = 3c - g_1 \div g_2$	8
2.3	Moe's Case 3: $b = 4c$ or $3c \div g_1 \div g_2$	9
2.4	Case I: $b = 4(c \div d) - g$	12
2.5	Critical Section, Case II (a) and (b)	13
2.6	ACI Committee 426, Critical Sections, Case IV	14
2.7	Hole Patterns for Mowrer and Vanderbilt's Tests	15
2.8	Section used by Zaidi, $b = 4c - g_1 - g_2$	16
2.9	Hole Pattern not Applicable to Zaidi's Equation	17
2.10	4 Corner Holes of Varying Size	18
2.11	Calculation of e : $e = e_1 + e_2$	21
2.12	Three Cases for Flexural Punching Failure	27
2.13	Interpolation of k_t	29
3.1	Boundary Conditions for Quarter Panel Model	32
3.2	Stress-Strain Curve for Concrete	34
3.3	Stress-Strain Curve for Steel	35
3.4	Section Before and After Cracking	37
3.5	Element Layering	38
3.6	Element Layout, Third Model	38
3.7	Element Layout, Fourth Model	39
3.8	Hole Patterns Investigated	40
3.9	Element Layout, Fifth Model	40
3.10	Hole Pattern One	42
3.11	Element Layout, Hole Pattern One	43
3.12	Yield Lines	46
3.13	Areas for External Work	49
3.14	Points for Deflection Readings	51
3.15	Deflection vs. Load for Model 5	52
3.16	Lines of Zero Flexural Stress, Solid Slab, 11.9 kPa	53
3.17	Lines of Zero Flexural Stress, Three Hole Patterns, 11.9 kPa	54
3.18	Deflections Along $x = 975$ mm, Hole Pattern One	55
3.19	Deflections Along Various Sections, 11.9 kPa, Hole Pattern 1	57

3.20	Deflections Along Various Sections, 11.9 kPa, Hole Pattern 1	58
3.21	Sections for Flexural and Shear Cracking	59
3.22	Sequence of Flexure-Shear Cracking, Solid Slab	60
3.23	Sequence of Flexure-Shear Cracking, Hole Pattern One	61
3.24	Sequence of Flexure-Shear Cracking, Hole Pattern Two	62
3.25	Sequence of Flexure-Shear Cracking, Hole Pattern Three	63
3.26	Column-Slab Interface	64
3.27	Reactions at the Column, Solid Slab	65
3.28	Reactions at the Column, Hole Pattern One	66
3.29	Reactions at the Column, Hole Pattern Two	67
3.30	Reactions at the Column, Hole Pattern Three	68
3.31	Restraintment of Finite Element Model	70
3.32	Possible Shape of Test Specimen	71
3.33	Deflected Laboratory Specimen	72
3.34	Edge Reactions of a Specimen	72
3.35	Shear Distribution, $x = 1.05\ m$, Load = 11.9 kPa	74
3.36	Shear Distribution, $y = 1.05\ m$, Load = 11.9 kPa	75
3.37	Elements and Integration Points, Inside $x = 1.05\ m$, $z = 90\ mm$	76
3.38	τ_{zz} Values, Inside $x = 1.05\ m$, $z = 90\ mm$	76
3.39	Elements and Integration Points, Outside $x = 1.05\ m$, $z = 90\ mm$	77
3.40	τ_{zz} Values, Outside $x = 1.05\ m$, $z = 90\ mm$	77
3.41	Area Considered for Equilibrium Check	78
4.1	Stress and Strain Diagrams	82
4.2	Method for Determining P_p Using Adapted Model	84
4.3	Radial Line Method	85
4.4	60 Degree Wedge Method, Hole on Centreline	86
4.5	Arbitrary Column Corner	87
4.6	Reduction for Holes Near Column Corner	88
4.7	Typical Reduction of Centreline-Symmetrical Specimen	90
4.8	Worst Case Hole Pattern	92
4.9	Corner - Symmetric, Radial Line Method, Using Adapted Equation	93
4.10	Corner - Symmetric, 90 Degree Wedge Method, Using Adapted Equation	94
4.11	Corner - Symmetric, 90 Degree Wedge Method, Using Code Equation	95
A.1	Column and Middle Strips	107
A.2	Moments at Critical Sections	108
A.3	Quarter Panel Reinforcing Steel, x Direction Only	112

List of Symbols

A_s = Area of nonprestressed tension reinforcement.

b = Length of the critical section.

b' = Length of the critical section, flexural mode of failure, measured at the column periphery.

b_0 = Length of the critical section, shear mode of failure, measured at $d/2$ from the column.

c = Side length of the column.

d = Effective depth of the reinforcement.

e = Eccentricity of the centroid of b .

f'_c = Compressive strength of the concrete.

f_y = Yield strength of the nonprestressed reinforcement.

k_b = Ratio of applied load to internal bending moment at column periphery.

k_t = Ratio of applied load to ultimate moment of resistance at failure.

k_{y1} = Moment factor for overall tangential yielding.

L = Span centre to centre of columns.

M_{bal} = Balanced resisting moment.

M_n = Nominal flexural resistance.

M_0 = Total factored static moment.

P_{flex} = Flexural strength of test specimen.

P_p = Predicted punching strength.

P_u = Punching strength of test specimen.

P_{vf} = Predicted flexural punching strength.

P_{vs} = Predicted shear punching strength.

r_f = Reduction coefficient to allow for column shape.

s = Side length of test specimen.

V_f = Factored shear force at a section.

V_r = Factored shear resistance.

w_{df} = Factored dead load per unit area of a slab.

w_f = Factored load per unit area of a slab.

w_{lf} = Factored live load per unit area of a slab.

β_1 = Ratio of depth of rectangular compression block to depth to neutral axis.

ρ = Ratio of nonprestressed tension reinforcement = $\frac{A_s}{bd}$.

σ_x = Stress in the x direction.

ω = Tension reinforcement index = $\rho \frac{f'_c}{f_y}$.

Chapter 1

Ultimate Shear Strength and Vertical Holes

1.1 Introduction

In designing a concrete flat slab, the major design consideration is the distribution of flexural reinforcement. Yet in almost every case, it is the shear forces in the area of the slab-column connection that are the governing factor. In attempting to design slabs without the use of drop panels or column capitals this area becomes increasingly important. The cost of column capitals and drop panels is very high

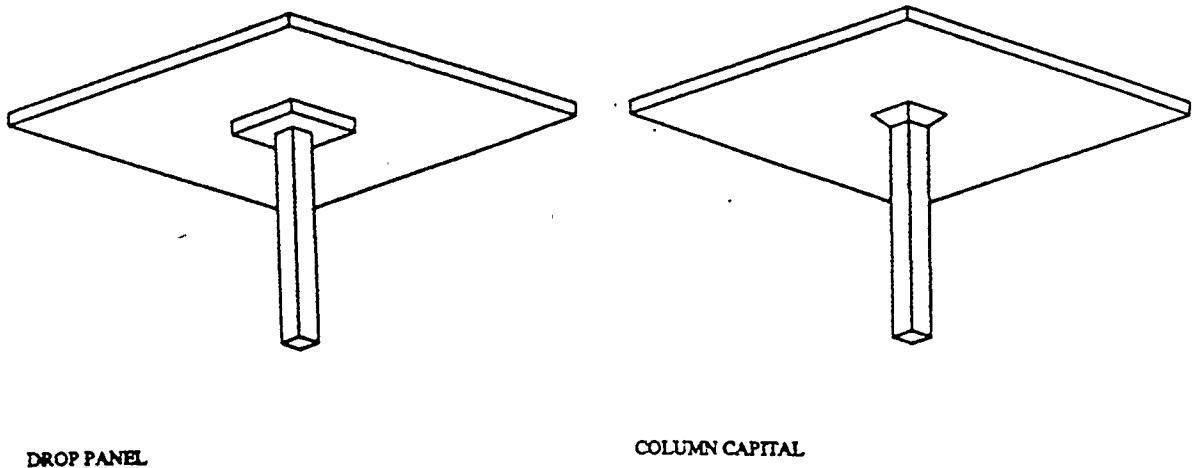


Figure 1.1: Drop Panel and Column Capital

and as such, their use should be avoided whenever possible. It is often the case that vertical holes through the slab, close to the column, are required for electrical and mechanical utilities.

1.2 Problem

The problem can be stated as:

What is the punching shear strength of an interior slab-column connection? And what is the effect of vertical holes on that strength?

The extent of the effect can be expected to be influenced by the size, shape and position of the hole.

In order to determine the effect of such holes, testing has been undertaken by several investigators. Initially the problem is one of size and type of specimens to be tested. To build a full scale, multipanel specimen would be both cost and space prohibitive.

1.3 Assumptions Made for a Laboratory Specimen

Consider a typical 300 mm x 300 mm interior column, and a flat plate, 150 mm thick with a span of 4.50 m o/c in each direction shown in Figure 1.2. The boundary conditions at the centre lines of the slab are known but not easily duplicated in a laboratory. As well, the specimens would still be quite large and expensive. Because of this nearly all tests to determine the shear strength of slab column connections have been based on the portion of the slab within the lines of zero moment.

If a cross section of a typical interior slab is considered the resulting deflected shape would be as shown in Figure 1.3. The idea is that the points of contraflexure form a square around the column and that the moment at these points is zero. Thus the slab-column connection can be simulated by a slab between $L/2.5$ and

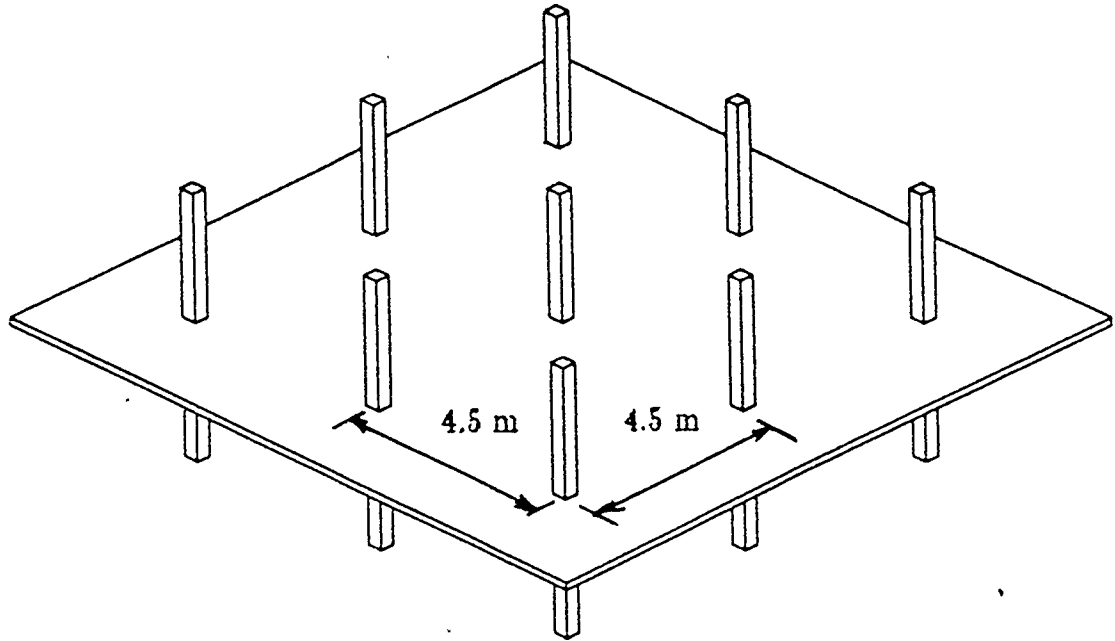


Figure 1.2: Slab-Column System, 4.5 m o/c

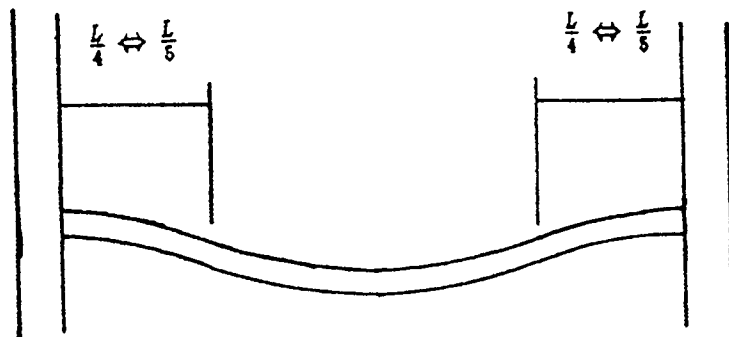


Figure 1.3: Points of Contraflexure, Deflected Slab

$L/2$ square. The edges could be simply supported and the load applied to the column stub as shown in Figure 1.4.

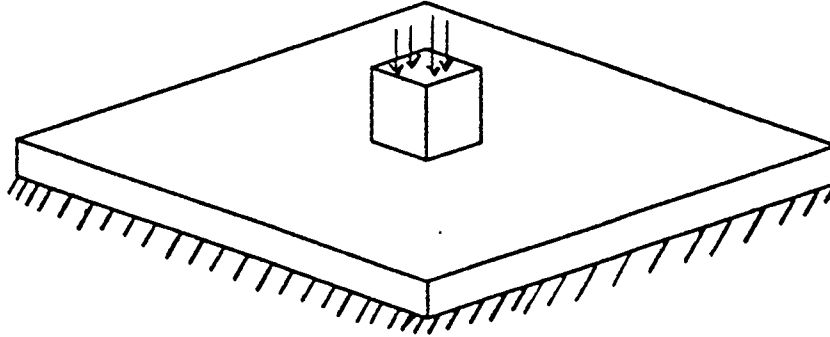


Figure 1.4: Simply Supported Slab

It should be noted that the applied loads acting on this portion of the slab surface are generally ignored in these tests.

1.4 Chapter Summary

Chapter 2 provides a literature review of two categories of investigation; those carried out on slabs with holes and those that deal with solid slabs only.

All of these prior investigations have assumed that the specimen used gives a realistic indication of what happens to a slab-column connection during loading. In Chapter 3 a study is presented to determine whether this assumption is indeed true. A finite element analysis of an $L \times L$ slab is described. The boundary conditions of such an interior panel are known and easily simulated on the computer. The analysis is nonlinear and examines several areas of interest up to ultimate load. The modelling was done using an 8 node brick element of the computer program ANSYS.

In Chapter 4 a model presented by Rankin and Long [24] is modified for slabs with vertical holes. Three methods for reduction of the critical section are compared.

The summary and conclusions are presented in Chapter 5:

Chapter 2

Literature Review

2.1 Introduction

The literature review is split up into two parts. The first deals with investigations on slab-column connections with holes, the second with investigations without holes.

2.2 Slab-Column Connections With Vertical Holes

2.2.1 Experiments and Testing Done by Moe

This 1961 paper [2] describes tests performed on a total of 43 specimens. These specimens were split into 5 different series, each series designed to test the effects of a different variable or condition. The series H specimens were slabs cast with holes immediately adjacent or close to the column. Series H consisted of a total of 15 different slabs, all 1.83 m (6 ft.) square with a thickness of 150 mm (6 in.). The specimens were centrally loaded through a 254mm (10 in.) square column stub with the edges of the slab simply supported. Reinforcement for all slabs except H14 consisted of 12, 16 mm ($\frac{5}{8}$ inch) bars in both the x and y directions. The average effective depth of the slab was 114 mm (4.5 in.) and the overall reinforcement ratio, ρ , was 1.15%. Slab H14 had 8 bars for a ρ of 0.77%.

The hole pattern for each of the slabs is shown in Figure 2.1.

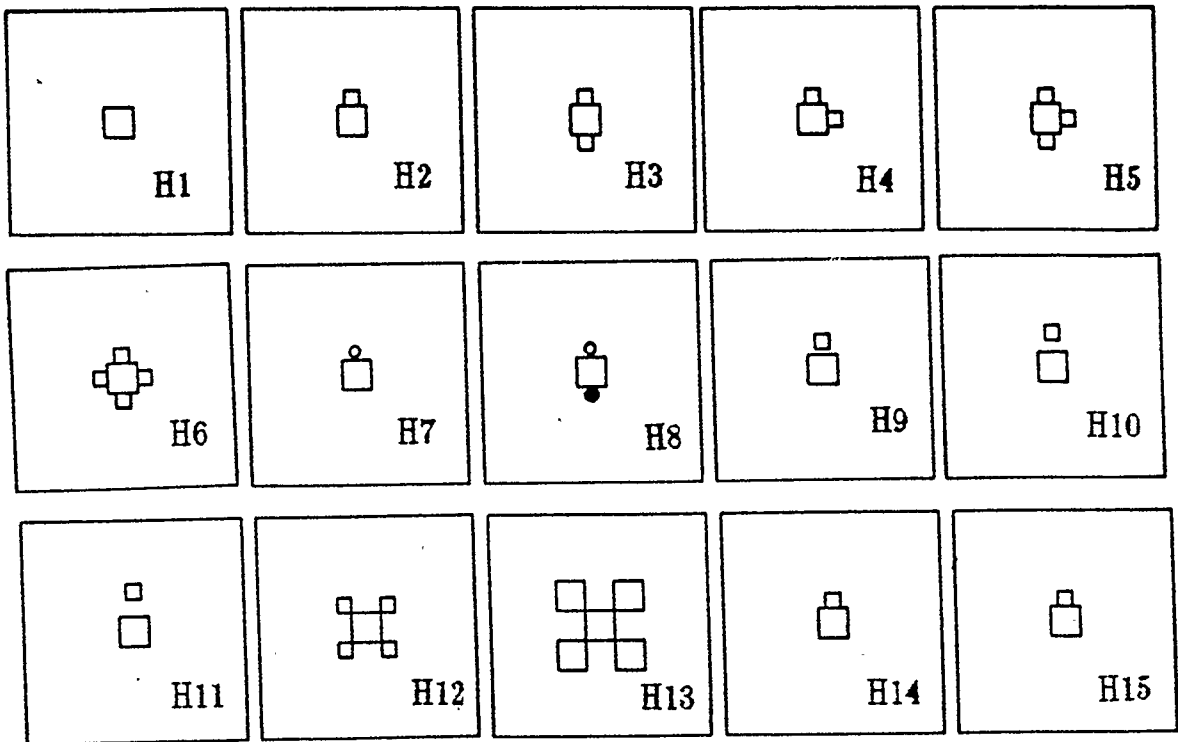


Figure 2.1: Hole Patterns for Moe's Tests

The following are the rules for the reduction of b , the length of the effective critical section, as quoted from Moe's paper:

1. "In cases of square holes adjacent to the column, b was taken as the total periphery minus the sum of the widths of the holes, measured along the periphery.
2. In cases with circular holes adjacent to the column, b was for the sake of simplicity measured along the shortest lines connecting the corners of the column to the periphery of the holes. It was realized that the holes reduced the shearing strength of the slabs, and the above-mentioned method of measuring b was believed to express this reduction satisfactorily, although the

failure did not take place along a section of the type in Figure 2.2.

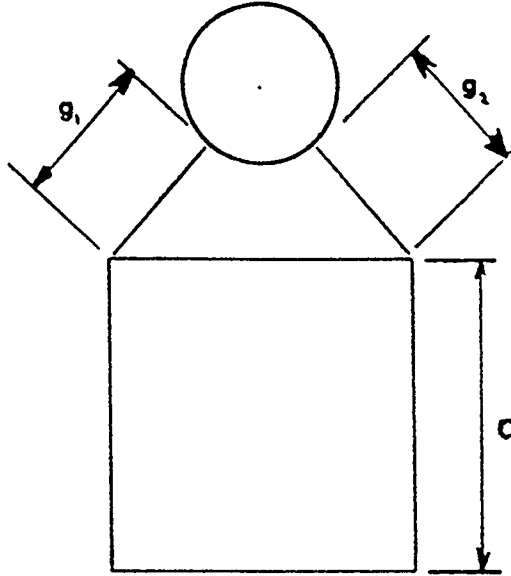


Figure 2.2: Moe's Case 2: $b = 3c + g_1 + g_2$

3. In cases in which the holes were placed at some distance from the column, b was measured along straight lines from the corners of the column stub to the nearest points on the periphery of the holes, whenever this yielded smaller values of b than the section along the periphery of the column." The critical section for this case is depicted in Figure 2.3.

For his analysis Moe used b measured along the periphery of the column face. However he also calculated $\frac{P_u}{\sqrt{f'_c}}$ for b measured at $d/2$ and d from the column face. From this he found the variance of the test results was lowest when b was taken at $d/2$.

In predicting the punching strength of a specimen Moe used the following formula:

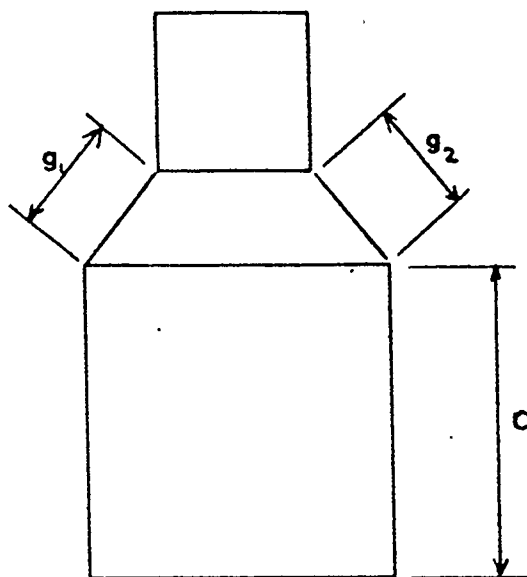


Figure 2.3: Moe's Case 3: $b = 4c$ or $3c + g_1 + g_2$

$$P_p = \frac{15bd\sqrt{f'_c}(1 - 0.075c/d)}{1 + 5.25bd\sqrt{f'_c}/P_{flex}} \quad (2.1)$$

Where:

P_p = The ultimate shearing capacity, *lbs*.

b = The effective critical perimeter around the loaded area, *in*.

d = The effective depth of the slab, *in*.

c = The side length of the column, *in*.

f'_c = The compressive strength of the concrete, *psi*.

P_{flex} = The shear force at which flexural failure occurs in solid slabs, *lbs*.

The equation for P_{flex} is the one developed by Elstner and Hognestad [1] using yield line theory.

$$P_{flex} = 8M_n \left(\frac{1}{1 - c/s} - 3 + 2\sqrt{2} \right) \quad (2.2)$$

Where:

$$M_n = \rho f_y d (1 - 0.59\omega) = f'_c \omega d (1 - 0.59\omega)$$

= The ultimate flexural moment per unit width.

$$\rho = A_s / (sd) = \text{The reinforcement ratio}$$

A_s = The area of reinforcement in each direction, in^2 .

s = The side length of a square slab, in .

f_y = The yield strength of reinforcing bar, psi .

$\omega = \rho f_y / f'_c$ = The tension reinforcement index.

Moe concluded that this equation fit his results well. His rules for the reduction of b (taken at the column periphery) do not allow for any loss of strength for slabs H12 and H13. However his results showed a significant reduction in the ultimate strength of these slabs.

2.2.2 Study by ASCE-ACI Committee 426

This study of 1962 [3] used the data from Moe's tests and attempted to come up with an alternative method for predicting the effect of holes on the critical section.

A simplified equation for predicting ultimate strength was proposed.

$$P_u = 4bd\sqrt{f'_c} \left(1 + \frac{d}{c} \right) \quad (2.3)$$

Where b is the critical section measured at the column face. However ACI Committee 426 noted that the results with the least scatter were obtained when the critical section is taken at $d/2$ from the column face. With this in mind they rearranged the original equation to:

$$P_u = 4b_o d \sqrt{f'_c} \quad (2.4)$$

where b_o is the length of the "pseudocritical" section measured at $d/2$ from the column face.

In addressing the problem of how much to reduce the critical section the committee proposed the following guidelines:

The positions and sizes of the holes were broken down into 4 cases.

Case I: Holes closer than $d/2$ to the column.

Case II: Holes between $d/2$ and $2d$ from the column.

Case III: Holes greater than $2d$ from the column.

Case IV: Holes large enough to be treated as free edges.

For each of the above cases various rules were applied:

Case I: "Radial lines should be drawn from the centroid of the loaded area to the edges of the opening ... If there are several openings, the sum of the radial projections should be subtracted from the original pseudocritical section." Figure 2.4 shows the critical section.

Case II: "The reduced perimeter should be taken as the smaller of the two given by the following criteria:

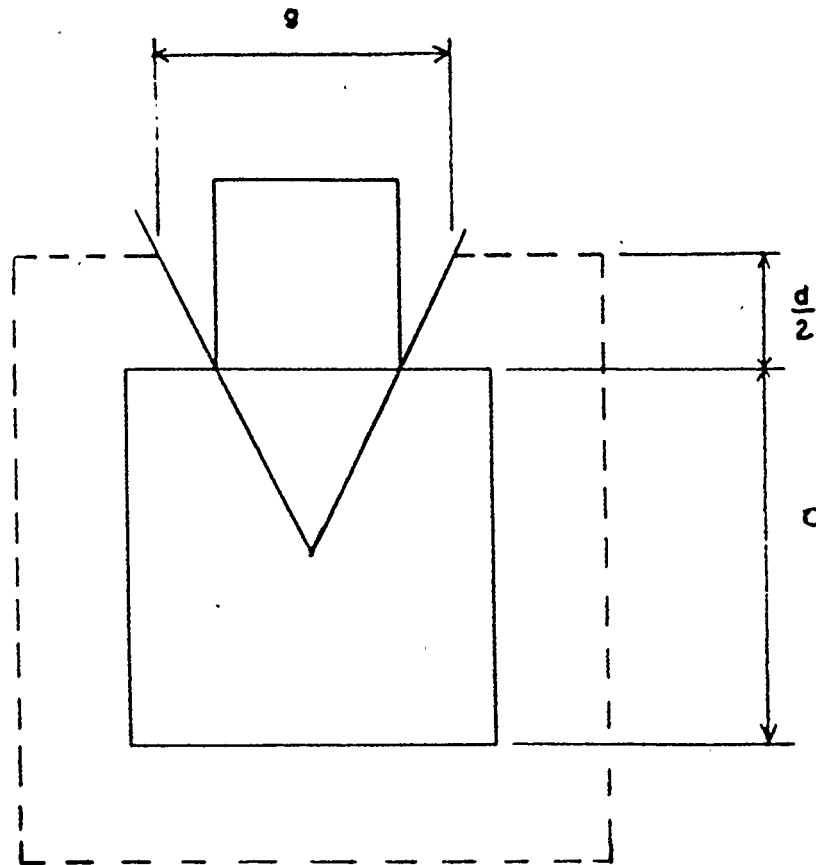


Figure 2.4: Case I: $b = 4(c + d) - g$

- (a) The shortest of all possible sections lying not less than $d/2$ from the loaded area.
- (b) The original pseudocritical section minus the sum of the radial projections of the openings as shown in Figure 2.5."

The report also stated that when the opening was close to the corner of the pseudocritical section, criterion (a) would provide for no reduction while criterion (b) would call for too much of a reduction.

Case III "Only criterion (a) (of Case II) and the original unreduced critical section need be investigated."

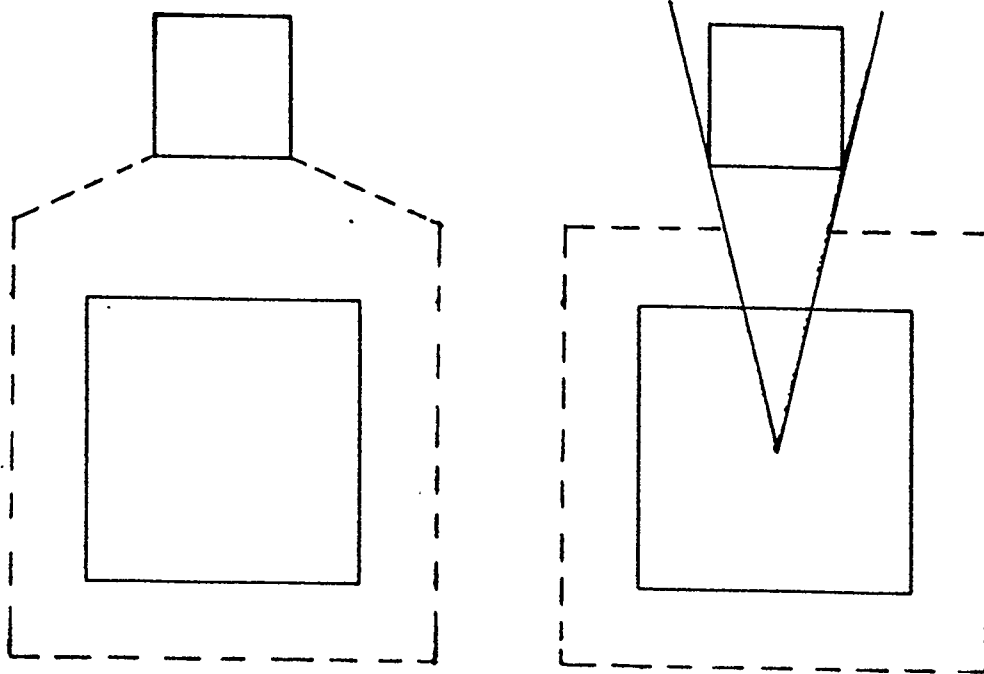


Figure 2.5: Critical Section, Case II (a) and (b)

Case IV: Finally the report states that for holes that are “large compared with the dimensions of the critical section”, that side of the critical section should be treated as a free edge. A free edge was to be reduced using criterion (a) of Case II. This definition is rather vague and is best illustrated by the examples of Figure 2.6.

2.2.3 Experiments Carried Out by Mowrer and Vanderbilt

Mowrer and Vanderbilt [7] tested 2 series of slabs, one of which was designed to test the effect of holes near the critical shear section. This series consisted of 17 lightweight and 8 normal weight slabs. The specimens were 914 mm (3 ft.) square and 76 mm (3 in.) thick. Each was loaded through a 150 mm (6 in.) column stub that was 150 mm high. Reinforcement consisted of varying numbers of $\frac{1}{2}$ inch

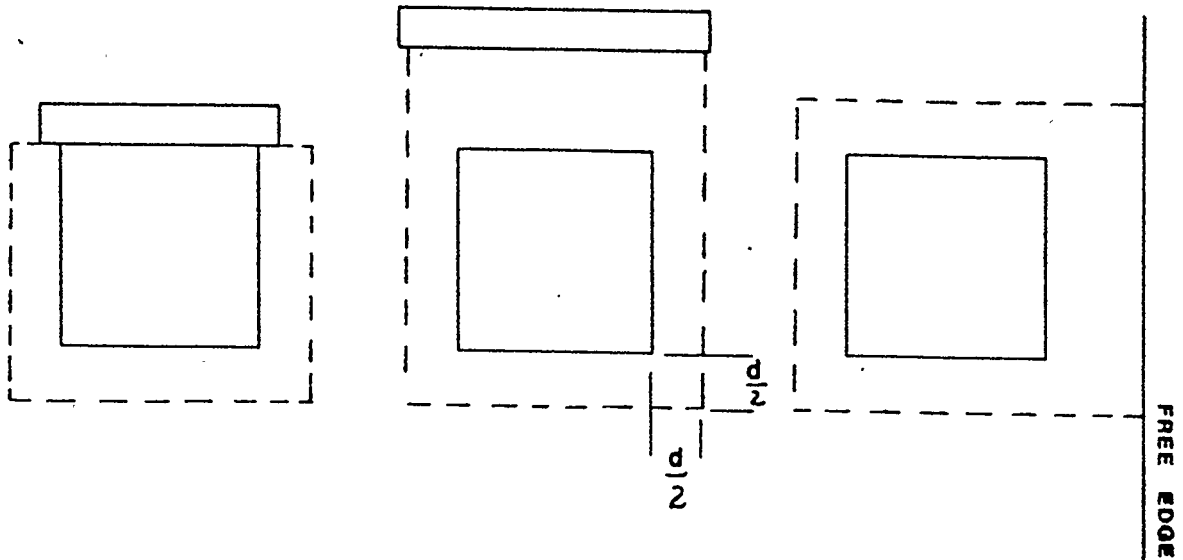


Figure 2.6: ACI Committee 426, Critical Sections, Case IV

(12mm) bars . Other variables included concrete strength and the pattern of the holes.

Like Moe's tests the slabs were simply supported at the edges and the hole patterns are as shown in Figure 2.7. The effective depth for all the slabs was 51 mm (2 in.). Once again b , the effective perimeter, was calculated at the periphery of the column. The rules used for reduction of b were the same as those suggested by Moe.

On the basis of their results Mowrer and Vanderbilt revised Moe's equation to:

$$\frac{P_u}{bd\sqrt{f'_c}} = \frac{9.7(1 - d/c)}{1 + 5.25bd\sqrt{f'_c}/P_{flex}} \quad (2.5)$$

2.2.4 Thesis by Zaidi

A thesis entitled "Shear Resistance of Perforated Reinforced Concrete Slabs" was written by S.T.H. Zaidi and published in 1968 at the University of Pennsylvania.[8]

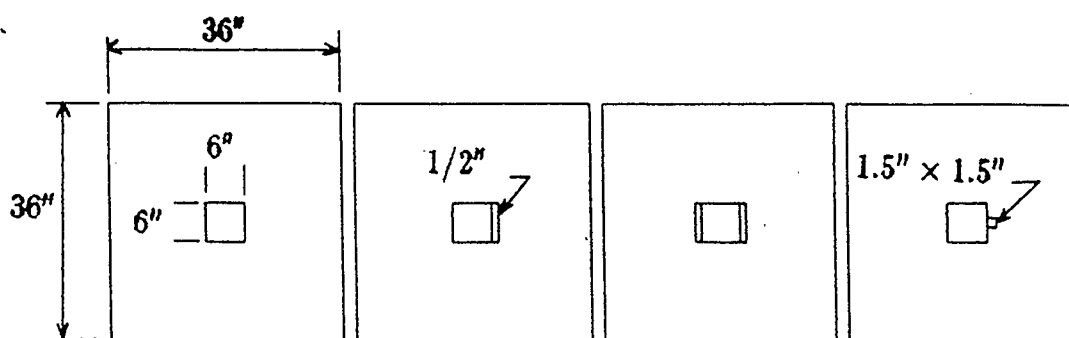


Figure 2.7: Hole Patterns for Mowrer and Vanderbilt's Tests

The specimens used were of the same nature as the ones tested by Moe, but at a smaller scale. The A series of specimens were 737 mm (29 in.) square and 61 mm (2.4 in.) thick. The slabs were centrally loaded through a 102 mm (4 in.) square column stub that was 152 mm (6 in.) high. All of the edges of the slab were simply supported.

Reinforcement consisted of # 2, ($\frac{1}{4}$ in.), (6 mm) bars and the average percentage of reinforcement, ρ , was 1.15. The effective depth of the reinforcement was 46 mm (1.8 in).

For the B series of slabs the effective depth of the reinforcement was reduced to 39 mm (1.55 in.) and the reinforcement ratio, ρ , increased to 1.34%.

A total of 78 slabs were tested in series A and 45 slabs in series B. Holes were circular, square, rectangular and L shaped. Other variables included the number, position and size of the holes. The method used to calculate b was similar to, but not exactly the same as the method proposed by ACI Committee 426. The critical section was taken at the column face. Figure 2.8 shows the amount subtracted for

a hole was the length within the lines of the radial projection of the hole.

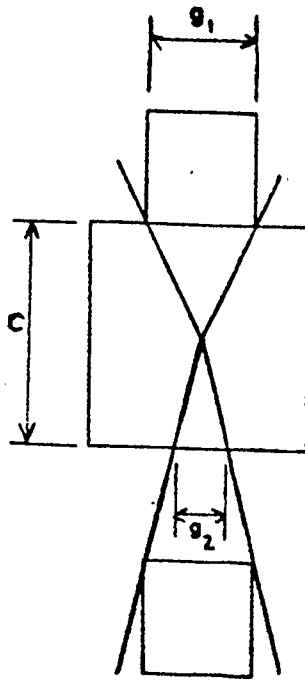


Figure 2.8: Section used by Zaidi, $b = 4c - g_1 - g_2$

Zaidi believed that the ultimate strength of the specimens was affected by the following parameters:

f'_c = The strength of the concrete.

b = The length of the critical section.

d = The effective depth of the slab.

c/d = The ratio of the side length of the column to the effective depth.

e/d = The ratio of the eccentricity in the centroid of b (caused by nonsymmetric hole patterns) to the effective depth.

P_{flex} = The flexural strength of the slab.

An initial statistical analysis led Zaidi to believe the prediction equation had the following form:

$$\frac{P_u}{bd\sqrt{f'_c}} = \frac{A(1 + Bc/d - Ce/d)}{1 + Dbd\sqrt{f'_c}/P_{flex}} \quad (2.6)$$

A final statistical analysis gave values for the constants and the final prediction equation was:

$$\frac{P_u}{bd\sqrt{f'_c}} = \frac{14(1 + 0.15c/d - 0.425e/d)}{1 + 10bd\sqrt{f'_c}/P_{flex}} \quad (2.7)$$

Once again this equation proved to be conservative for slabs with the hole pattern shown in Figure 2.9.

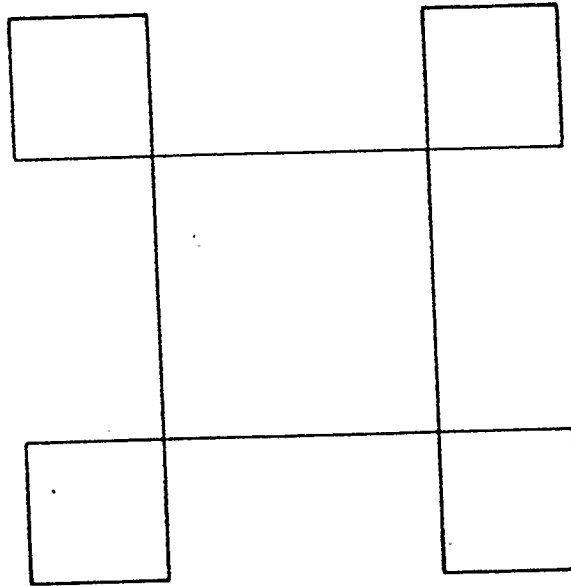


Figure 2.9: Hole Pattern not Applicable to Zaidi's Equation

2.2.5 Paper by Roll, Zaidi, Sabinis and Chaung (ACI SP-30)

This 1971 paper [9] is the publication version of Zaidi's thesis with a few additions.

Four series of tests are described.

1. Test series A1 which is the data from series A of Zaidi's thesis.
2. Test series A2, the data from series B of Zaidi's thesis.
3. Test series B, 20 new slabs with # 3, ($\frac{3}{8}$ inch), (9 mm) bars instead of # 2 bars as used in the previous two series. This increased the reinforcement ratio ρ to 2.53%.
4. Series H, a series of 14 tests to determine the effect of 4 corner holes of varying size. The hole pattern is shown in Figure 2.10.

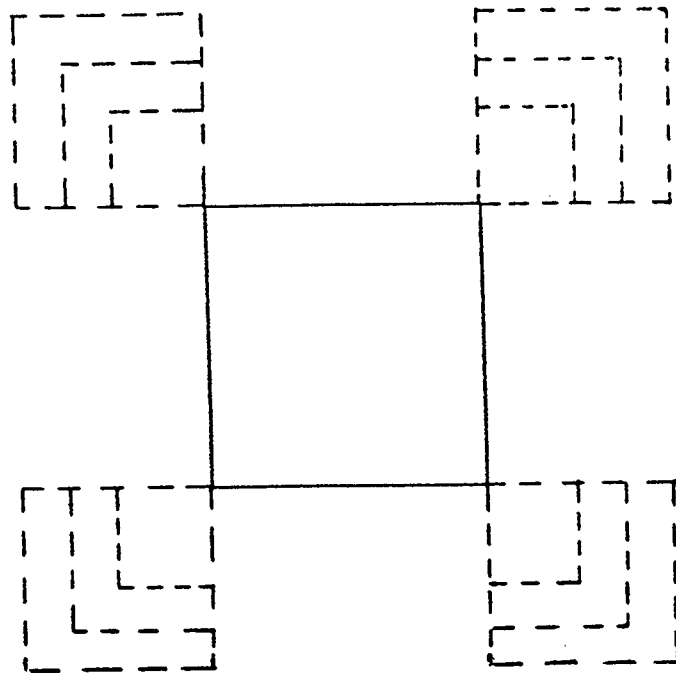


Figure 2.10: 4 Corner Holes of Varying Size

All the specimens were of the same type and size as the ones used in Zaidi's thesis. The method of reduction of b was the same one used by Zaidi.

The analysis in this paper resulted in 2 different equations. The first is Equation 2.7, the one developed by Zaidi in his thesis.

The second is a design equation developed for small values of $\frac{P_{flex}}{bd\sqrt{f'_c}}$ and as such “should not be used in the case of 4 large holes adjacent to the column face.”

$$\frac{P_u}{bd\sqrt{f'_c}} = \frac{6.1}{1 + 5.2bd\sqrt{f'_c}/P_{flex}} + 0.23\frac{P_{flex}}{bd\sqrt{f'_c}} \quad (2.8)$$

2.2.6 Paper by Hawkins, Criswell and Roll (ACI SP-42)

This paper [11] is an analysis of previous work. No new specimens were tested. The section on perforated slabs begins with the presentation of the equation developed by Zaidi in his thesis.

Roll noted that most of the specimens used to derive this equation had a c/d ratio of about 2.2. By looking at cases with varying c/d values Roll concluded that the c/d term should be flipped and the equation altered to the following form:

$$\frac{P_u}{bd\sqrt{f'_c}} = \frac{14(1 - 0.75d/c - 0.425e/d)}{1 - 10bd\sqrt{f'_c}/P_{flex}} \quad (2.9)$$

Roll further hypothesized that if a nonsymmetric hole pattern were used the connection acts as if it were transferring moment. Thus c and not d , should be linked with e . Finally Roll states that if $\frac{P_u}{P_{flex}}$ is set to unity the specimen will reach its maximum flexural strength before its shear strength. Thus the prediction equation is reduced to:

$$\frac{P_u}{bd\sqrt{f'_c}} = 4\left(1 + 2.58\frac{d}{c} - 3.3\frac{e}{c}\right) \quad (2.10)$$

Or by rounding off to produce a reasonable lower limit.

$$\frac{P_u}{bd\sqrt{f'_c}} = 4\left(1 + 2\frac{d}{c} - 3\frac{e}{c}\right) \quad (2.11)$$

But not less than:

$$4\frac{(\text{Perimeter for shear flow normal to the column})}{b} \quad (2.12)$$

Where:

d = The effective depth of the slab.

f'_c = The concrete strength.

c = The side length of the loaded area.

b = the length of the critical section measured at the column face minus the radial projections of the holes, as shown in Figure 2.7.

e = The eccentricity of the centroid of b caused by nonsymmetric hole layouts defined by Figure 2.11.

(Perimeter for shear flow normal to the column) = Defined by Roll as: "the length of the column perimeter within lines normal to each column face and tangent to the holes. For example, for Figure 2.8 a lower limit to P_u is $16cd\sqrt{f'_c}$."

2.2.7 Summary

Each of the previous investigations present data collected on slabs with holes. Each then performs a statistical analysis on that data to derive a prediction equation

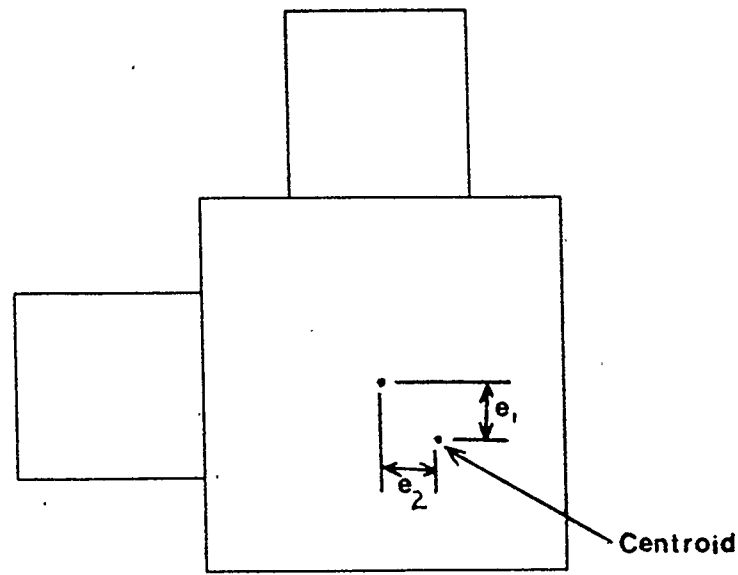


Figure 2.11: Calculation of e : $e = e_1 + e_2$

for the punching shear strength of a laboratory specimen. The equations are not given any sort of logical basis.

In the hopes of finding a logical model for punching shear, a second literature review was done. This time the punching shear strength of slab-column connections without holes is investigated.

2.3 Slab-Column Connections Without Vertical Holes

2.3.1 Punching Strength of Reinforced Concrete Slabs

In a paper presented in 1966 Yitzhaki [5] states that there are two types of punching shear failure. One in which the flexural reinforcement fully yields, the second where failure occurs before full yielding of the reinforcement.

For the first type of failure, he introduces the equation:

$$P_{ult} = 8\rho f_y d^2 \left(1 - 0.5\rho \frac{f_y}{f'_c}\right) \quad (2.13)$$

Yitzhaki states that the effect of the concrete strength is represented by the factor $(1 - 0.5\rho \frac{f_y}{f'_c})$.

For an "over-reinforced section" failure occurs when P_{pun} is attained. P_{pun} is affected by the size of the column and is less than P_{ult} . Yitzhaki introduces $\frac{c}{d}$ and ρf_y as "linearly independent multipliers" with constants that are "evaluated from available test data." Using these the second equation is presented.

$$P_{pun} = 8\left(1 - 0.5\rho \frac{f_y}{f'_c}\right)d^2(149.3 - 0.16\rho f_y)\left(1 + 0.5\frac{c}{d}\right) \quad (2.14)$$

(Note that imperial units are used for this equation.)

2.3.2 Shear Strength of Continuous Plates

In a paper presented in 1972 M.D. Vanderbilt [10] draws three conclusions about the punching strength of slab-column connections.

1. The shear strength is a function of the column shape, as well as size, with circular columns showing higher strength than square columns of equal periphery. This difference is attributed to stress concentrations at the corners of the square columns.
2. Doubling the reinforcement resulted in only a modest increase in shear strength.
3. None of the available equations or procedures proved to be satisfactory for predicting punching shear strength.

2.3.3 Shear Strength of Slabs: Basic Principle and Their Relation to Current Methods of Analysis

In a paper presented in 1974 by Criswell and Hawkins [13] the following conclusions are drawn:

1. "Most methods of analysis for ultimate shear strength fall into two broad groups. For one group, the strength is presumed to be governed primarily by the concrete strength and for the other by flexural effects. Because of the strong interaction of the shear and flexural effects, idealized models ... are needed to provide methods of analysis that are conceptually realistic."
2. The simply supported test specimens fail earlier than expected of a slab. A ductile failure is difficult to achieve with a test specimen.
3. Not enough is known about the mechanisms of punching shear failures. The failures seem to be punching shear failures or flexural shear failures. "Future investigations should attempt to identify whether the more likely mechanism is primarily one of shear or flexure or if a division of failure modes is meaningful."

2.3.4 The Punching Strength of Slabs, A Flexural Approach Using Finite Elements

The finite element model developed by Masterson and Long in their paper [14] is used in Long's subsequent publications. Its relevance is made clear in the review of those papers.

2.3.5 A Two Phase Approach to the Prediction of the Punching Strength of Slabs

In this paper of 1975 [16] Long uses the idea that there are 2 basic modes of punching shear failure.

1. The steel yields before the concrete fails. As a consequence the failure can be considered to be strongly influenced by flexural strength.
2. The concrete fails before the steel yields.

Flexural Punching Strength

The yield line approach was found to be unsatisfactory for the following reasons:

1. From inspection of the tested specimens it was evident that a full yield line pattern had not developed.
2. Only the tension reinforcement right next to the column yields before punching. Blakey [6] concluded that punching occurs when a plastic hinge forms around the column periphery.
3. Dowel forces in the reinforcement contribute 30% to the shear capacity. Thus, if a slab develops a full yield line pattern the failure load should be in the order of $1.3P_{flex}$. This correction overestimates the capacity of the specimen.

The approach for the flexural mode is based on a lower bound elastic theory which allows for the development of local plasticity around the column periphery. The flexural punching capacity is predicted using:

$$P_{vf} = 1.30k_bM_n \quad (2.15)$$

Where:

1.30 accounts for the dowel action.

k_b relates the column load to the internal slab moment.

M_n is the ultimate moment of resistance per unit width of the slab.

The constant k_b is obtained from finite element work done by Masterson.

$$k_b = \frac{1}{0.255 - 1.17c/L} \quad (L = 2.5s) \quad (2.16)$$

M_n is defined by the 1971 ACI code. The expression for flexural punching strength is:

$$P_{vf} = \frac{\rho f_y d^2 (1 - 0.59\rho f_y / f'_c)}{(0.2 - 0.9c/L)} \quad (2.17)$$

Shear Punching Strength

Four assumptions are made about shear punching strength. These assumptions are based on design curves provided by Long [16].

1. P_{vs} varies with $(100\rho)^{0.25}$.
2. P_{vs} varies with $(f'_c)^{0.4}$. However for the normal range of design strengths $\sqrt{f'_c}$ is adequate.
3. P_{vs} varies with $\left(\frac{1}{0.75 + 4c/L}\right)$.

4. The critical section is assumed to be at $d/2$ from the column face.

Based on test data Long states that the final equation for shear punching strength is:

$$P_{vs} = \frac{1.66(c + d)d(100\rho)^{0.25}\sqrt{f'_c}}{(0.75 + 4\frac{c}{L})} \quad (2.18)$$

In comparing predicted values to test values two areas of concern were noted by Long.

- Correlation was bad for slabs with low values of $\rho f_y / f'_c$ (less than 0.1). This was probably due to a much more extensive yield line pattern developing than is assumed for the lower bound solution of the flexural mode formula.
- Correlation was bad for slabs with high values of f'_c . This is due to the use of $\sqrt{f'_c}$ instead of $(f'_c)^{0.4}$.

2.3.6 Predicting the Punching Strength of Conventional Slab-Column Specimens

This 1987 paper by Rankin and Long [24] extends the two phase approach by giving a more rational approach to the flexural mode of punching failure.

Flexural Punching Strength

A flexural punching failure can occur by one of three modes. For a lightly reinforced section a full yield line pattern will develop. For a heavily reinforced section, failure will occur due to localized compression failure of the concrete around the column. All other flexural punching failures fall between these extremes as shown in Figure 2.12.

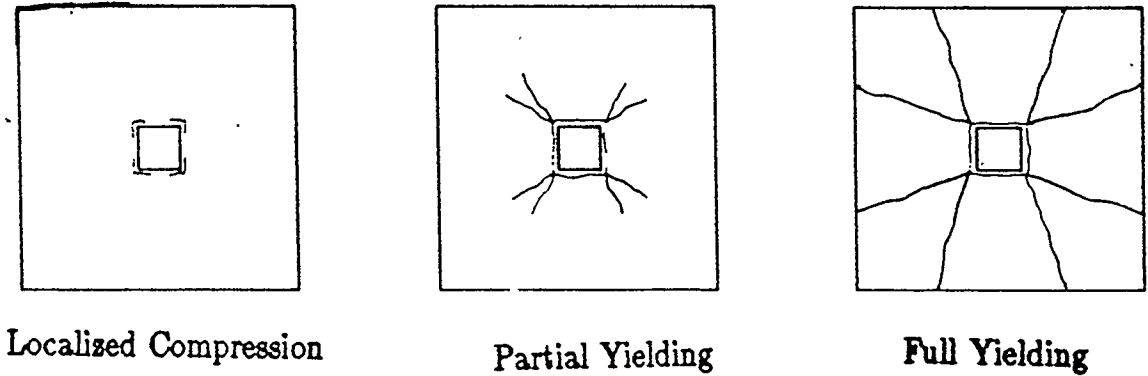


Figure 2.12: Three Cases for Flexural Punching Failure

Full Yielding

Using the yield line pattern shown in Figure 2.12 the load required is:

$$P_{vf} = k_{y1} M_n \quad (2.19)$$

Where:

$$k_{y1} = 8 \left(\frac{s}{s-c} - 0.172 \right) \quad (2.20)$$

Note that this is the same as the P_{flex} used by Moe, Zaidi, Roll, etc. in their equations. It applies to simply supported laboratory specimens.

Localized Compression Failure

This type of failure occurs when a plastic hinge develops only at the critical section. This section is the periphery of the column. The ratio of

$$k_b = \frac{P}{M} = \frac{\text{load applied to the column}}{\text{internal moment at critical section}}$$

is called the elastic moment factor. Long and Masterson developed the equation:

$$k_b = \frac{1}{0.255 - 1.17 \frac{e}{L}} \quad (L = 2.5s) \quad (2.21)$$

This relationship has been improved by Long and Rankin to:

$$k_b = \frac{25}{[\ln(2.5s/c)]^{1.5}} \quad (2.22)$$

Partial Yielding

The failure load in this case lies somewhere between the load causing localized compression failure and the load that causes full yielding. Thus a third constant, (k_t), is introduced.

$$P = k_t M_n \quad (2.23)$$

Long states that " k_t can be closely approximated by linearly interpolating between the moment factor for full yielding k_{y1} , and the elastic moment factor k_b ." Figure 2.13 and Equation 2.24 define k_t .

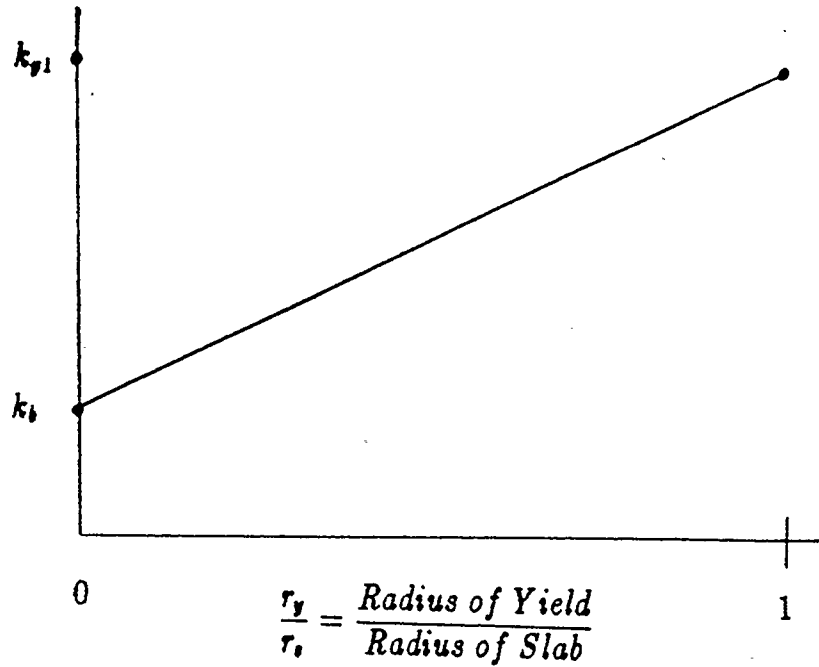
$$k_t = k_b + (k_{y1} - k_b) \frac{r_y}{r_s} \quad (2.24)$$

Slab Ductility

The value of r_y/r_s is found from the following:

$$\frac{r_y}{r_s} = 1 - \left(\frac{M_n}{M_{bal}} \right) \quad (2.25)$$

Where:

Figure 2.13: Interpolation of k_t

$$M_n = \rho f_y d^2 \left(1 - 0.59 \frac{\rho f_y}{f'_c}\right) \quad (2.26)$$

and:

$$M_{bal} = 0.333 f'_c d^2 \quad (2.27)$$

The moment factor for partial yielding is:

$$k_t = k_{y1} - (k_{y1} - k_b) \left(\frac{M_n}{M_{bal}}\right) \quad (2.28)$$

Column Shape Factor

This factor is to account for the stress factors found in and around the corners of a square column. Regan [19] has suggested that circular columns are 15% stronger

than square columns. Thus $r_f = 1.0$ for circular columns and 1.15 for square columns. k_t is altered one last time.

$$k_t = k_{y1} - (k_{y1} - \frac{k_b}{r_f}) (\frac{M_n}{M_{bal}}) \quad (2.29)$$

And the expression for the flexural punching strength is set at:

$$P_{vf} = k_t M_n \leq \frac{k_b}{r_f} M_{bal} \quad (2.30)$$

Shear Punching Strength

This equation is the one developed by Long in his 1974 [16] paper.

$$P_{vs} = 1.66(c + d)d(100\rho)^{0.25} \sqrt{f'_c} \quad (2.31)$$

Note that the $\frac{L}{c}$ term has been dropped.

2.4 Discussion

The papers describing investigations of connections with holes seemed to follow the same format; in each case the authors fit an empirical equation to the test data. The literature on solid interior slab-column connections showed a general trend toward a two phase approach to punching shear strength. Two papers, one by Long, the other by Rankin and Long put forth and developed logical arguments for the prediction of punching shear strength.

Chapter 3

Suitability of Laboratory Specimen

3.1 Introduction

When examining interior slab-column connections full scale tests of multiple slab-column systems are not usually done. High cost and shortage of lab space force one to look for a smaller, more economical type of test.

Nearly all of the investigations considered in the literature review used the same type of laboratory specimen. This specimen, a square slab with simply supported edges, was presumed to represent the area of a flat plate within the lines of contraflexure. In service such a flat plate would be subjected to a uniformly distributed load and a typical interior slab-column connection would be considered.

Thus the previous experiments have all been based on the following assumptions:

1. The lines of contraflexure form a square about the column.
2. The position of such lines are constant throughout the test.
3. The deflection along such a line is uniform. (Although the corners of the test specimens were allowed to uplift.)

In order to determine if these are valid assumptions a finite element analysis was performed under the following conditions. Consider the slab-column system of Figure 1.2 where the columns are spaced at 4.5 m o/c in both directions.

If the load is considered to be uniformly distributed then a typical interior column can be isolated by the centrelines between the columns. Thus a slab 4.5 m by 4.5 m with a column stub in the centre can be examined. Because of symmetry only one quarter of the column and slab need be considered. If the column is assumed rigid then Figure 3.1 shows the boundary conditions that apply.

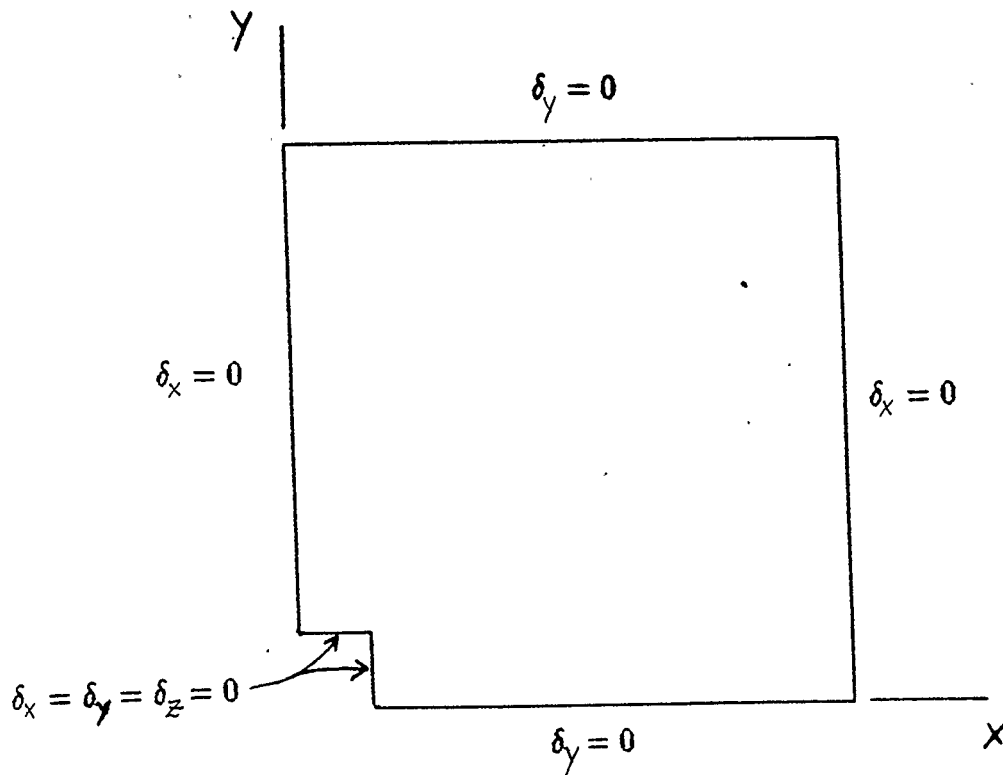


Figure 3.1: Boundary Conditions for Quarter Panel Model

3.2 Choice of Computer Program

Because of its pre and postprocessing capabilities the computer program ANSYS was chosen for the analysis. Since all of the tests in the laboratory were carried up to the failure load of the specimen it must be concluded that a linear elastic

analysis would not be satisfactory. The element chosen for the model was STIF65, an 8 node brick element with a number of nonlinear capabilities.

3.2.1 Element STIF65

This element is called the 3-D Reinforced Concrete Solid and is capable of cracking in tension, crushing in compression and can model up to 3 separate groups of reinforcing steel. The element is defined by 8 nodes, each node having 3 translational degrees of freedom. The element material is reinforced concrete and the following linear and nonlinear material data is input:

1. E_c the initial tangent modulus was set at 25000 MPa
2. f'_c the specified compressive strength was set at 25 MPa
3. The tensile cracking stress was set at $0.6\sqrt{f'_c}$, in this case 3.0 MPa
4. The shear transfer coefficient for an open crack was set at 0.25. In other words 0.25 of the shear would be transferred across a crack.
5. The shear transfer coefficient of a closed crack was set at 0.75.
6. The stress strain curve utilized the multilinear kinematic hardening option. This allowed for piecewise linear curve to be specified using the data points shown in Figure 3.2.
7. The uniaxial crushing stress was set at the f'_c value of 25 MPa
8. The biaxial crushing stress was set to a default value of $1.2f'_c = 30 \text{ MPa}$.

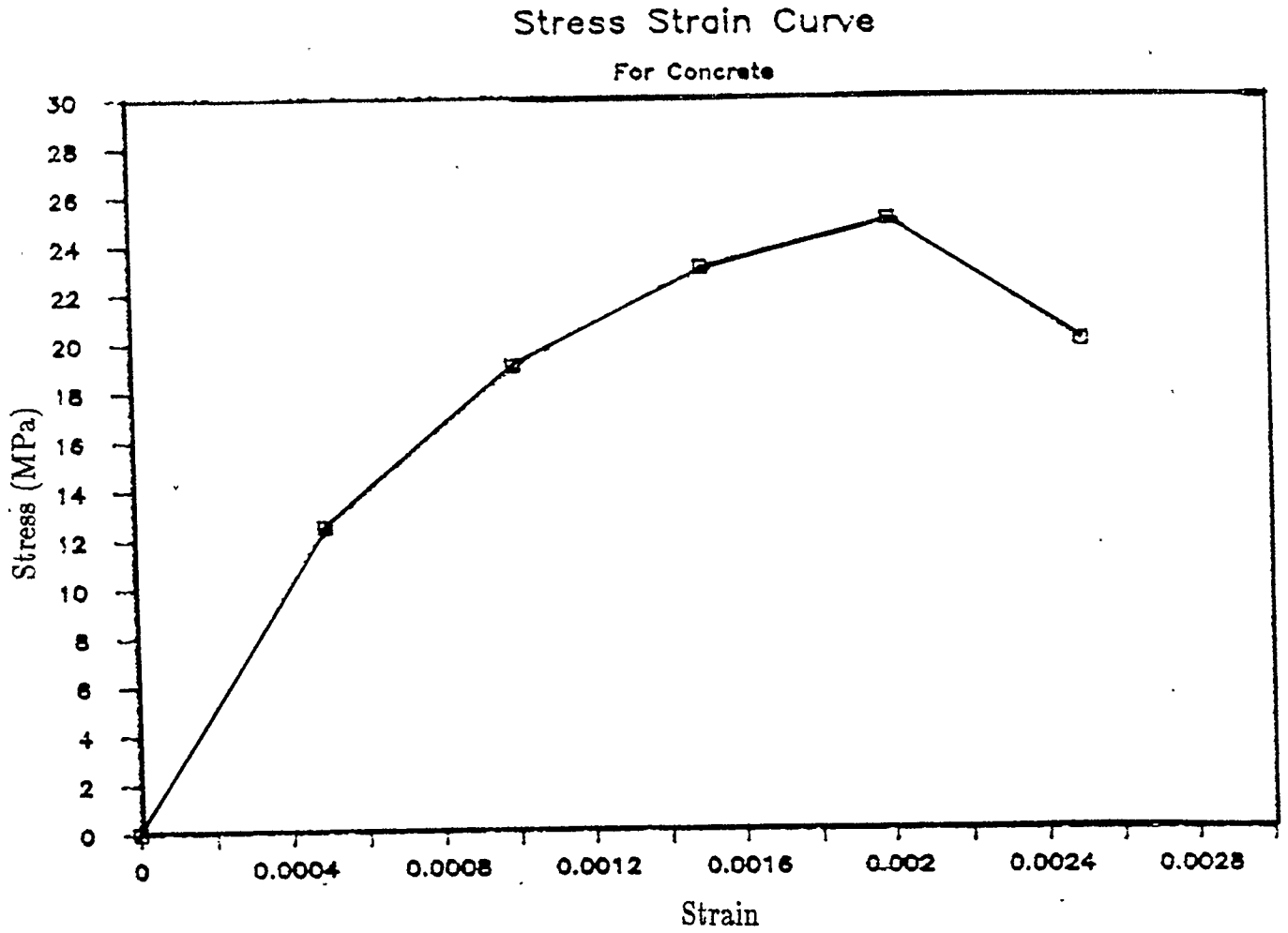


Figure 3.2: Stress-Strain Curve for Concrete

If the element contained reinforcing steel the the following material properties were utilized:

1. The yield strength was set at 400 MPa.
2. The initial elastic modulus was set at 200 GPa.
3. The classical bilinear kinematic hardening curve was used with a second slope of 2 GPa as shown in Figure 3.3.

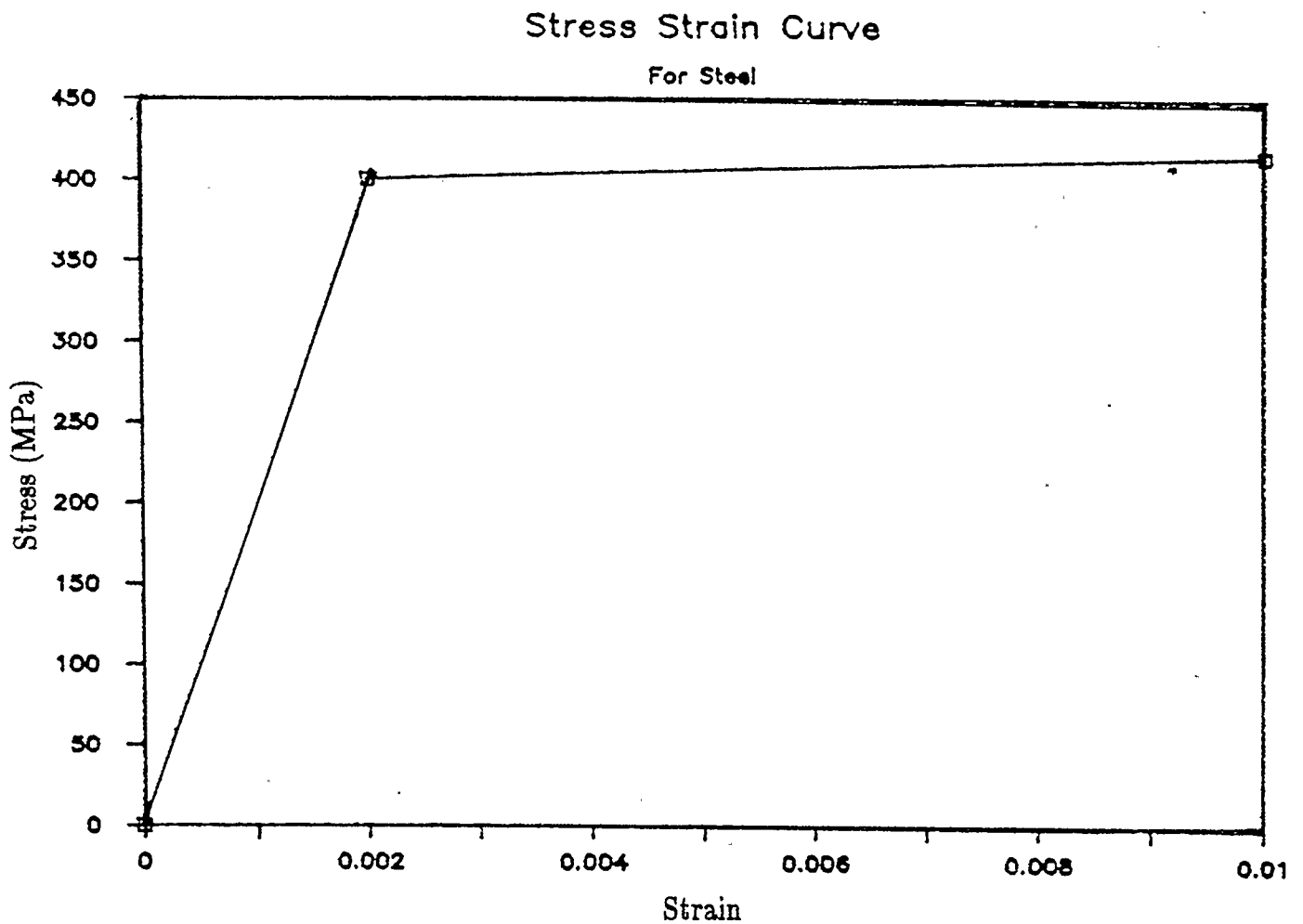


Figure 3.3: Stress-Strain Curve for Steel

3.3 Design of Reinforcing Steel

In order to proceed with the modelling the amount and placement of the reinforcing steel is required. The design was carried out following example 5.3 of the CPCA Concrete Design Handbook [22]. Details of the design are placed in the appendix.

3.4 Element Layering

The design of the reinforcement called for both the positive and negative steels to be set 30 mm from the top and bottom surfaces of the 150 mm thick slab. The area of greatest interest is located next to the column. A couple of points need to be considered.

1. The reinforcement is smeared throughout an entire element containing steel.
2. The top of the slab is expected to crack extensively, rendering the concrete somewhat ineffectual.

Consider a cross section of a concrete beam. Before cracking the entire depth of the section shown in Figure 3.4a is assumed to be acting to resist moment.

However once the section is cracked the concrete in tension is ignored and only the concrete to a depth of c is assumed effective.

The value of c depends on the material properties and changes as cracking progresses within the plate. To more accurately model the plate the compression zone should have more layers of elements than the tension zone. The elements in the tension zone will simply crack while adjacent to the compression zone the elements may or may not crack and if they do, the cracks may close up again.

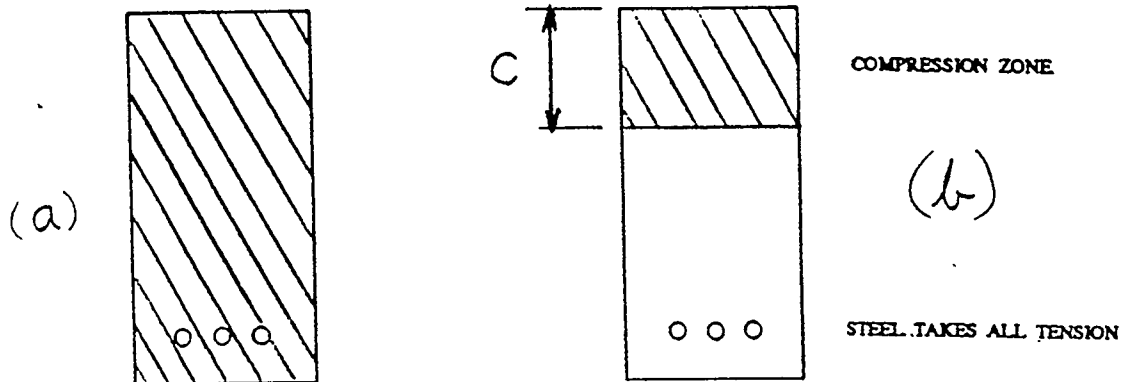


Figure 3.4: Section Before and After Cracking

An element with a closed crack is assumed to have greater shear strength due to aggregate interlock.

Figure 3.5 starts with the bottom of the slab as $z = 0$, the first layer, with no steel, was set at 15 mm thick. The second layer, centred on the positive steel was 30 mm thick. The third layer is set at 45 mm thick and the final layer, centred on the negative steel was set at 60 mm thick.

It was hoped that by minimizing the number of layers the overall run times could be reduced.

3.5 Element Layouts

Three separate element layouts, all representing solid slabs were run. The models were called the third, fourth and fifth models respectively.

The third model is shown in Figure 3.6 and used 680 nodes and 512 elements. The smallest elements were 150 mm by 150 mm and as such would not allow for the input of holes next to the column.

However this model could be run fairly quickly and gave some idea of the

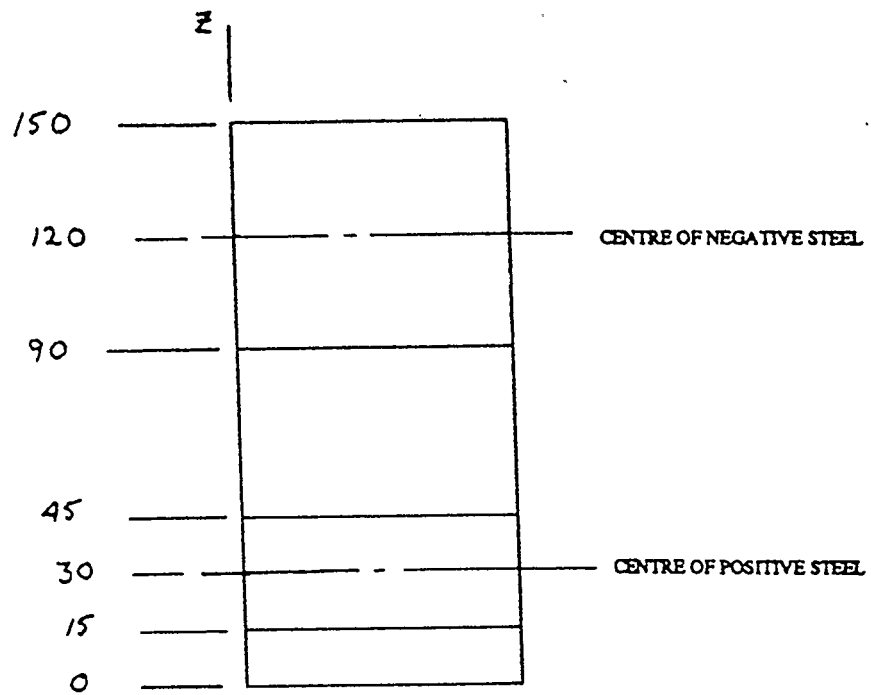


Figure 3.5: Element Layering

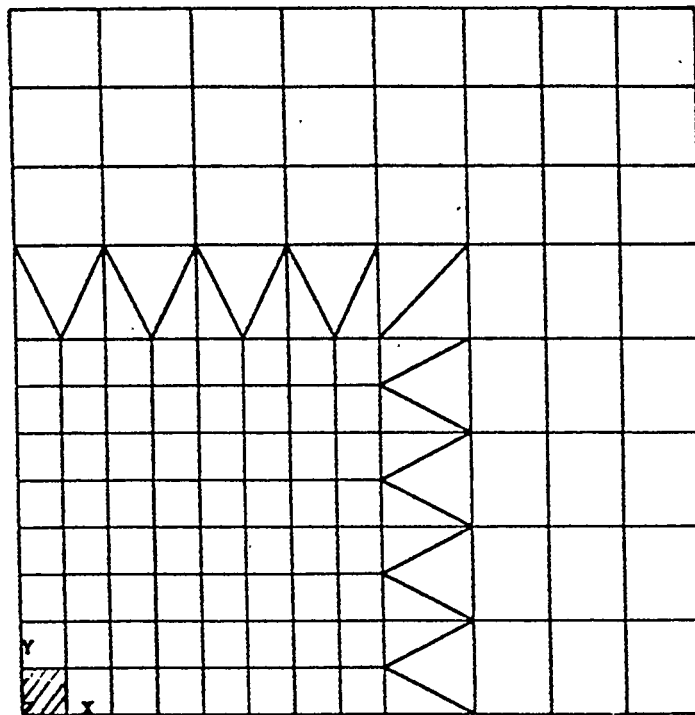


Figure 3.6: Element Layout, Third Model

expected results.

The fourth model used 830 nodes and 660 elements and is shown in Figure 3.7. The elements next to the column were 75 mm square and would allow for holes 150 mm square in a pattern shown in Figure 3.8.

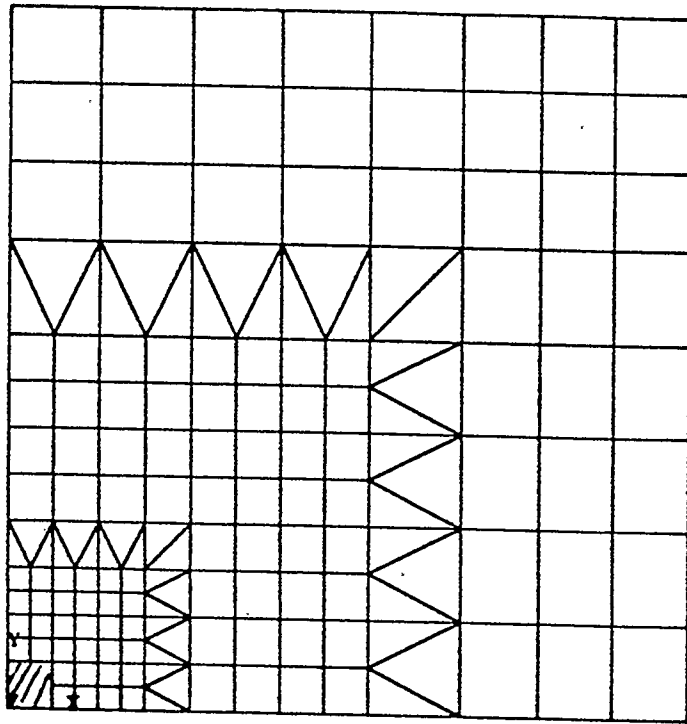


Figure 3.7: Element Layout, Fourth Model

The fifth model allowed for the second band of wedge shaped elements to be moved further out from the column. It was hoped that this would eliminate any effect these elements might have on the position of the line of contraflexure. This model contained a total of 975 nodes and 784 elements and is shown in Figure 3.9.

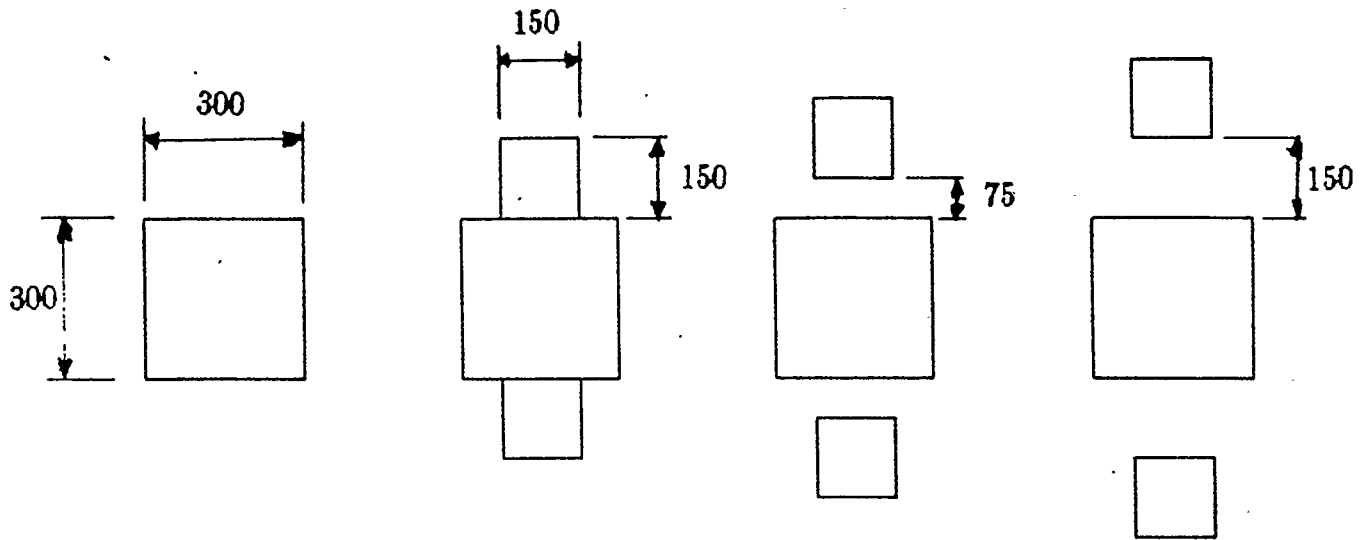


Figure 3.8: Hole Patterns Investigated

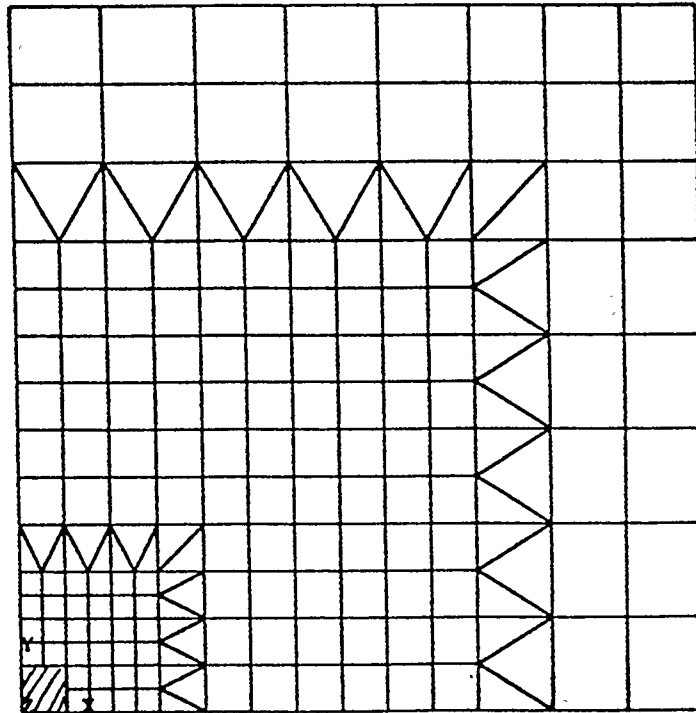


Figure 3.9: Element Layout, Fifth Model

3.6 Run Times and Iterations

The following table gives some of the statistics on the analyses run on the various models.

Model	Total Number of Load Steps	Total Number of Iterations	Approx. CPU Time/Iteration (min.)	Total CPU Time (hrs.)
3	32	176	11	32.3
4	44	418	15	104.5
5	30	428	20	142.7

3.7 Analysis of Slabs With Holes

The first 3 runs established the procedure and the limits of the finite element analysis of a solid slab. The next three runs examined the effects of holes next to the column.

Everything for these subsequent models remained the same except for the element layout. The concrete and steel material properties, the layout of the reinforcing steel and the element layering are all identical to the solid slab. The first hole pattern used is shown in Figure 3.10. The quarter panel model has the element layout shown in Figure 3.11.

The nodes along the hole are allowed to move freely subject to the constraints of the column and/or symmetry. The holes are introduced by "unselecting" the appropriate elements. This means that such elements, and the steel they may contain, are not considered in the model. No steel was added to the surrounding elements. This makes the model a little weaker than it should be, as normally any

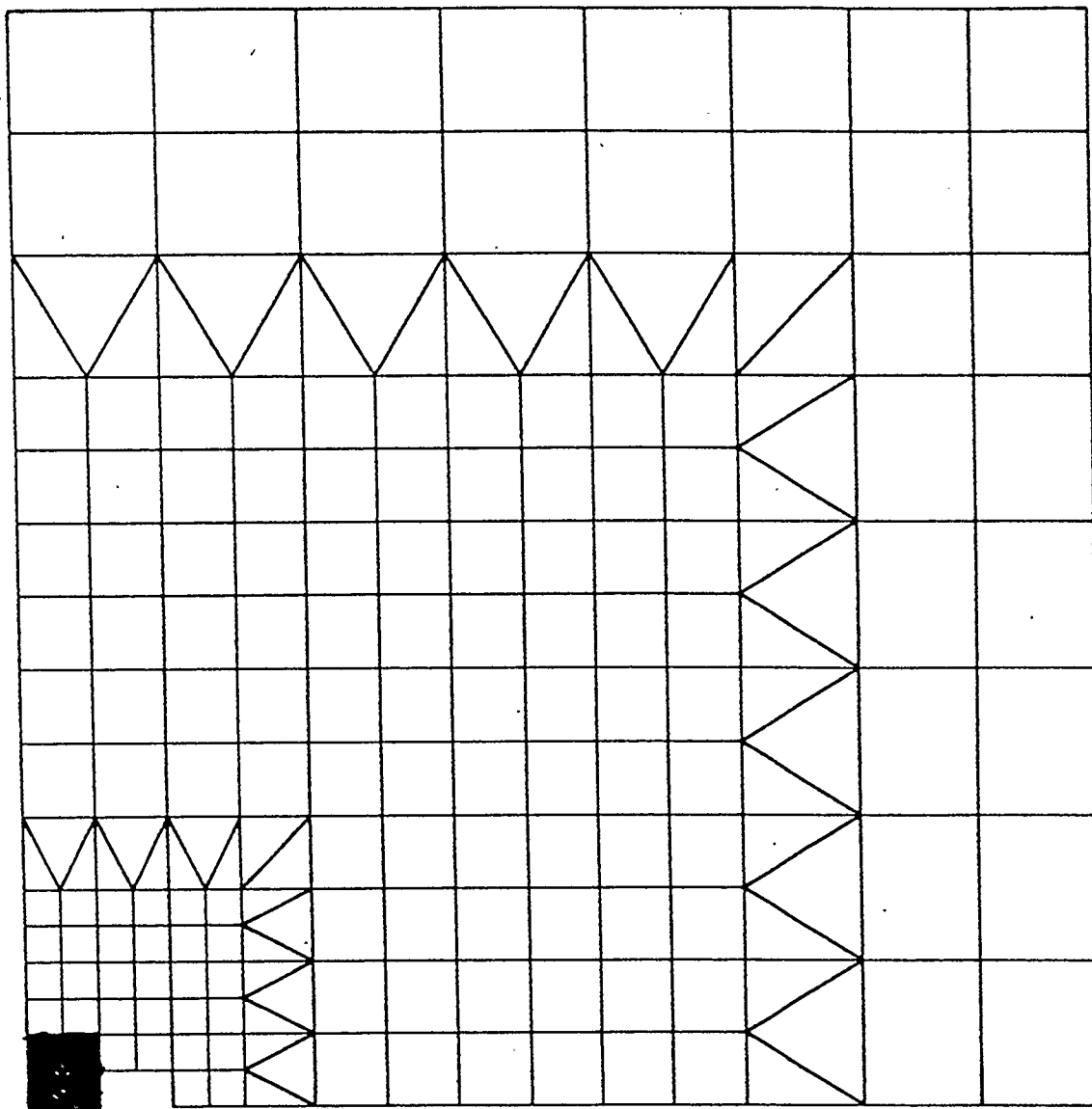


Figure 3.11: Element Layout, Hole Pattern One

steel would be shifted over and not eliminated.

3.8 Data Recorded

The following groups of data were recorded:

1. Load Deflection curves
2. Position of the line of zero flexural stress
3. Deflections along the line of zero flexural stress
4. Deflections at various cross sections parallel to the x axis
5. Shear cracking
6. Reactions at the nodes in the slab-column connection

3.9 Failure Criteria for the Model

In an experiment in the laboratory, the failure of the specimen is generally obvious. The specimen collapses under load, the test is over.

This is not the case for this computer simulation. One is forced to choose a failure criterion. For this model the failure criterion could be based on the following:

1. Nonconvergence of one or more elements within a given number of iterations in one loadstep.
2. Application of the load as determined by analysis using the design code.

3. Excessive deflections at midspan.
4. Application of the ultimate load using yield line analysis.

The decision as to which criterion to use is not always clear.

Nonconvergence

The ultimate strength is unknown at the start of the analysis. If the model does not converge at a very low load then it might be concluded that there is some problem or weakness within the model or the program. In this study there were no convergence problems except perhaps that the 10 loadsteps past 13.1 kPa each required an average of 25 iterations. Up to that point the average was about 9 iterations per loadstep with a maximum of 17 iterations. Also the position of the line of zero stress had become rather erratic due to cracking so these results had become meaningless at a load of 19.1 kPa.

Design Code Standards

Using CAN3-A23.3-M84 as a guide the failure of the slab could be set at the minimum required load. The loading could also be stopped upon violation of serviceability requirements.

For the design of the reinforcement within the slab the loads were set at 7.2 kPa unfactored and 9.65 kPa factored.

The code (Table 9-2, Pg. 54) [21] specifies that if immediate deflection due to a specified live load exceeds $L/360 = 4.5/360 = 12.5 \text{ mm}$ then the slab has failed through lack of serviceability.

Yield Line Analysis

The following describes two methods for determining the flexural failure load using yield line analysis.

Assume the flexural failure of the slab will be of the form shown in Figure 3.12.

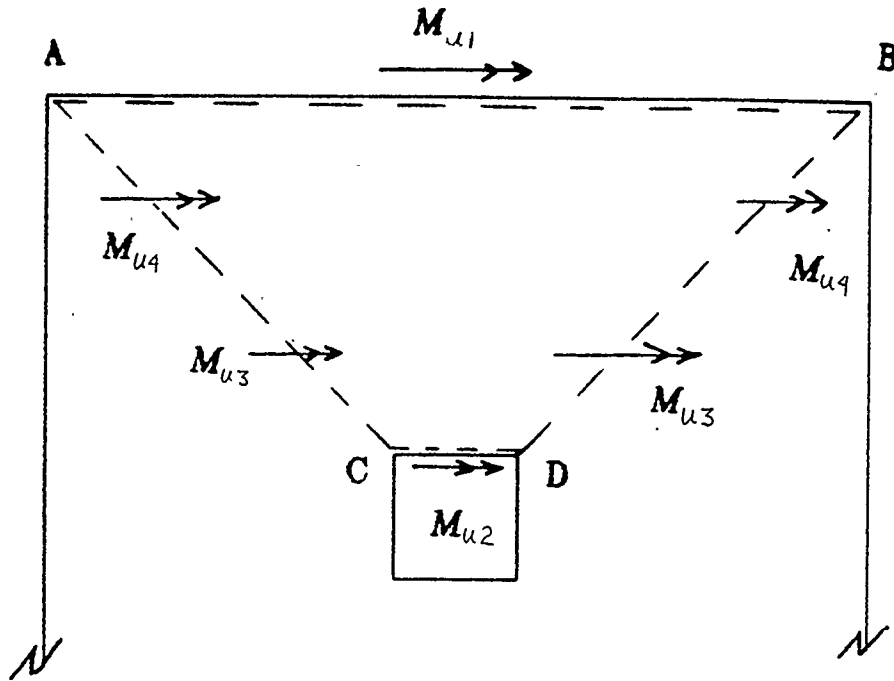


Figure 3.12: Yield Lines

M_{u1} (the ultimate moment of resistance per unit length) is calculated using the original design of the reinforcement. There are 8 number 10 bars spread over 2.25 m, thus the area per metre of the positive steel is:

$$A_s = \frac{8(100)}{2.25} = 355 \frac{\text{mm}^2}{\text{m}}$$

Recall that for a reinforced section:

$$M_u = \phi_s A_s f_y \left(d - \frac{\beta_1 c}{2} \right)$$

Where:

$$c = \frac{\phi_s A_s f_y}{0.85 \phi_c f'_c \beta_1 b}$$

With the following numbers substituted in:

$$d = 0.120 \text{ m}$$

$$b = 1.0 \text{ m}$$

$$A_s = 355 \text{ mm}^2/\text{m}$$

$$f_y = 400 \text{ MPa}$$

$$f'_c = 25 \text{ MPa}$$

$$\beta_1 = 0.85$$

Thus:

$$M_{u1} = 16.6 \text{ kN} \cdot \text{m}$$

From Figure 3.12 M_{u1} is a sagging moment while M_{u2} , M_{u3} and M_{u4} are hogging moments. However there is no steel near the top of the slab from 0.25L to 0.5L. Therefore

$$M_{u4} = 0$$

And the steel near the top of the slab close to the column is evenly distributed.

Thus:

$$M_{u2} = M_{u3}$$

In the negative steel region there are 7 number 10 bars in 1.125 m. Thus:

$$A_s = \frac{7(100)}{1.125} = 622 \frac{mm^2}{m}$$

And:

$$M_{u2} = 28.4 \text{ kN} \cdot \text{m}$$

Assuming the line AB of Figure 4.39 is displaced δ :

Energy Dissipated

$$= M_n \sum (\text{Proj. Length of Yield Line on Axis of Rotation}) \\ \times (\text{Rotation of the Segment about that axis})$$

$$E = M_{u1} L \left(\frac{2\delta}{L-c} \right) + M_{u2} \left(\frac{L}{2} \right) \left(\frac{2\delta}{L-c} \right) \\ = 16.6(4.5) \left(\frac{2\delta}{4.5-0.3} \right) + 28.4 \left(\frac{4.5}{2} \right) \left(\frac{2\delta}{4.5-0.3} \right) \\ = 35.6\delta + 30.4\delta = 60.0\delta$$

External Work (uniform load q , see Figure 3.13)

$$\text{Work Done} = W = \sum (\text{Load})(\text{Area of Segment}) \\ \times (\text{Displacement of Centroid of Segment}) \\ = 2qA_1 \frac{2}{3}\delta + qA_2 \frac{1}{3}\delta$$

Where:

$$A_1 = \frac{L}{2} \left(\frac{L-c}{2} \right) \left(\frac{1}{2} \right) \quad A_2 = c \left(\frac{L-c}{2} \right) \left(\frac{1}{2} \right)$$

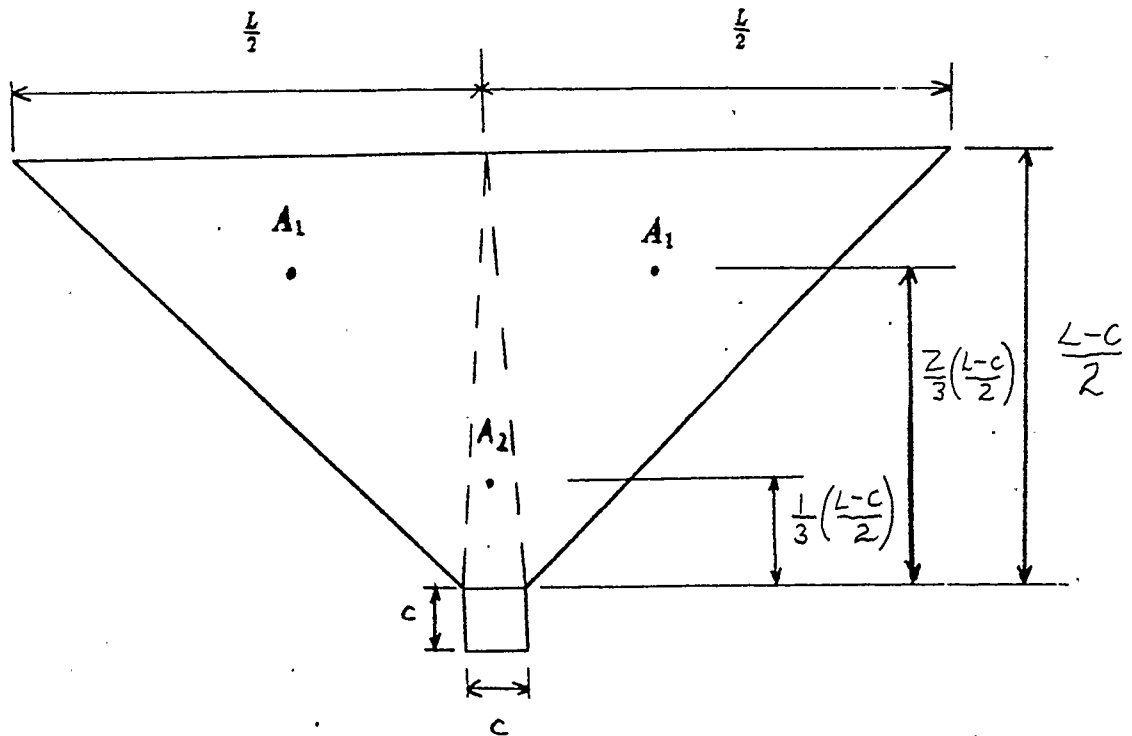


Figure 3.13: Areas for External Work

If: $L = 4.5 \text{ m}$ and $c = 0.3 \text{ m}$ then:

$$A_1 = 2.363 \text{ m}^2 \quad A_2 = 0.315 \text{ m}^2$$

Thus:

$$W = 3.256q\delta$$

Equating: $W = E$

$$3.256q\delta = 66.0\delta$$

Therefore according to yield line analysis failure can be expected to take place at a load of 20.3 kPa.

Choice of Final Analysis Load

The data recorded for the line of zero flexural stress was rather erratic at a load of 19.1 kPa. Yield line analysis gave a maximum load of 20.3 kPa. Serviceability deflections were not exceeded in either case. It was decided that the finite element analysis should be concentrated on the first 60% of a failure load. This gave a maximum load of $(0.6)(19.1) \approx 11.9 \text{ kPa}$. No load data was recorded for less than the self weight of the slab (3.5 kPa) although some of the load steps were less than 3.5 kPa to avoid false cracking. The load steps were taken at 0.6 kPa intervals.

3.10 Results

3.10.1 Load Deflection Curves

Readings were taken at the points shown in Figure 3.14. The deflections were affected by cracking within the slab. A significant amount of cracking between two

loadsteps produced results with a certain degree of nonlinearity as shown in Figure 3.15. The holes in the slab did not affect the deflection readings.

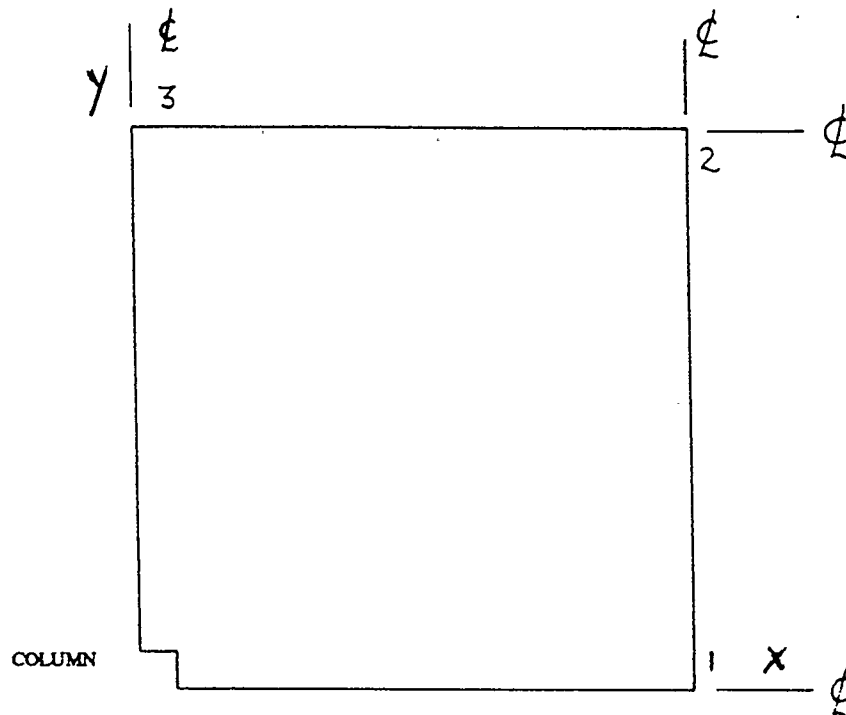


Figure 3.14: Points for Deflection Readings

3.10.2 Position of the Line of Zero Flexural Stress

The lines $\sigma_x = 0$ and $\sigma_y = 0$ formed a rough square around the column about 975 mm from the centre of the column. The holes did not significantly affect the position of these lines.

Figure 3.16 shows the lines of zero flexural stress ($\sigma_x = 0$) for two layers within the elements in layer one of the solid slab. These layers are separated by 15 mm.

Figure 3.17 shows the effect of the hole in the three positions. All three patterns are based on a load of 11.9 kPa.

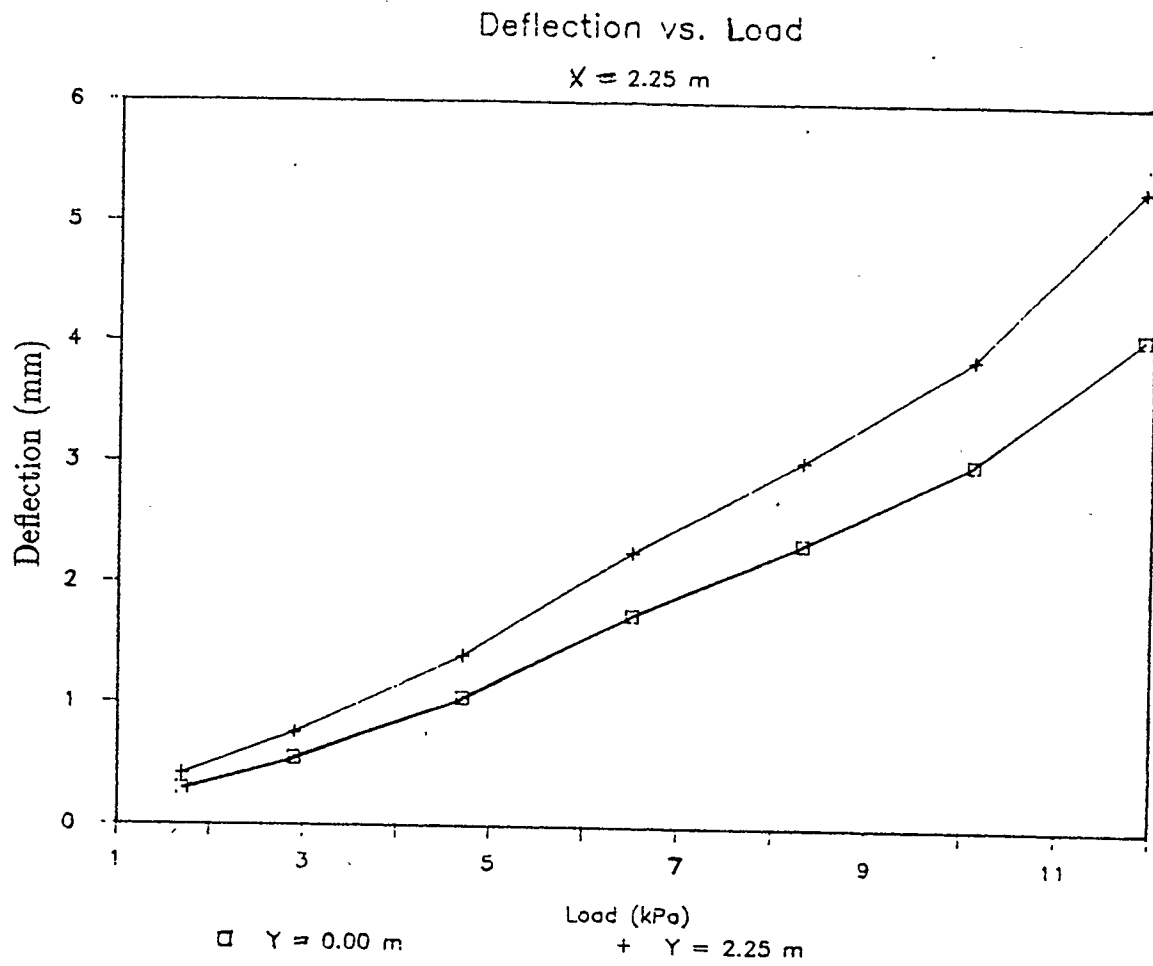
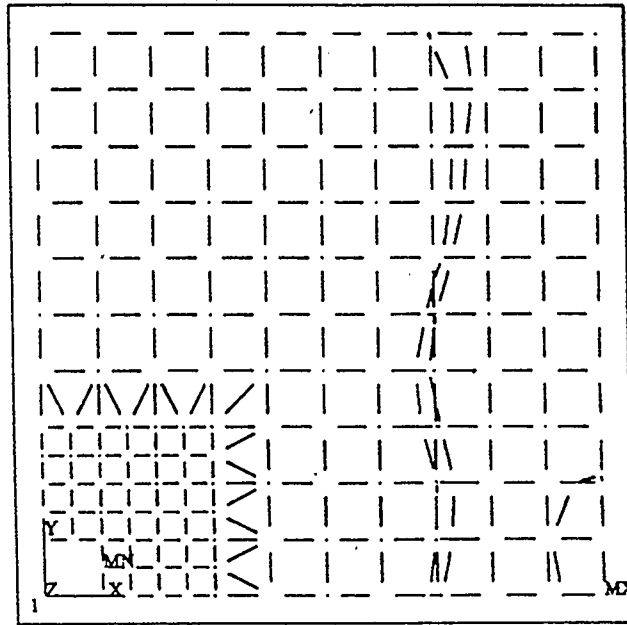


Figure 3.15: Deflection vs. Load for Model 5



LOAD = 11900

Figure 3.16: Lines of Zero Flexural Stress, Solid Slab, 11.9 kPa

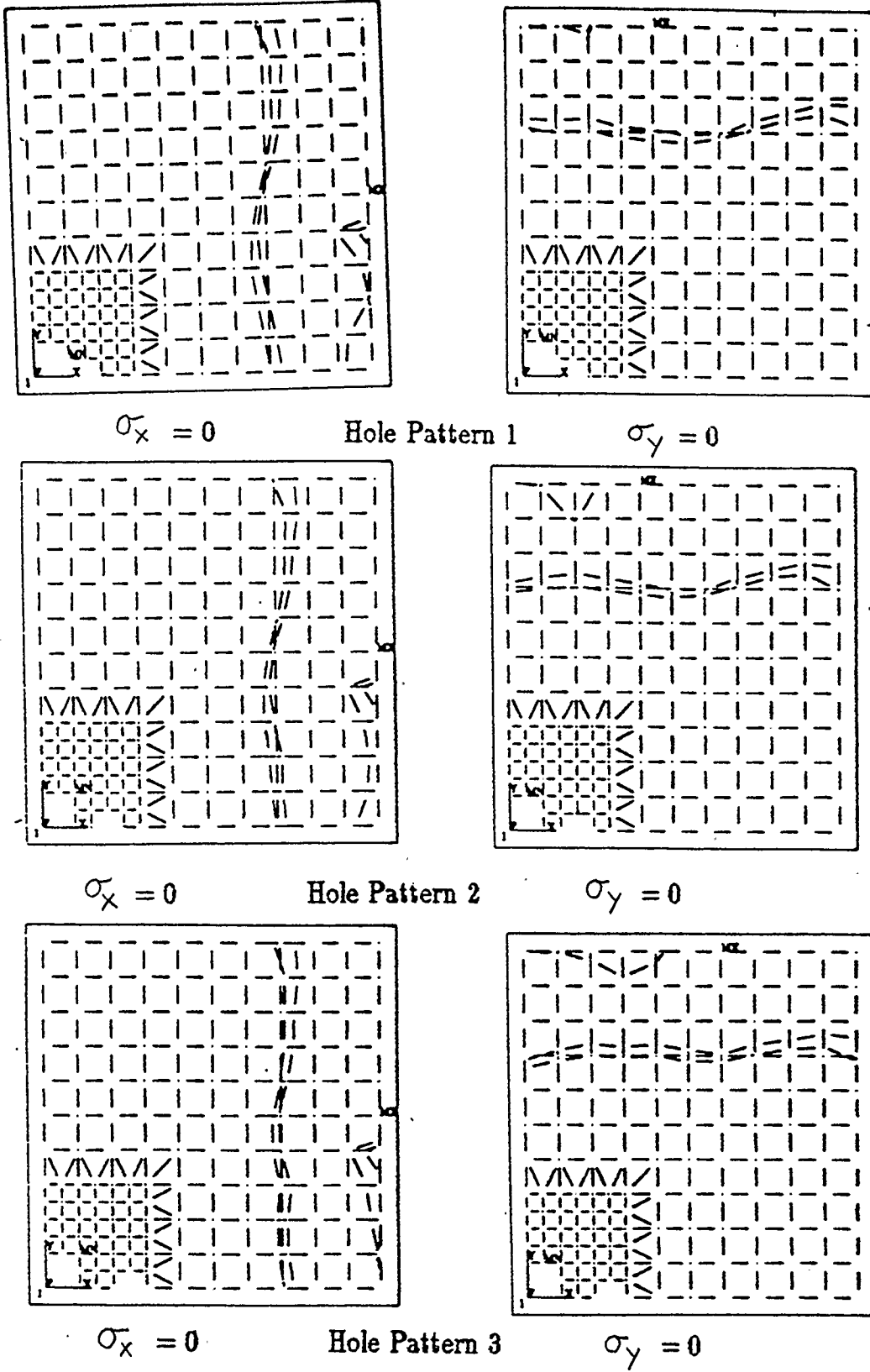


Figure 3.17: Lines of Zero Flexural Stress, Three Hole Patterns, 11.9 kPa

3.10.3 Deflections along Lines of Zero Flexural Stress

These deflections, taken at the top surface of the slab, were virtually identical for each of the hole patterns. The results from Hole Pattern One are shown in Figure 3.18.

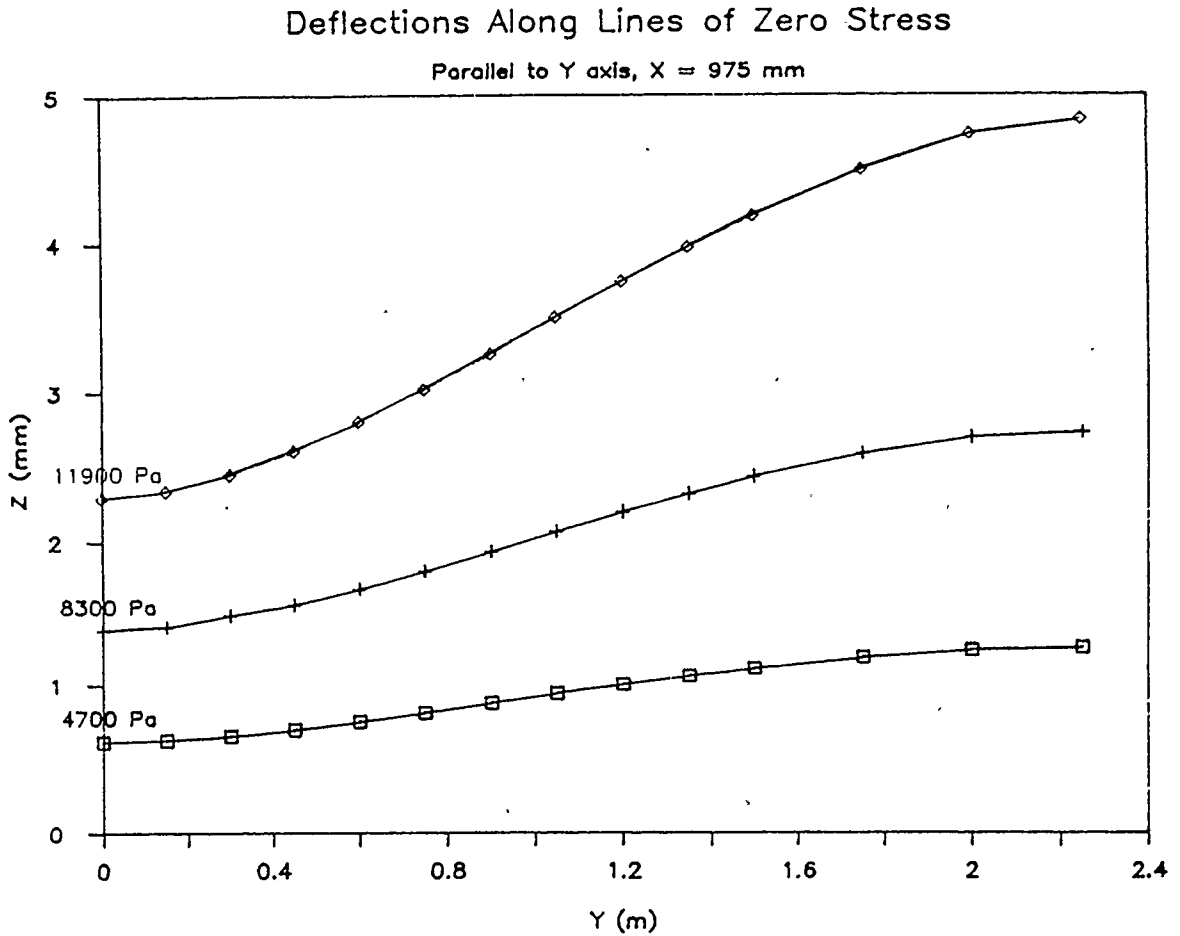


Figure 3.18: Deflections Along $x = 975 \text{ mm}$, Hole Pattern One

3.10.4 Deflections Along Various cross Sections

These deflections were not affected by the varying hole patterns. The deflections for Hole Pattern One are shown in Figure 3.19 and 3.20. The disturbing feature of these figures is that the points of contraflexure are not all 975 mm from the centre of the column. In Figure 3.19 for $y = 0$ to 300 mm the point of contraflexure is at about $x = 350$ to 400 mm. For the rest of the cross sections the point is less well defined but appears to be closer to $x = 900$ to 1000 mm. One would have expected the point of contraflexure and the point of zero flexural stress, shown in Figure 3.17, to be in the same place.

3.10.5 Flexural and Shear Cracking

The progression of shear cracking was recorded for each of the sections shown in Figure 3.21.

Only the sections at $y = 16$ and 91 mm were recorded for the solid slab. The shear cracking was affected by the holes, especially in the section at $y = 91$ mm. The cracking in this section is shown for the various hole patterns and various loads in Figures 3.22 to 3.25. The presence of the holes seems to increase the amount of cracking and alter the position of the cracks so that they are right beside the hole.

A problem with the finite element analysis is evident from these figures. The horizontal cracks that form in the bottom of the slab should not be there. The tensile stress in this area should not be enough to produce cracking, yet for some reason it seems to be artificially high.

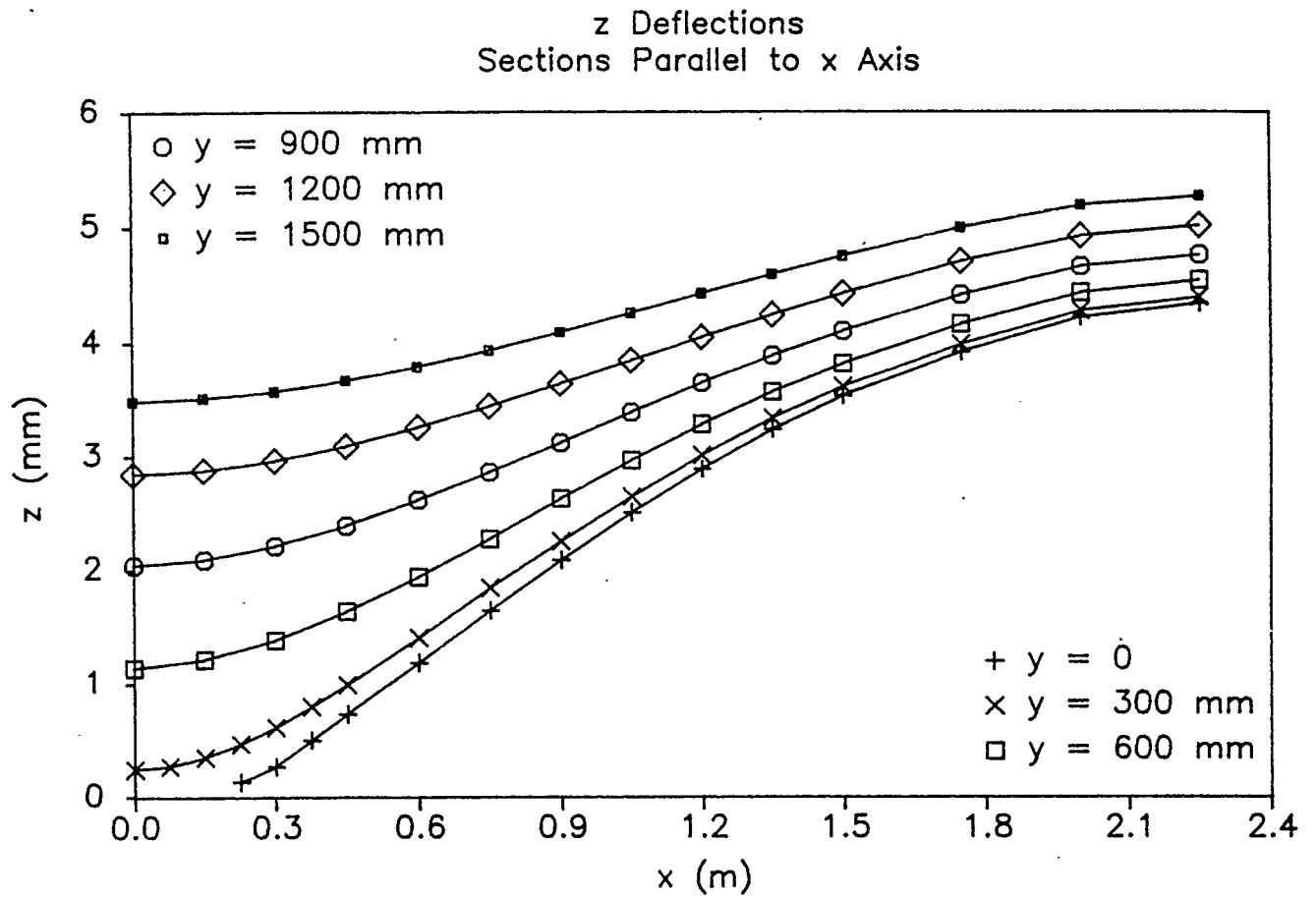


Figure 3.19: Deflections Along Various Sections, 11.9 kPa, Hole Pattern 1

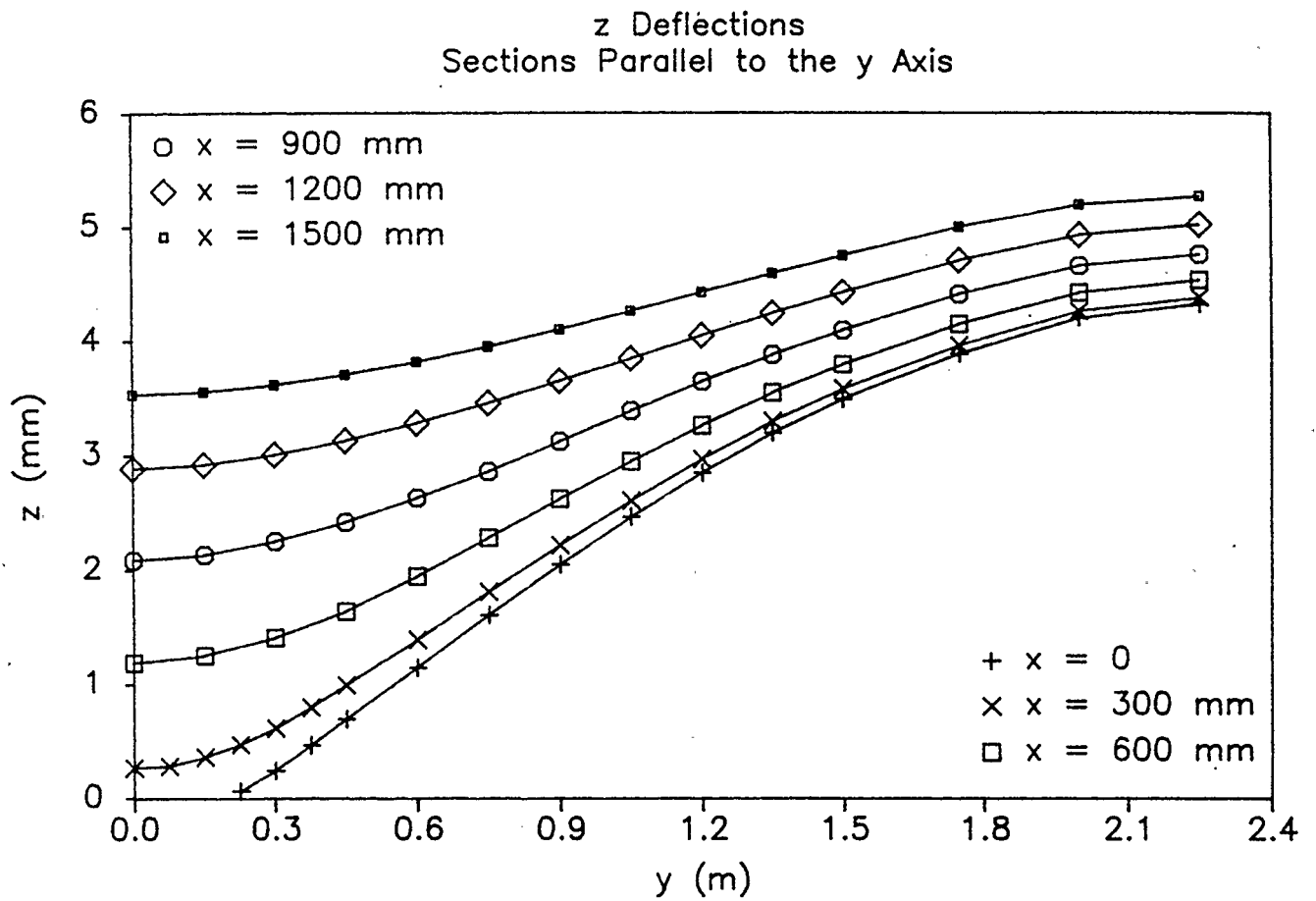


Figure 3.20: Deflections Along Various Sections, 11.9 kPa, Hole Pattern 1

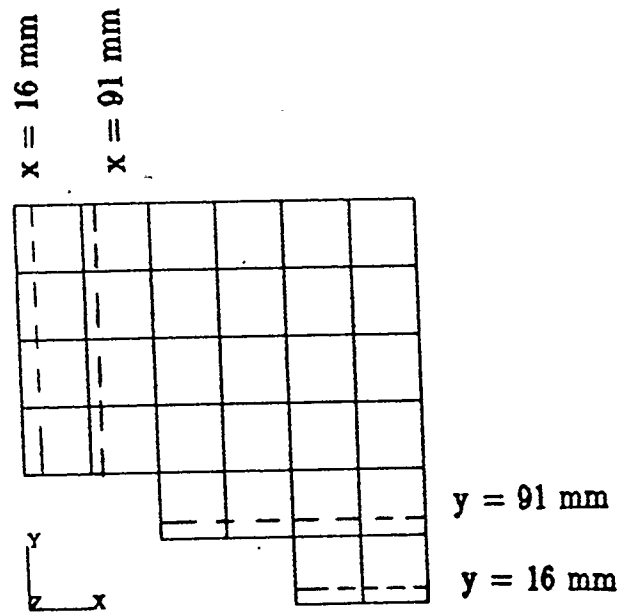


Figure 3.21: Sections for Flexural and Shear Cracking

Section at 91 mm

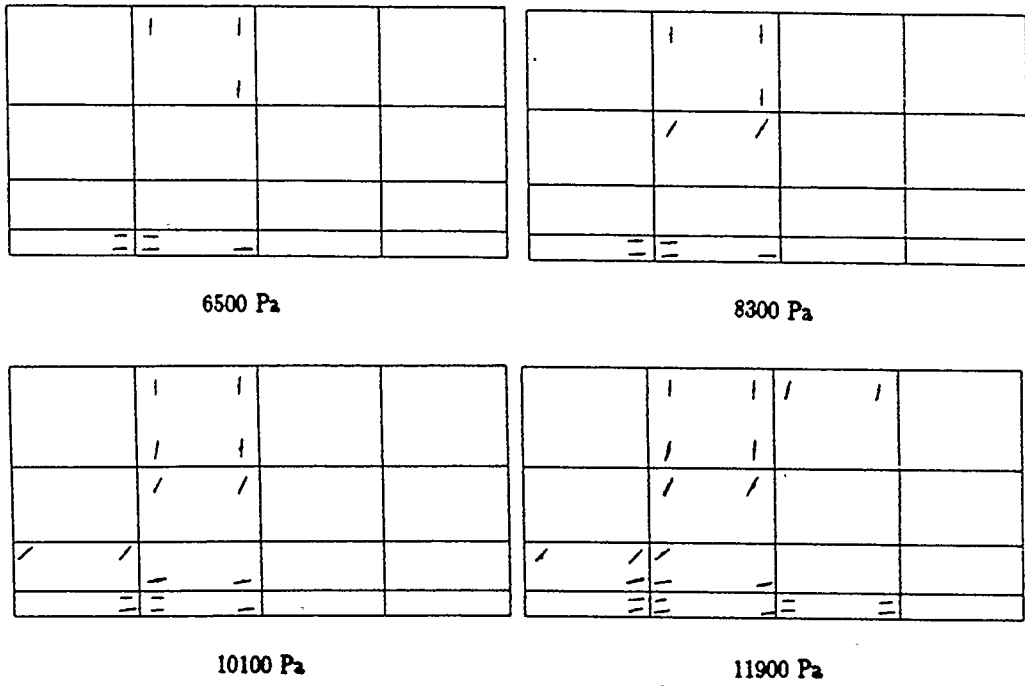
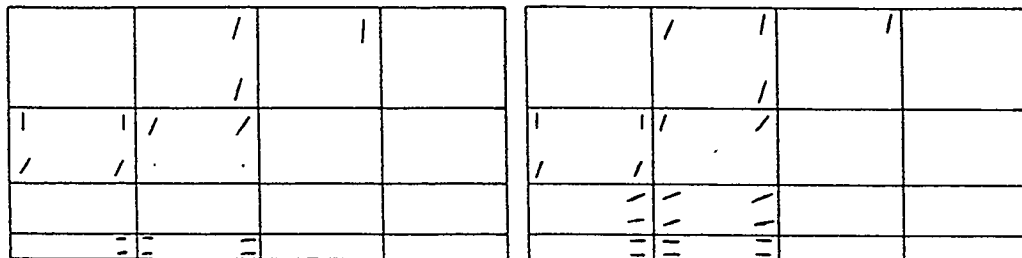


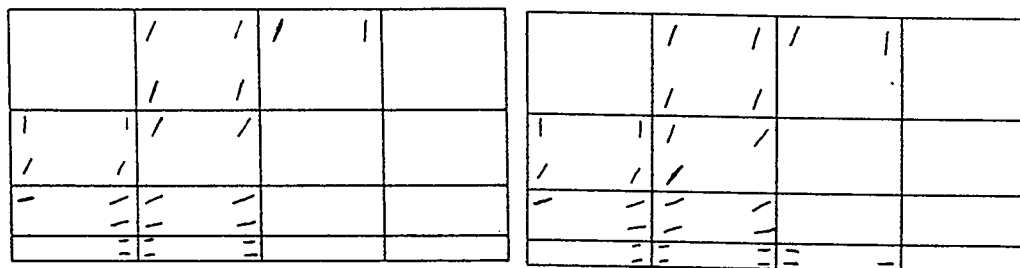
Figure 3.22: Sequence of Flexure-Shear Cracking, Solid Slab

$y = 91 \text{ mm}$



6500 Pa

8300 Pa



10100 Pa

11900 Pa

Figure 3.23: Sequence of Flexure-Shear Cracking, Hole Pattern One

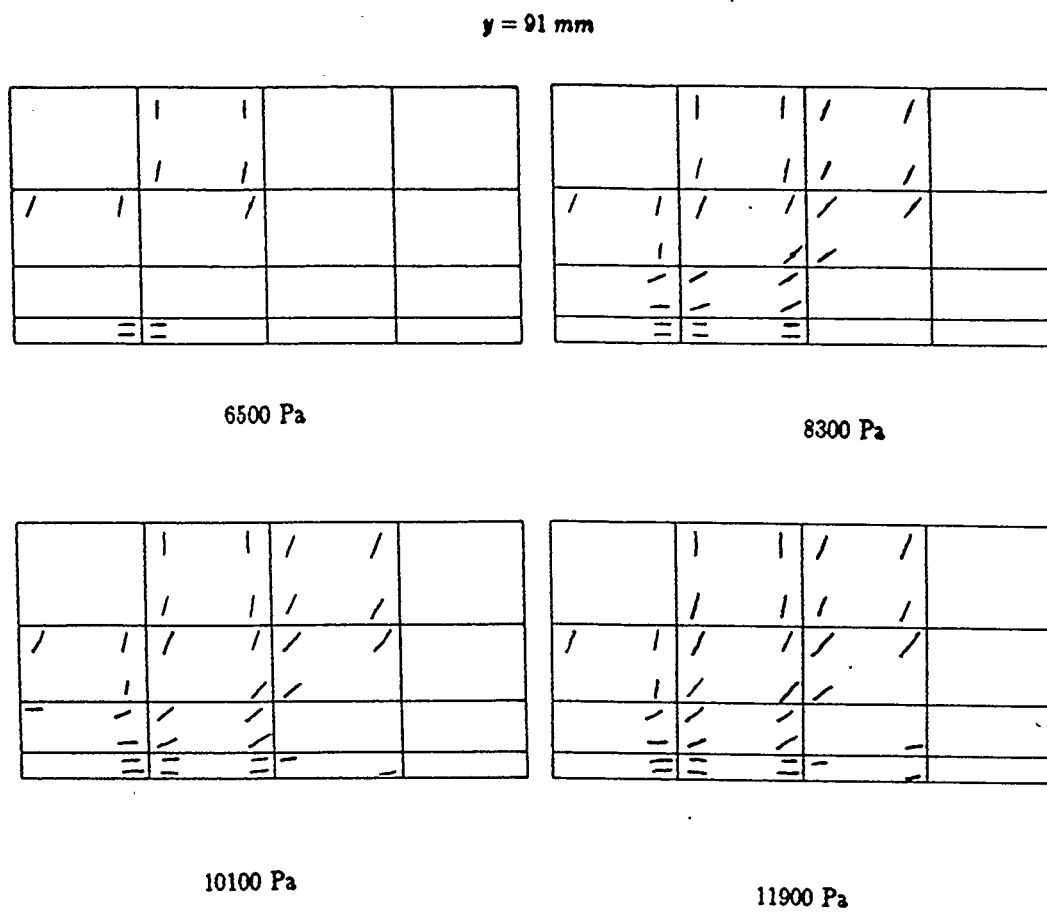
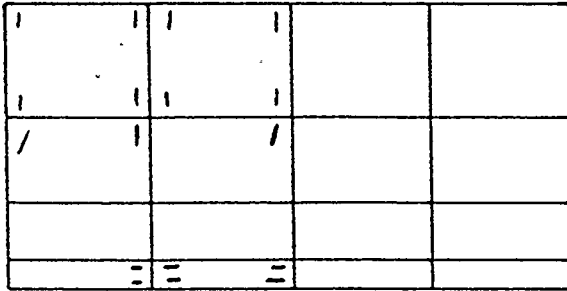
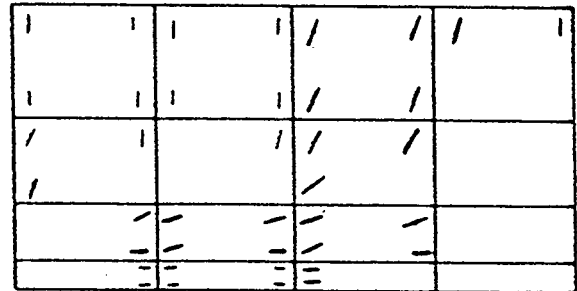


Figure 3.24: Sequence of Flexure-Shear Cracking, Hole Pattern Two

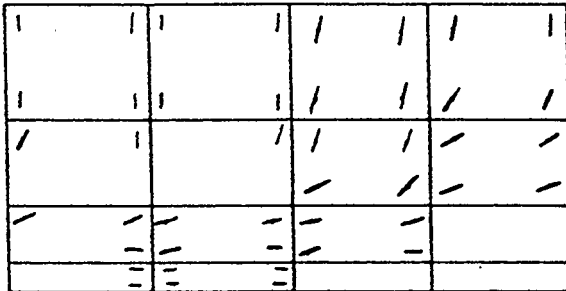
$y = 91 \text{ mm}$



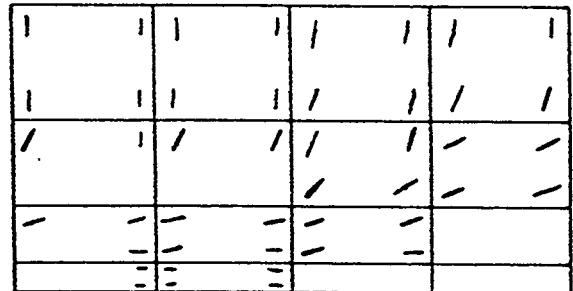
6500 Pa



8300 Pa



10100 Pa



11900 Pa

Figure 3.25: Sequence of Flexure-Shear Cracking, Hole Pattern Three

3.10.6 Reactions at the Column

In this model the nodes at the slab-column joint are fixed. That is, no movement is allowed in any of the x , y or z directions. Consider the slab-column interface shown in Figure 3.26.

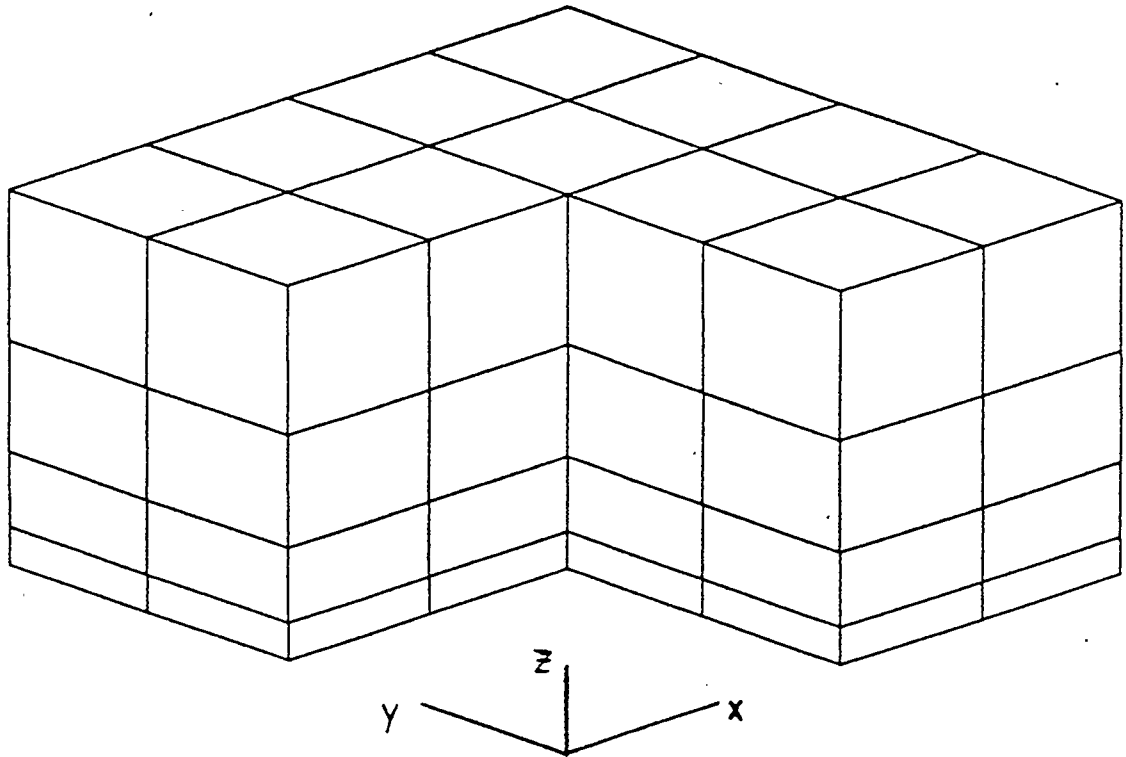


Figure 3.26: Column-Slab Interface

The connection is made up of a total of 25 nodes in 5 stacks at the coordinates shown in Table 3.1. The reaction in the z direction for each of the stacks at a load of 11.9 kPa is shown in Figures 3.27 to 3.30. The bulk of the load is carried at the corner of the column in each case. A hole close to the face of the column drives the peak load up slightly.

x (mm)	y (mm)
0	150
75	150
150	150
150	75
150	0

Table 3.1: Coordinates for Node Stacks at Column

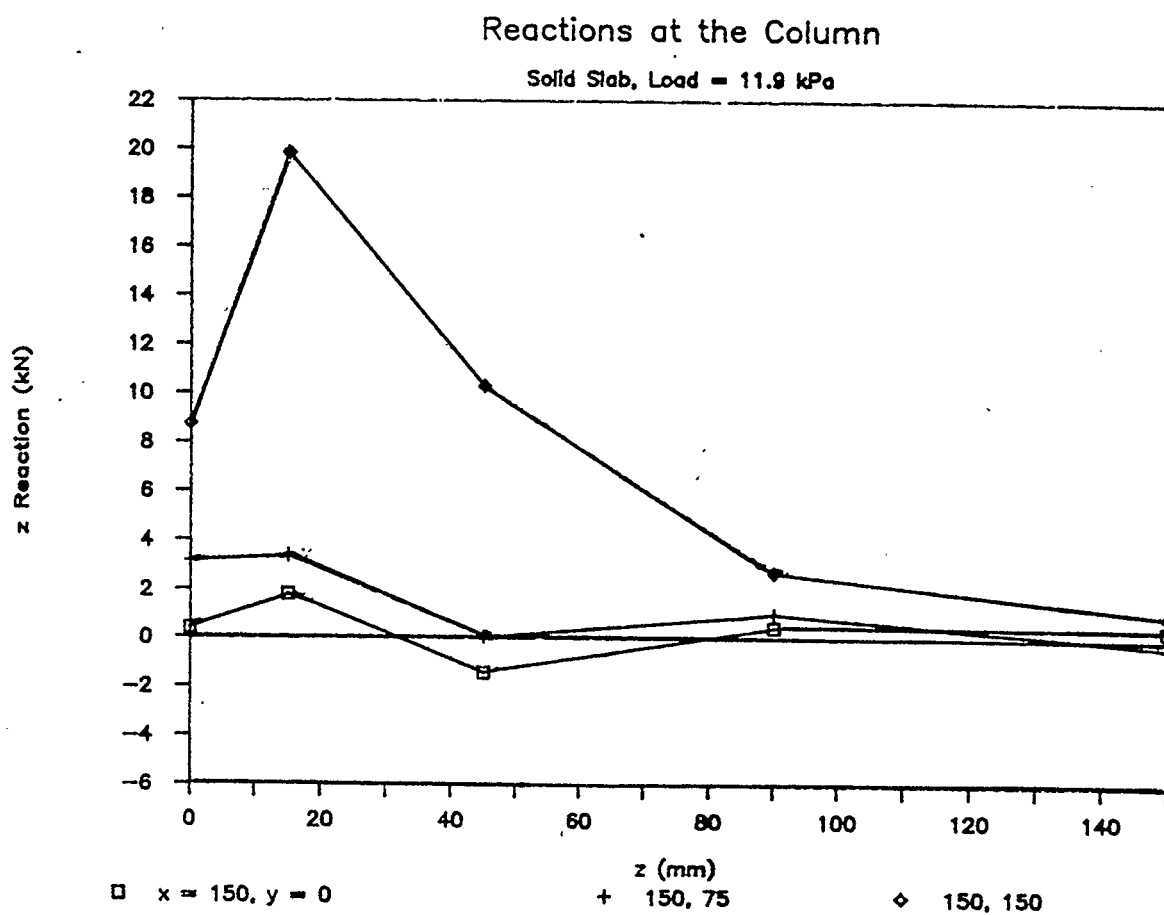


Figure 3.27: Reactions at the Column, Solid Slab

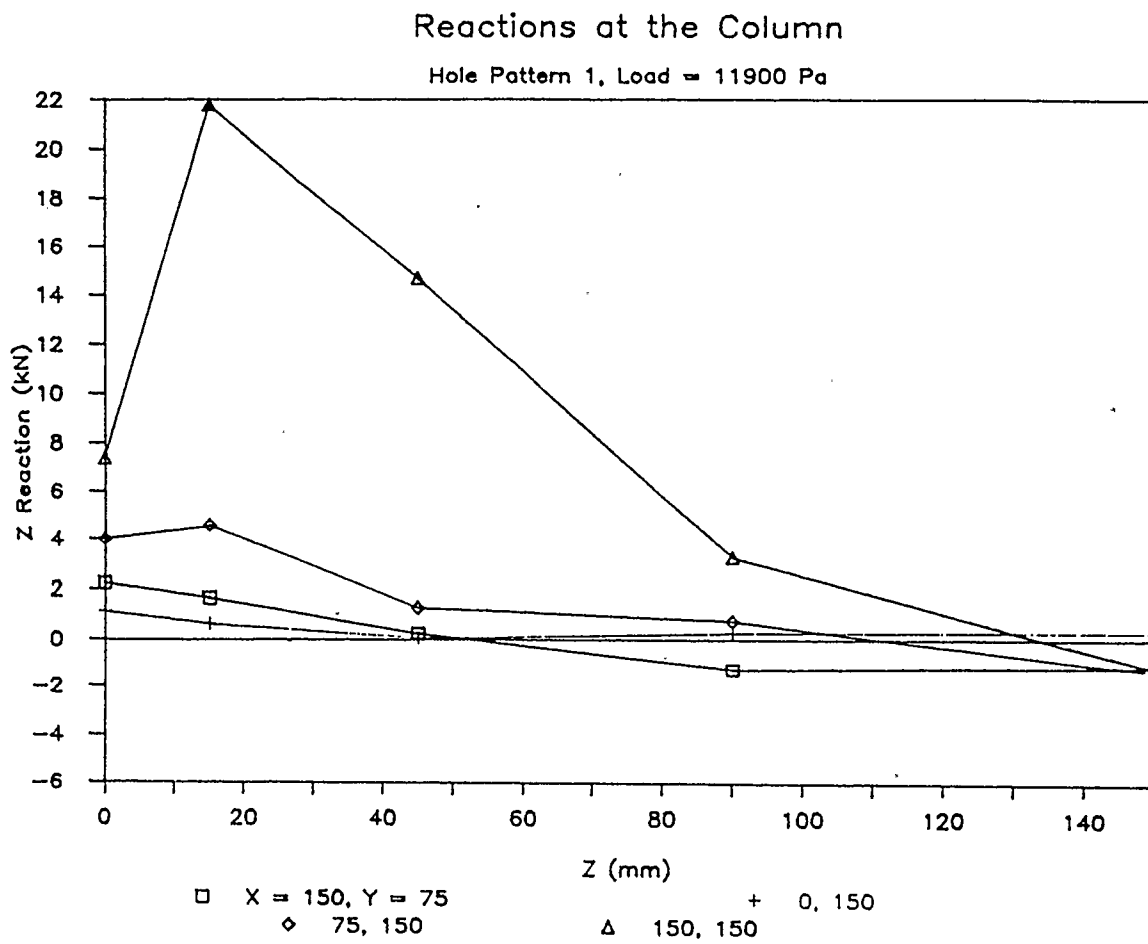


Figure 3.28: Reactions at the Column, Hole Pattern One

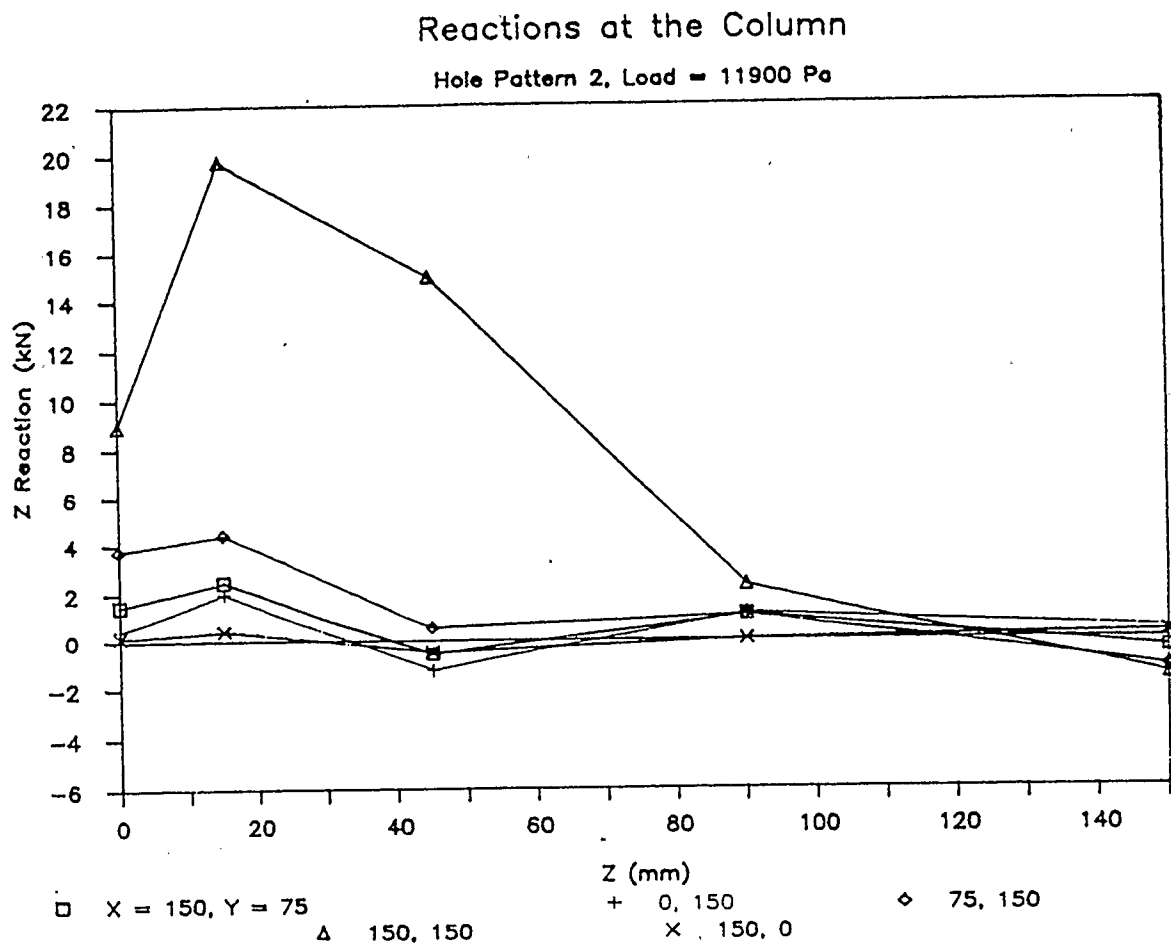


Figure 3.29: Reactions at the Column, Hole Pattern Two

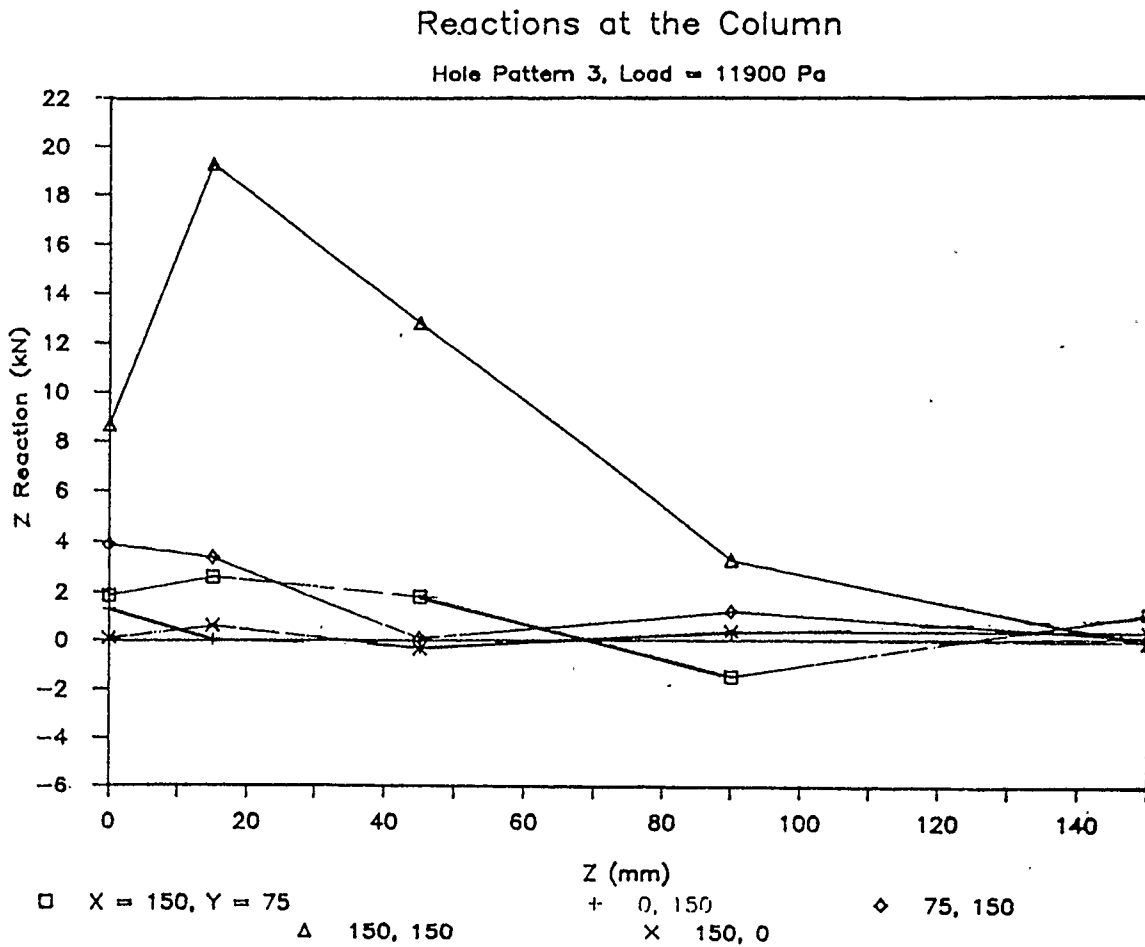


Figure 3.30: Reactions at the Column, Hole Pattern Three

3.11 Analysis and Discussion of Finite Element Results

In order for reality to be correctly represented by a laboratory specimen the following must be true:

1. The lines of zero flexural moment form a square around the column.
2. The position of these lines is constant throughout the test.
3. The deflections along these lines are uniform, or at least match the deflections of the test.

Assumption 1

The main idea in choosing a simply supported specimen is: the simply supported edge represents the point where the bending moment in the slab is zero. At this point one would expect the following:

- The curvature of the slab would be zero, this would be the point of contraflexure of the slab.
- The flexural stresses in the slab would be zero.

The results of the finite element analysis have shown that these two points are not always coincident. Along a section where $y = 0$ the point of contraflexure is at about $x = 375 \text{ mm}$, while the point of zero flexural stress is at about 975 mm .

The line of zero flexural stress forms a rough square around the column at about $x = 975 \text{ mm}$ or $\frac{0.975}{4.5}L = 0.22L$. This is the assumption made for a simply supported specimen, a square somewhere between $0.2L$ and $0.25L$. But for $y = 0$ this line is not anywhere near the point of contraflexure.

Restraint Conditions

The boundary conditions for the model are such that the nodes at the column are allowed *zero* deflection and at the centreline of the slab the nodes are allowed *zero* translation. Consider the profile of the slab between the column and the centreline. The model restrains the section as shown in Figure 3.31. The tension force is needed to keep the ends at a constant horizontal distance from each other. This tension could affect the position of the line of zero flexural stress.

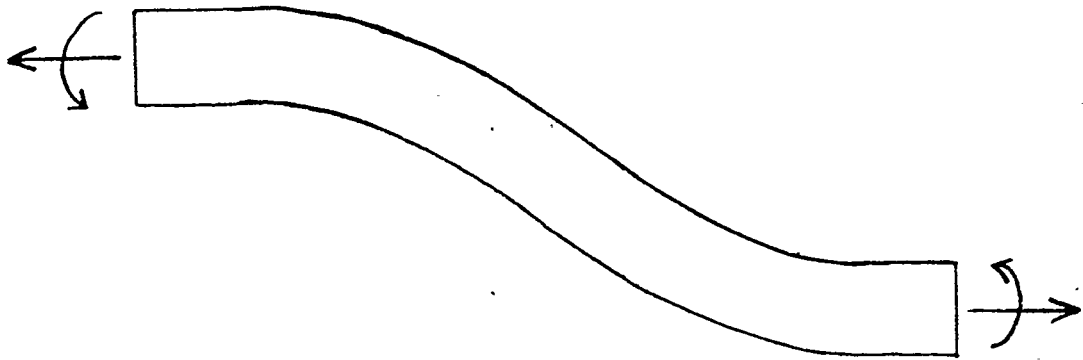


Figure 3.31: Restraintment of Finite Element Model

Overall Effect

The effect of the tension force could lead one to believe that the point at which the moment in the slab is zero lies between 375 and 975 mm (for $y = 0$). Recall however that for $y = 600$ mm or greater the position of contraflexure and zero flexural stress agree at about $x = 975$ mm. Therefore if the position at $y = 0$ is an average value of about 675 mm then one ends up with a test specimen like the one shown in Figure 3.32.

If only the line of zero flexural stress is considered then test specimens used thus far are adequate.

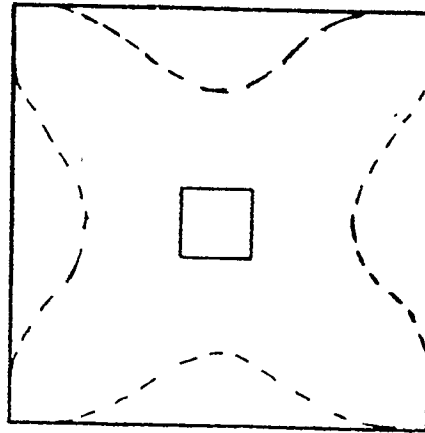


Figure 3.32: Possible Shape of Test Specimen

Assumption 2

The results over several load steps show that the position of the line of zero flexural stress did not change by more than 5% of the centre to centre span of the slab.

Assumption 3

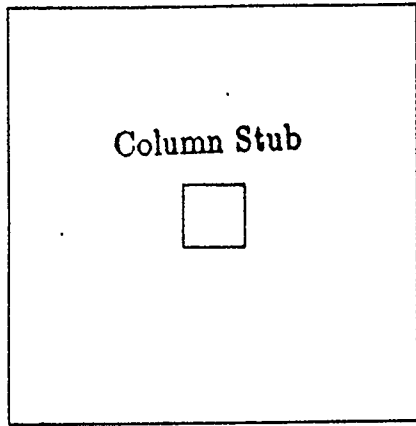
The deflections along the lines of zero flexural stress were found to be nonuniform. This would indicate that the distribution of shear stresses along the line is also nonuniform.

Recall that some of the past investigators, in describing their testing procedures, have made the following statement: *The corners of the specimen were allowed to uplift.*

Consider a deflected laboratory specimen. (To match reality the specimen is shown with the column stub down, see Figure 3.33.)

Along an edge of the specimen the reaction load must be distributed over the length that still touches the support (Figure 3.34).

The shear stress along sections at $x = 1.05 \text{ m}$ and $y = 1.05 \text{ m}$ is shown in



All Edges Simply Supported

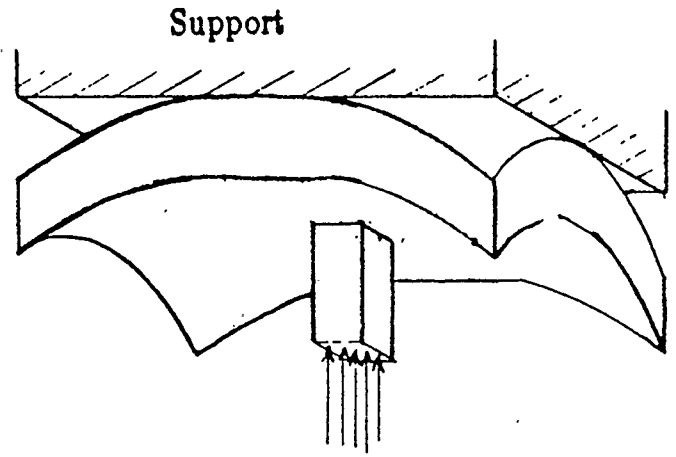


Figure 3.33: Deflected Laboratory Specimen

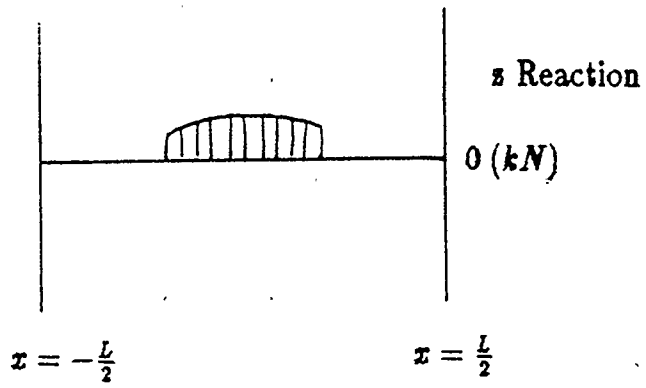


Figure 3.34: Edge Reactions of a Specimen

Figures 3.35 and 3.36. The results are from the finite element analysis of Hole Pattern three at a load of 11.9 kPa.

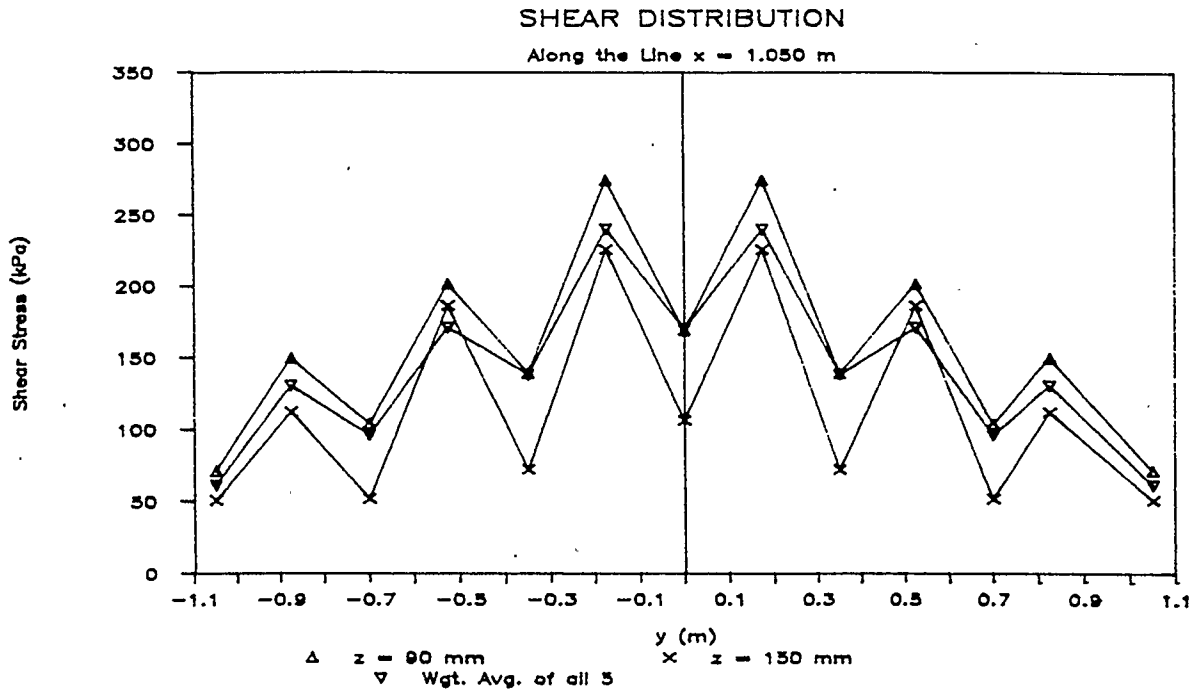
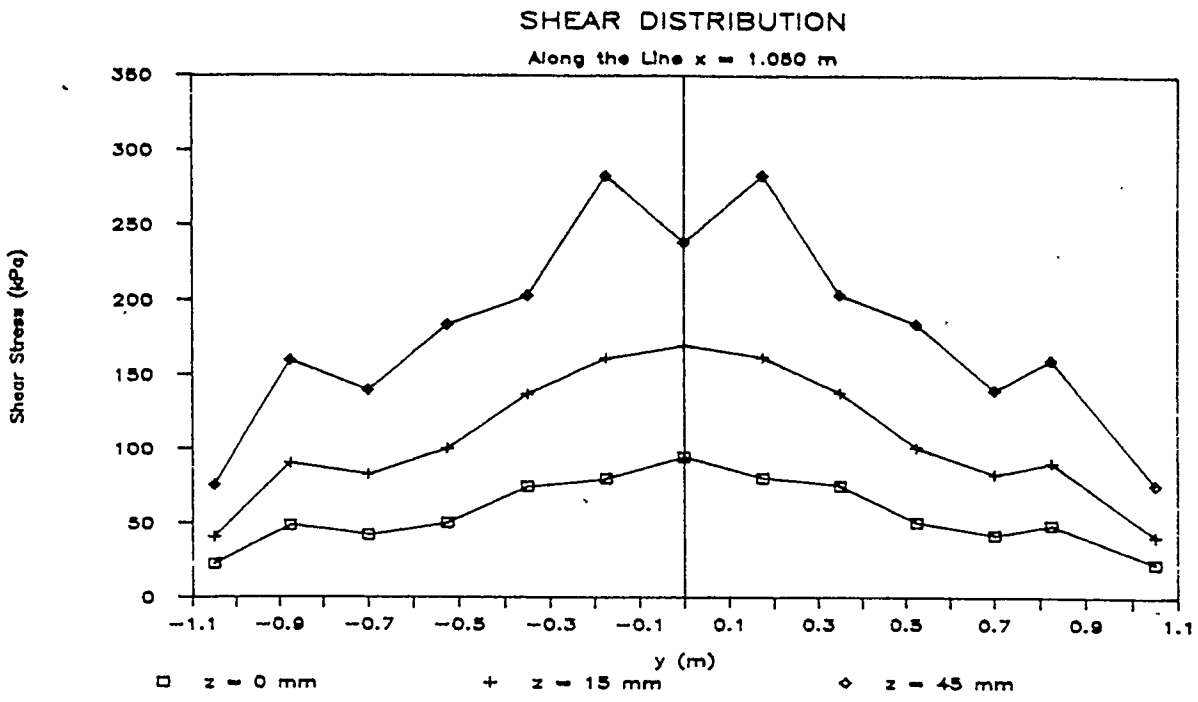


Figure 3.35: Shear Distribution, $x = 1.05$ m, Load = 11.9 kPa

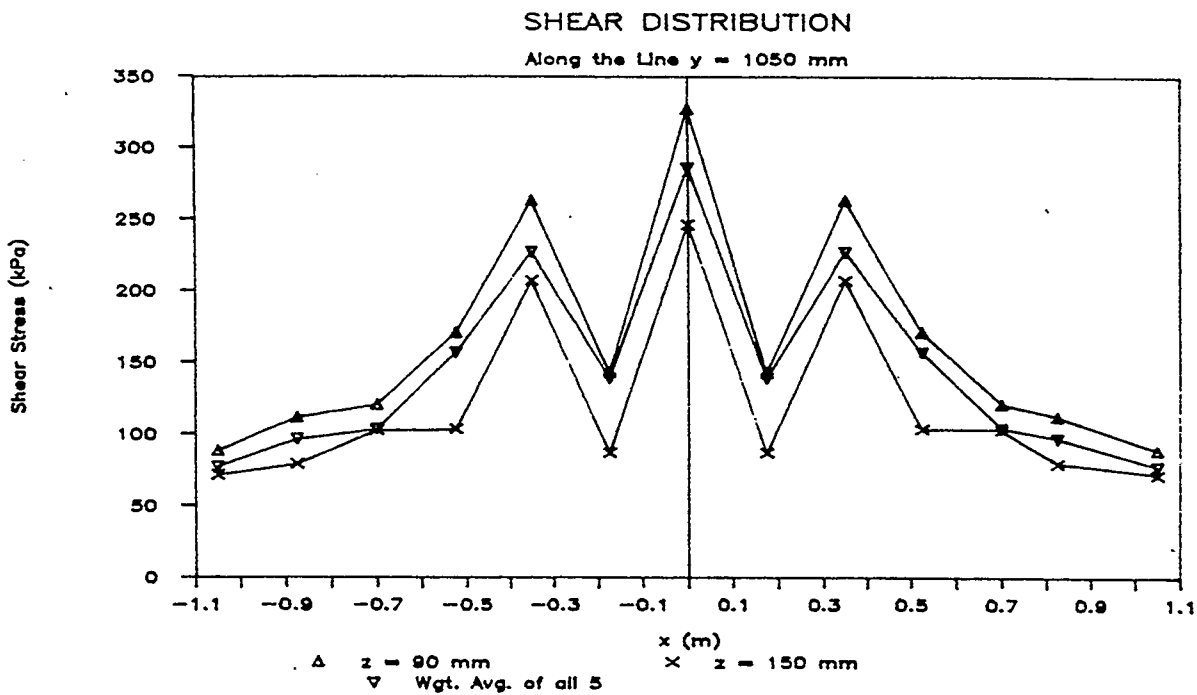
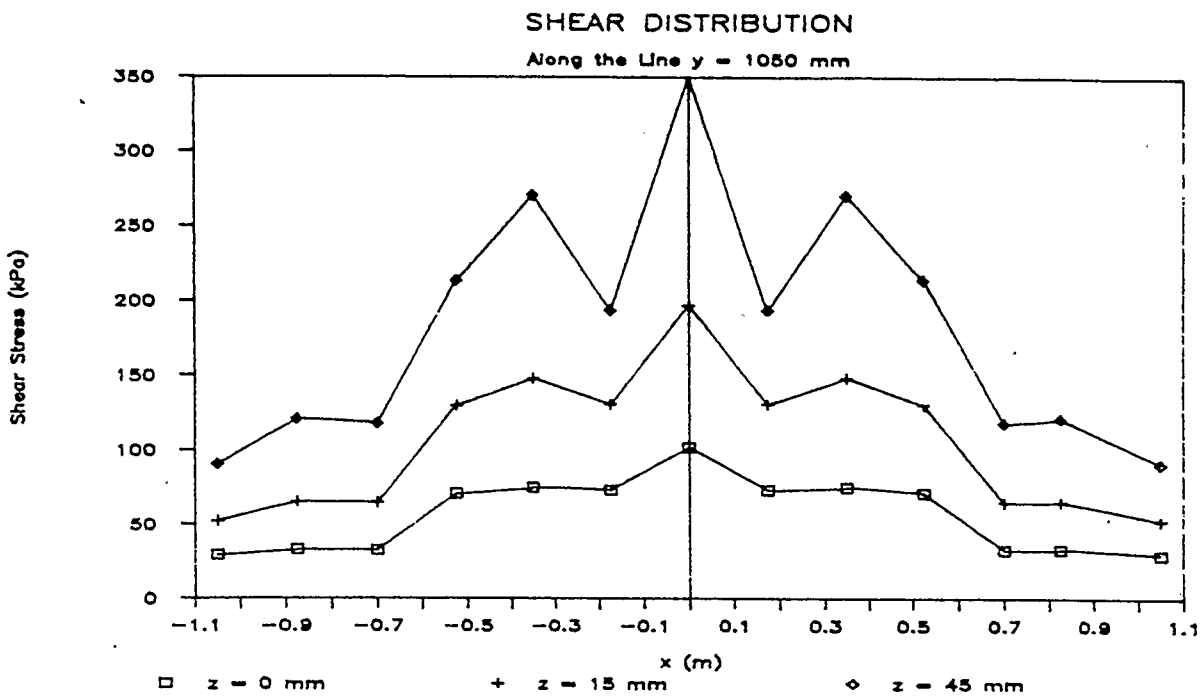


Figure 3.36: Shear Distribution, $y = 1.05$ m, Load = 11.9 kPa

The points on the graph do not give a smooth curve when averaged. The line $x = 1.05 \text{ m}$ is a border between two elements and the shear distribution is plotted for each of the layers of nodes within the model. The graph shows that the results for the levels at $z = 0, 15$ and 45 mm are reasonable. For the levels $z = 90$ and 150 mm the results oscillate too much.

Consider the line at $z = 90 \text{ mm}$. The τ_{zz} are obtained from the integration points within the adjoining elements. The weighted average of those values gives the nodal value. Choose first the elements just inside (closer to the column) of the line $x = 1.05 \text{ m}$, $z = 90 \text{ mm}$. The elements in question are shown in Figure 3.37. This figure also shows the integration points to be considered.

355		359		363	
5	7	5	7	5	7
307		311		315	
6	8	6	8	6	8

Figure 3.37: Elements and Integration Points, Inside $x = 1.05 \text{ m}$, $z = 90 \text{ mm}$.

The τ_{zz} values at these integration points are shown in Figure 3.38.

149	307	268	2	141	288
315	397	421	205	256	299

Figure 3.38: τ_{zz} Values, Inside $x = 1.05 \text{ m}$, $z = 90 \text{ mm}$.

Now choose the elements just outside (farther from the column) of the line

$x = 1.05 \text{ m}$, $z = 90 \text{ mm}$. Figures 3.39 and 3.40 show the elements and the corresponding τ_{xz} values.

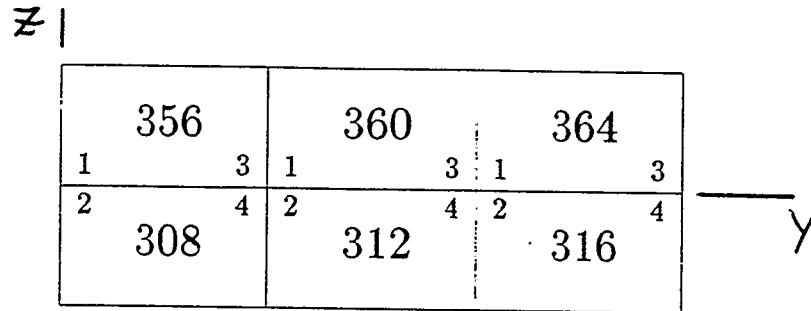


Figure 3.39: Elements and Integration Points, Outside $x = 1.05 \text{ m}$, $z = 90 \text{ mm}$.

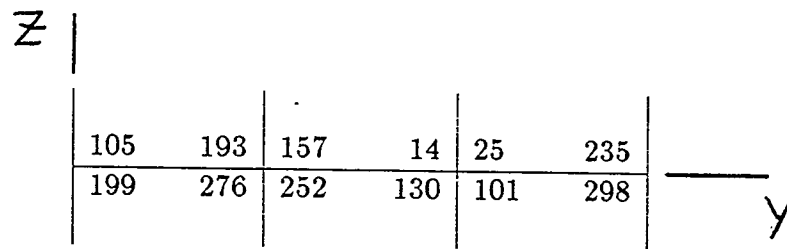


Figure 3.40: τ_{xz} Values, Outside $x = 1.05 \text{ m}$, $z = 90 \text{ mm}$.

While these values do not seem to present any obvious pattern they do satisfy equilibrium. When all the shear stresses along the face $x = 1.05 \text{ m}$ are added up they equal the load placed on the area shown in Figure 3.41.

The cause of the oscillation is not clear. There is some cracking in the upper elements, but not along the entire length of the line. The only differences between the upper and lower layers are their relative thicknesses and the reinforcing steel in the top layer. Since the average values of the nodal shear stresses do satisfy equilibrium one can speculate about the true shape of the average distribution. It is possible that the curve is an average of the oscillating curve. If this is true then some of the load is being carried all along the face $x = 1.05 \text{ m}$.

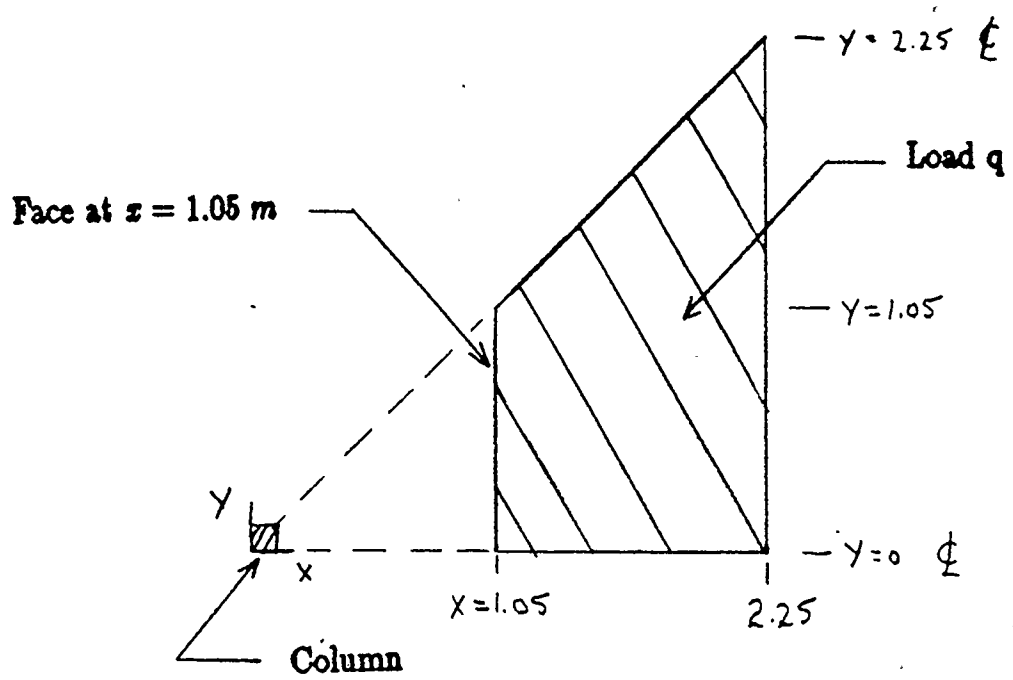


Figure 3.41: Area Considered for Equilibrium Check

Acceptance or Rejection of Test Specimen

The finite element model has shown that there is some question as to the best shape for a test specimen. Even if a square specimen is acceptable, the deflection along the edge of the specimen should not be considered uniform. To obtain test conditions which match the conditions in a floor slab, some acceptable kind of support system needs to be created which gives the required deflections. This would divert some of the load to the corners of the specimen.

However there were problems with the finite element model itself. The formation of horizontal cracks near the bottom of the slab, the difference in the positions of the points of contraflexure and zero flexural stress and the erratic shear distribution all undermine confidence in the model. Because of this the results from the laboratory tests cannot be rejected solely on the basis of this finite element analysis.

Chapter 4

Examination of Prediction Equations

4.1 Introduction

The literature review of Chapter 2 revealed that many different prediction equations have been developed. Almost all are based on a statistical analysis of data gathered from tests on laboratory specimens. The laboratory specimens are all simply supported sections of slab with square column stubs. The model presented by Rankin and Long [24] is one of the few papers that gives a logical basis for prediction of punching shear strength. The aim of this chapter is to adapt this model to handle slabs with holes and compare the subsequent predictions to test results. Also three methods for reducing the critical section will be investigated.

4.2 Application of Rankin and Long's Model to Slabs with Holes

Any application of Rankin and Long's model to slabs with holes must be done for both the equation for flexural punching strength and the equation for shear punching strength.

4.2.1 Flexural Punching Strength

Consider the three cases for flexural punching shear failure shown in Figure 2.12. When a full yield line pattern develops the effect of the hole is minimal. This is because the reinforcement usually is not cut off through the hole, it is simply shifted over. Thus the resisting moment of the sections close to the hole increases, making up for any loss of flexural strength due to the hole.

The equation for a localized compression failure is:

$$k_b = \frac{25}{[\ln(2.5s/c)]^{1.5}}$$

and was developed using finite element analysis [14]. Without doing further finite element study there is no way of knowing what the effect of holes on such an equation would be. It has been assumed that this constant is unaffected by the holes.

For partial yielding the constant k_t gives the point between k_{y1} and k_b at which the strength should be taken. This point is determined by the ratio:

$$\frac{M_n}{M_{bal}} = \frac{\text{nominal flexural resistance}}{\text{balanced resisting moment}} \quad (4.1)$$

Both of the above values are per unit width. The effect of the holes is to reduce M_{bal} .

Long gives M_{bal} as:

$$M_{bal} = 0.333 f'_c d^2$$

And states that it is based on the Whitney stress block. For sections with holes it is more convenient to use the total moments which are obtained by multiplying by $b = 4c$ in the case of M_n and by b' for M_{bal} .

Consider the reinforced concrete section of width b' shown in Figure 4.1.

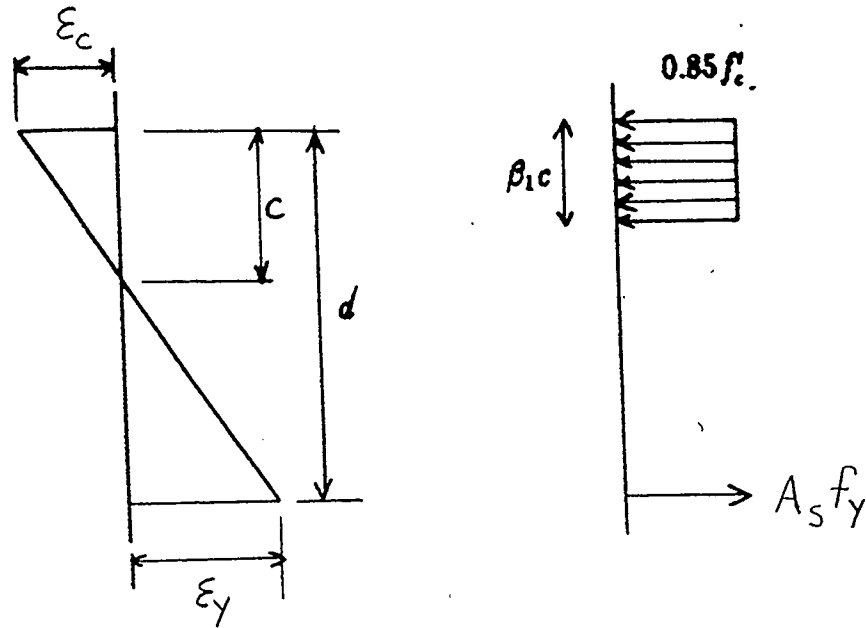


Figure 4.1: Stress and Strain Diagrams

Note that for the following three equations “ c ” is the depth to the neutral axis.

Assume: $\epsilon_y = 0.002$ and $\epsilon_c = -0.003$ (compression)

$$\text{Therefore: } \frac{c}{d} = \frac{-\epsilon_c}{-\epsilon_c + \epsilon_y} = \frac{0.003}{0.005} = 0.6$$

$$C = 0.85 f'_c \beta_1 c b' = 0.85 f'_c \beta_1 (0.6d) b'$$

M_{bal} is the balanced moment around the column periphery.

$$\begin{aligned} M_{bal} &= C \left(d - \frac{\beta_1 c}{2} \right) \\ &= 0.85 f'_c \beta_1 (0.6d) b' d \left(1 - \frac{\beta_1 0.6d}{2d} \right) \end{aligned}$$

Substituting:

$$M_{bal} = 0.51(1 - 0.3\beta_1)\beta_1 f'_c d^2 b' \quad (4.2)$$

M_{bal} is proportional to b' , the critical section at the column periphery, reduced by one of the methods introduced in the next section. The reduction of M_{bal} tends to drive k_t toward k_b (the constant for localized compression failure).

M_n is taken as the total nominal resisting moment over the length $b = 4c$. (Note that in this case c is the side length of the column.)

$$M_n = \rho f_y d^2 (1 - 0.59 \rho f_y / f'_c) 4c$$

4.2.2 Shear Punching Strength

Recall equation 2.31:

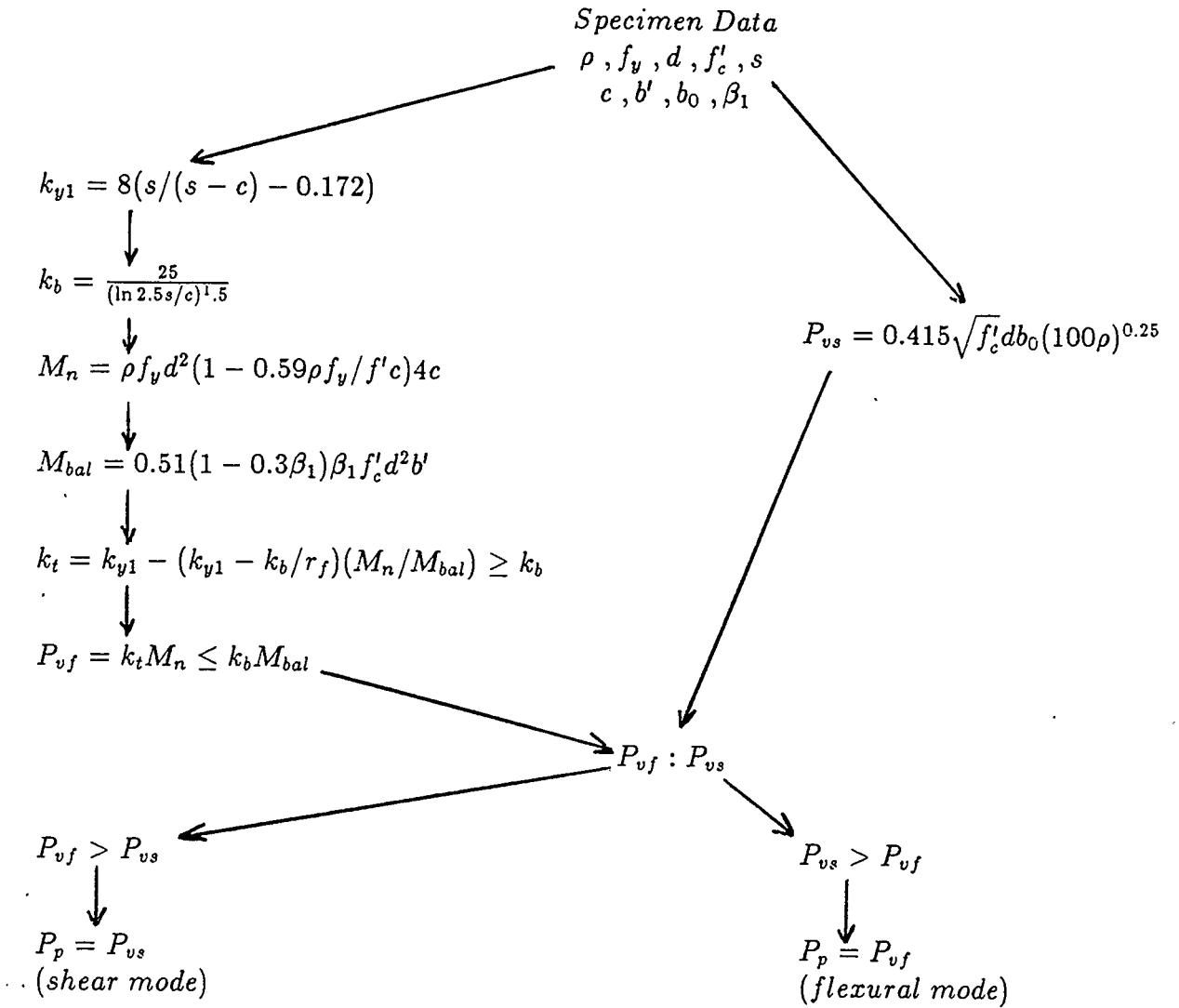
$$\begin{aligned} P_{vs} &= 1.66 \sqrt{f'_c} d (c + d) (100\rho)^{0.25} \\ &= 0.415 \sqrt{f'_c} d 4(c + d) (100\rho)^{0.25} \end{aligned}$$

The critical section is taken at $d/2$, thus $b_0 = 4(c + d)$ and the prediction equation for shear punching failure takes the form:

$$P_{vs} = 0.415 \sqrt{f'_c} d b_0 (100\rho)^{0.25} \quad (4.3)$$

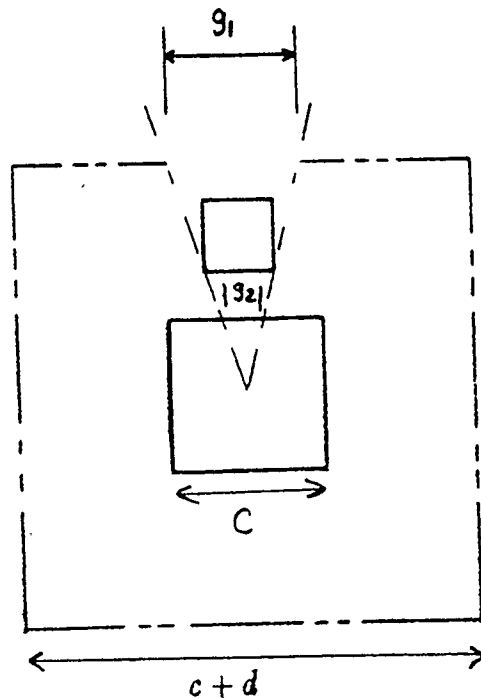
The method to reduce b_0 should be the same type that is used to reduce b' .

Figure 4.2 shows the method to determine P_p using the adapted model.



Note : $2.5s = L$

Figure 4.2: Method for Determining P_p Using Adapted Model



$$b_0 = 4(c + d) - g_1$$

$$b' = 4c - g_2$$

Figure 4.3: Radial Line Method

4.3 Methods for Reduction of b

Whether the critical section is at the column face or at $d/2$ the method of reduction of b should be the same. Three methods will be presented here and used for comparison later.

Radial Line Method

This is the method currently used by the Canadian design code [21]. Lines are drawn from the centre of the loaded area (the column) to points where these lines are tangent to the opening as shown in Figure 4.3.

Note that with this method, for a hole inside the critical section, the length that is ignored is wider than the hole itself. It is believed that this is one of the two basic flaws of this method. The other is that no matter how far the hole is

from the column, it is always required to have some effect on the shear strength. (Clause 11.10.6 of the Canadian design code [21] states that any hole within the column strip must be considered when calculating the punching shear strength.)

60 Degree Wedge Method

This is a new method, initially suggested by R.E. Loov that calls for two tangent lines to be drawn around the opening. These lines are subtended by a 60 degree angle as shown in Figure 4.4. As well, the lines stop at the tangent points and then continue back along the edge of the hole or straight back at 90 degrees to the column face.

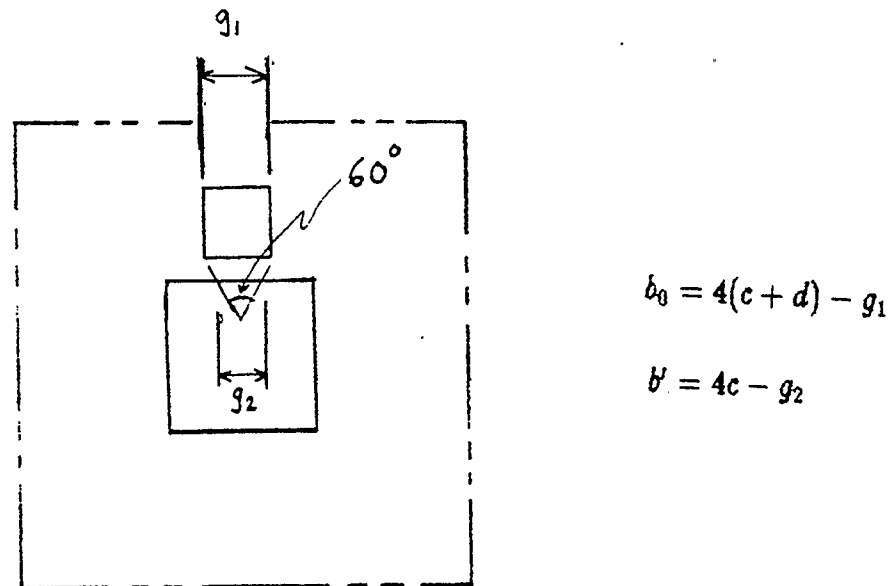


Figure 4.4: 60 Degree Wedge Method, Hole on Centreline

Normally the centreline of the wedge is drawn at right angles to the column face. However when a hole approaches the corner of a column the following guidelines apply.

Consider a corner of a column ABC of angle θ with line DE drawn bisecting

the angle shown in Figure 4.5.

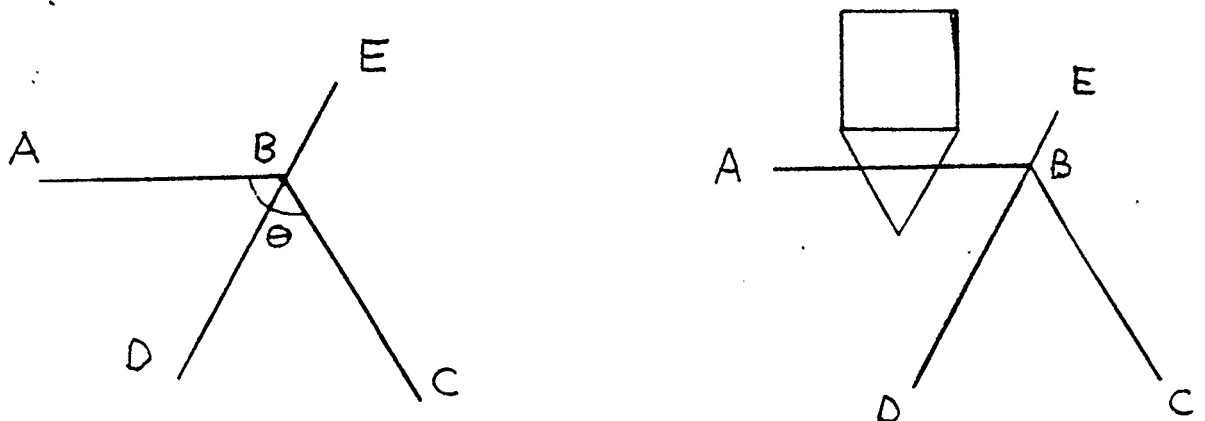


Figure 4.5: Arbitrary Column Corner

As the hole approaches the corner from the left the wedge is drawn at 90° to face AB. When the apex of the wedge contacts line DE the wedge is assumed to progressively swing around until it is 90° to face BC. From there it continues on at right angles to face BC as shown in Figure 4.6.

90 Degree Wedge Method

This method has the same guidelines as the 60 degree wedge method except that the angle subtended at the apex of the wedge is 90 degrees.

4.4 Comparison With Test Results

The comparisons are with test results obtained from Moe, Zaidi and Roll. All three used only square columns in these particular tests.

The hole patterns tested by Moe are shown in Figure 2.1. Hole layouts used by Zaidi and Roll can be determined by the labels of the corresponding test specimens.

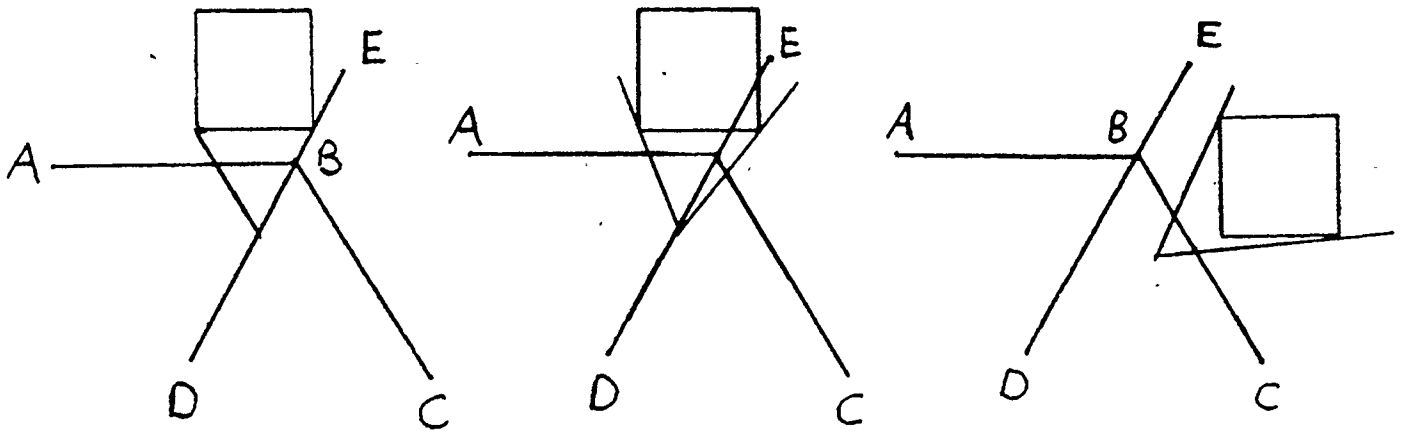


Figure 4.6: Reduction for Holes Near Column Corner

Zaidi and Roll both used the same scheme when labelling their slabs. Each label is made up as follows:

$$S - BCD - E - F - G$$

Where:

S= Square, the shape of the hole.

B= Type of hole layout, 1 indicating a hole on the centreline of the column, 2 indicating a hole off the corner of the column.

C= Size of the hole in inches.

D= The number of holes.

E= The type of reinforcement layout as shown in references [8] and/or [9].

F= Distance to the hole from the column in inches.

P_u/P_p Values						
	Radial Line		60 Wedge		90 Wedge	
Hole Pattern	Average	Variance	Average	Variance	Average	Variance
Centreline Symmetrical	1.48	0.03	1.26	0.03	1.26	0.03
Centreline Nonsymmetrical	1.26	0.02	1.21	0.02	1.21	0.02
Corner Symmetrical	2.08	0.39	1.65	0.16	1.20	0.05
Corner Nonsymmetrical	1.31	0.08	1.22	0.04	1.03	0.01

Table 4.1: Comparison of Various Methods for Hole Reduction, Using Adapted Prediction Equation

G = Number of the slab tested for each type.

Tables in Appendix B list the input data required for the adapted prediction equations for each of the categories. The predicted values (P_p) are compared to the test strengths (P_u) in each case. Table 4.1 shows the average value and variance of $\frac{P_u}{P_p}$ for each of the categories of hole patterns using the adapted prediction equations.

4.4.1 Results Using Adapted Equations

Long and Rankin [24] achieved an average $\frac{P_u}{P_p}$ value of 1.19 with a variance of 0.11 for slabs without holes. Table 4.1 shows that the radial line method is too

conservative for each category. By comparison the 60 and 90 degree wedge methods produce good results. Note that for holes on the centreline of the column the 60 and 90 degree methods are nearly the same. For the particular specimens examined, including the one shown in Figure 4.7, the angle at the apex of the wedge rarely made any difference. The advantage of the 90 degree method is most obvious for the corner-symmetric hole patterns. While this type of hole pattern is not likely to occur in practice it does provide some indication of the flaws in the radial line method.

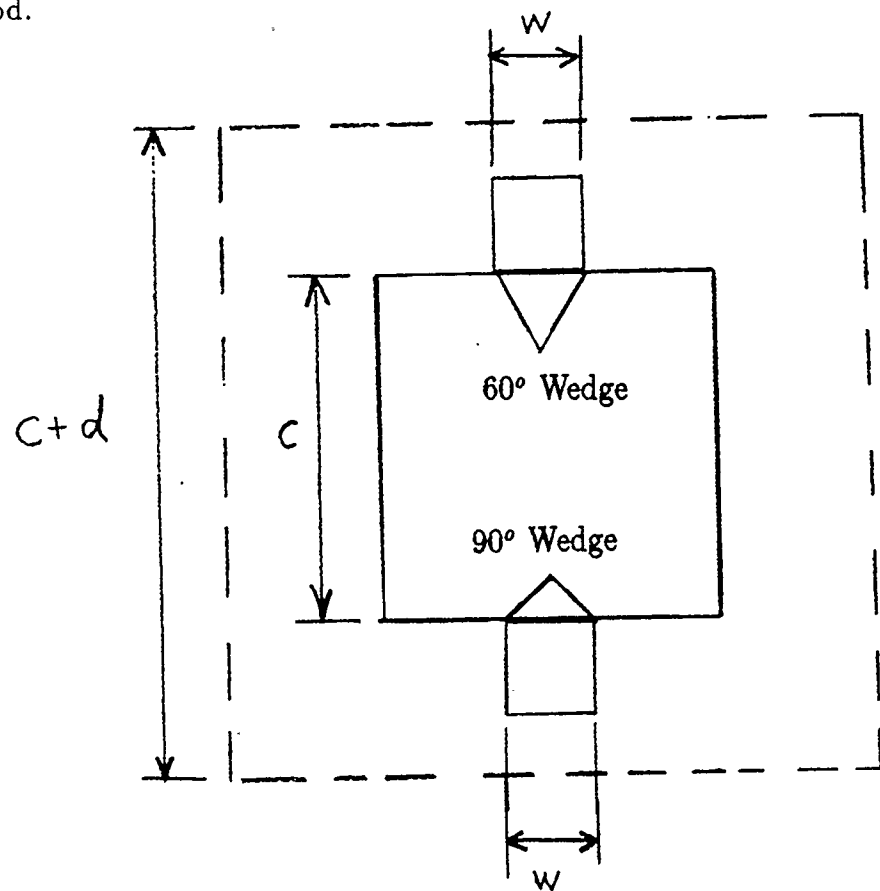


Figure 4.7: Typical Reduction of Centreline-Symmetrical Specimen

Comparisons were also made using the Canadian design code equation. This

P_u/P_p Values						
Hole Pattern	Radial Line		60 Wedge		90 Wedge	
	Average	Variance	Average	Variance	Average	Variance
Centreline Symmetrical	1.64	0.12	1.31	0.05	1.31	0.05
Centreline Nonsymmetrical	1.26	0.05	1.16	0.03	1.16	0.03
Corner Symmetrical	2.37	0.53	1.88	0.23	1.18	0.04
Corner Nonsymmetrical	1.50	0.15	1.38	0.09	1.15	0.05

Table 4.2: Comparison of Various Methods for Hole Reduction, Using Design Code Prediction Equation

equation uses only one b value, namely b_0 which is measured at $d/2$. Clause 11.10.6 of the code predicts the following capacity for square columns:

$$P_p = 0.4\phi_c\lambda\sqrt{f'_c}b_0d \quad (4.4)$$

In order to make comparisons to test results ϕ_c is set to 1.0 and $\lambda = 1.0$ (normal density concrete). Tables listing the parameters for the equation are included in the Appendix B. Table 4.2 gives a summary of the averages and variances for each category.

4.4.2 Results Using Code Equation

Once again the radial line method proves to be too conservative. If one hopes to achieve an average $\frac{P_u}{P_p}$ of 1.20 (to match the results obtained for solid slabs) then the correct method to use is the 90 degree wedge. In each of the categories the $\frac{P_u}{P_p}$ values for this method are close to 1.20 and the variances are small. Only for the centreline-symmetrical holes patterns is the average a little high. This category consisted of 10 specimens and two high results for Roll's B series [9] pushed the average up. This series had high values of ρ (2.53%).

Graphical Comparison of Results

Figures 4.9 and 4.10 show P_u/P_p values for the adapted equation, using the radial line and 90 degree wedge methods respectively. The points that are furthest above $P_u/P_p = 1.0$ in both cases are slabs with S-244-9-0-2 hole patterns shown in Figure 4.8 with 4 corner holes.

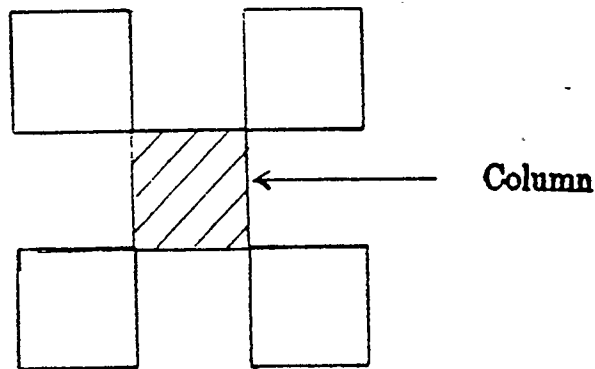


Figure 4.8: Worst Case Hole Pattern

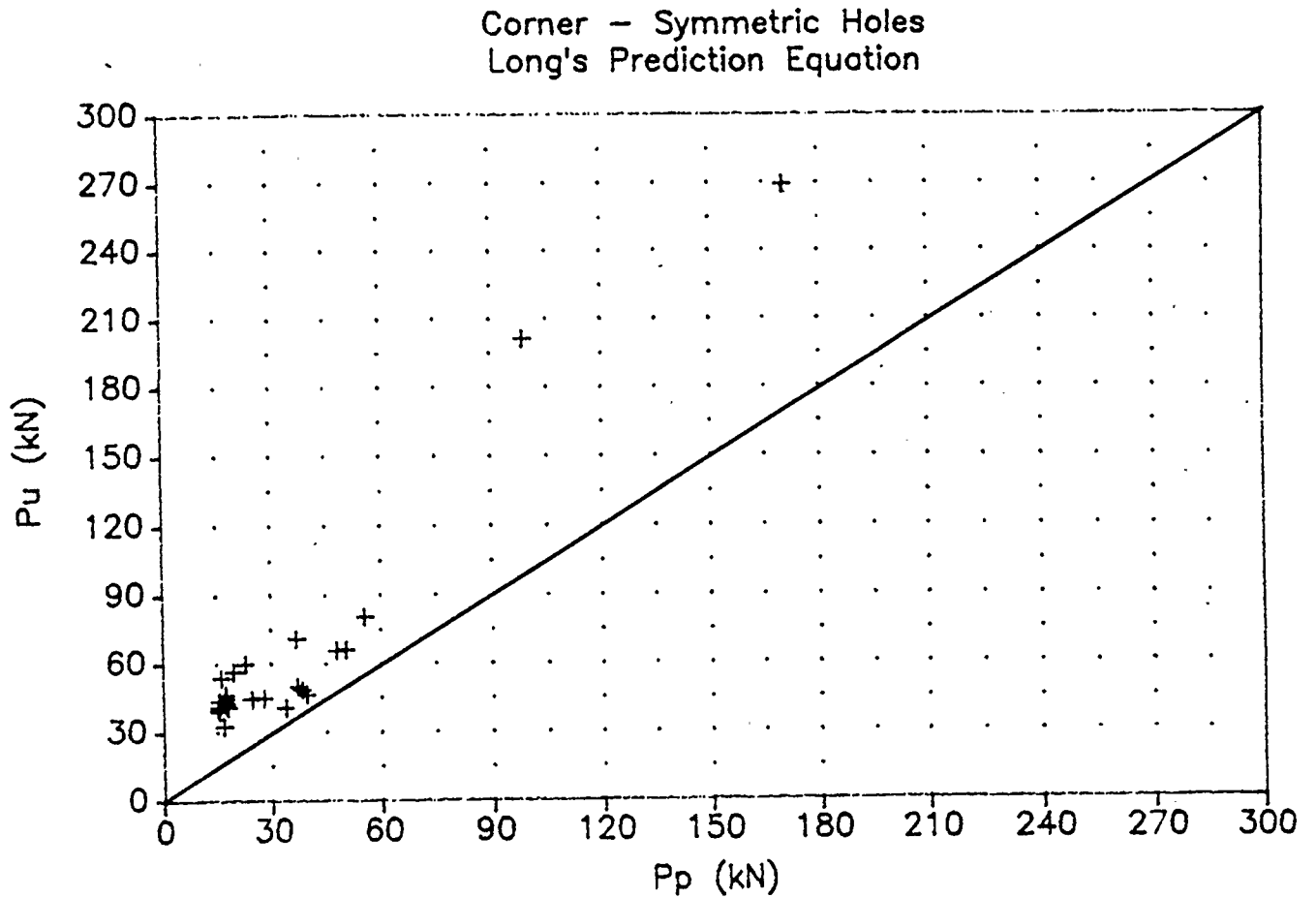


Figure 4.9: Corner - Symmetric, Radial Line Method, Using Adapted Equation

The graphs show that the 90 degree wedge method reduces the scatter of the data significantly.

Compare Figures 4.10 and 4.11. Both figures use the 90 degree wedge method, one with the adapted equation and the other with the code equation. The pattern of the data is changed because the code equation does not consider flexural punching failures.

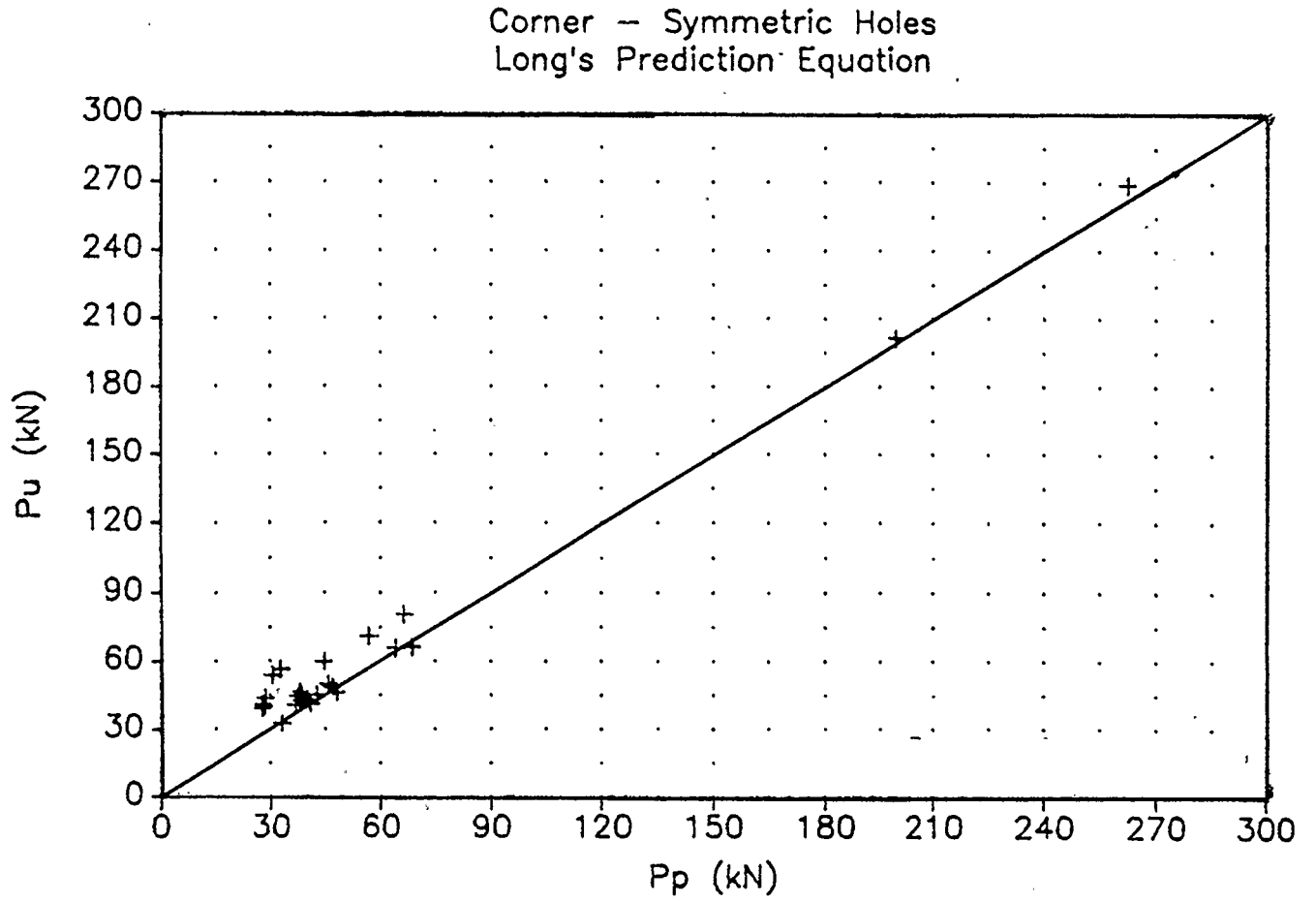


Figure 4.10: Corner - Symmetric, 90 Degree Wedge Method, Using Adapted Equation.

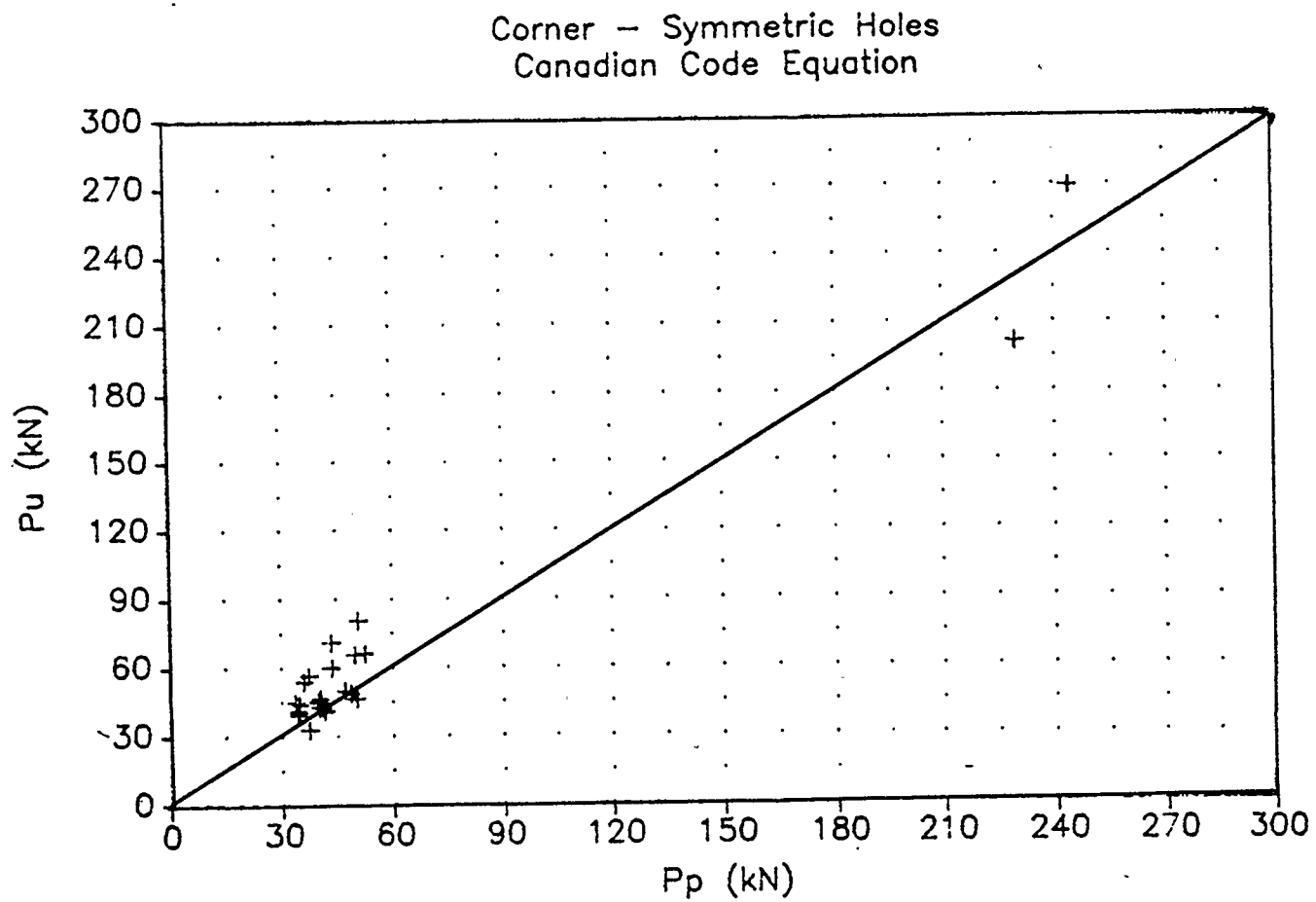


Figure 4.11: Corner - Symmetric, 90 Degree Wedge Method, Using Code Equation

4.5 Summary

A method was developed for adapting Rankin and Long's model to incorporate slabs with holes. The flexural punching strength equation is altered by reducing M_{bal} using the critical section b' . This critical section is reduced using one of the methods described in Section 4.3. The shear punching strength equation uses a critical section at $d/2$ from the column. This section, b_0 , should be reduced the same way as b' .

The results are tabulated so that comparisons can be made. Figures 4.8 to 4.10 compare the radial line method to the 90 degree wedge method and the adapted equation to the code equation.

Chapter 5

Summary and Conclusions

5.1 Restatement of Problem

Given an interior slab-column connection with a square column and equal spans in both directions:

1. What is the punching shear strength of the connection?
2. What are the effects of holes through the slab, close to the column, on that strength?

5.2 Summary

In examining these questions the following steps were taken:

Literature Review This is a review of of research done on slab-column connections both with and without holes.

Suitability of Laboratory Specimen A typical interior column was isolated at the centrelines between the columns. Because of symmetry only one quarter of the column and slab were considered. It was hoped that a finite element analysis would help determine the validity of the simply supported laboratory specimen.

Examination of Prediction Equations A model presented by Rankin and Long [24] is adapted to handle slabs with holes. Three methods of reducing the critical section are examined. The model is also compared to the equation currently used in the Canadian design code [21].

5.3 Conclusions

Literature Review

The investigators of slabs with holes have used many methods to reduce the critical section. None of these equations gives a reliable estimate of the punching strength.

The trend in the studies of slab-column connections with no holes was toward a two phase approach. Rankin and Long proposed a logical model [24] which they claim gives better results than other equations for slabs with no holes.

Suitability of Laboratory Specimen

The finite element analysis showed that the laboratory specimen may not be the correct shape and that there may be some problems with the assumed support conditions; however there were some problems with the finite element model. Because of this the results were not conclusive enough to reject the data obtained using the laboratory specimen.

Examination of Prediction Equations

Of the three methods outlined for reducing b the 90 degree wedge method proved to be the best. *It is recommended that this method replace the radial line method currently used in the Canadian design code.*

Comparison showed that the prediction equations proposed by Long and Rankin, adapted for slabs with holes, are better than the equation presently used by the Canadian design code because they provide a logical basis for punching shear.

Bibliography

- [1] Elstner, R.C., and Hognestad, E., (1956), "Shearing Strength of Reinforced Concrete Slabs", Journal of the American Concrete Institute (ACI Journal), Volume 53, July 1956, pp 29-58.
- [2] Moe, J., (1961), "Shearing Strength of Reinforced Concrete Slabs and Footings under Concentrated Loads", Portland Cement Association, Skokie, Illinois.
- [3] ACI-ASCE Committee 426, (1962), "Shear and Diagonal Tension", ACI Journal, Volume 59, March 1962, pp 353-396.
- [4] Hognestad, E., Elstner, R.C., and Hanson, J.A., (1964), "Shear Strength of Reinforced Structural Lightweight Aggregate Concrete Slabs", ACI Journal, Volume 61, June 1964, pp 643-655.
- [5] Yitzhaki, D., (1966), "Punching Strength of Reinforced Concrete Slabs". ACI Journal, Volume 63, May 1966, pp 527-540.
- [6] Blakey, F.A., (1966), "A Review of Some Studies of Slab-Column Junctions", Bulliten d'Information No. 58, Comité Européen du Béton, Paris, October 1966, pp51-66.
- [7] Mowrer, R.D., and Vanderbilt, M.D., (1967), "Shear Strength of Lightweight Aggregate Reinforced Concrete Flat Plates", ACI Journal, Volume 64, November 1967, pp 722-729.

- [8] Zaidi, S.T.H., (1968), "Shear Resistance of Perforated Reinforced Concrete Slabs", University of Pennsylvania, Ph.D. thesis.
- [9] Roll, F., Zaidi, S.T.H., Sabnis, G.M., Chuang, K., (1971), "Shear Resistance of Perforated Reinforced Concrete Slabs", ACI Special Publication 30, Cracking, Deflection and Ultimate Load of Concrete Slab Systems, Detroit, Michigan, pp 77-102.
- [10] Vanderbilt, M.D., (1972), "Shear Strength of Continuous Plates", ASCE Journal of the Structural Division, Volume 98, May 1972, pp 961-973.
- [11] Hawkins, N.M., Criswell, M.E., and Roll, F., (1974), "Shear Strength of Slabs Without Reinforcement", American Concrete Institute, Special Publication 42, Shear and Diagonal Tension, Detroit, Michigan, Volume 2, pp 677-720.
- [12] ACI-ASCE Committee 426, (1974), "The Shearing Strength of Reinforced Concrete Memembers - Slabs", ASCE Journal of the Structural Division, Volume 100, May-Aug 1974, pp 1543-1591.
- [13] Hawkins, N.M., and Criswell, M.E., (1974), "Shear Strength of Slabs: Basic Principle and their Relation to Current Methods of Analysis", American Concrete Institute, Special Publication 42, Shear and Diagonal Tension, Detroit, Michigan, Volume 2, pp 641-676.
- [14] Masterson, D.M., and Long, A.E., (1974), "The Punching Strength of Slabs, A Flexural Approach Using Finite Elements", American Concrete Institute, Special Publication 42, Shear and Diagonal Tension, Detroit, Michigan, Volume 2, pp 921-938.

- [15] Park, R., and Paulay, T., (1975), Reinforced Concrete Structures, Wiley and Sons, Toronto.
- [16] Long, A.E., (1975), "A Two Phase Approach to the Prediction of Punching Strength of Slabs", ACI Journal, Volume 72, February 1975, pp 37-45.
- [17] Meriam, J.L., (1978), Dynamics, Wiley and Sons, Toronto.
- [18] Ghali, A., and Neville, A.M., (1978), Structural Analysis, Chapman and Hall, London and New York.
- [19] Regan, P.E., (1981) Behavior of Reinforced Concrete Flat Slabs, Construction Industry Research and Information Association, London, 1981, Report 89.
- [20] Cope, R.J., and Clark, L.A., (1984), Concrete Slabs, Analysis and Design, Elsevier Applied Science Publishers, London and New York.
- [21] Canadian Standards Association, (1984), "Design of Concrete Structures for Buildings", Canadian Standards Association, CAN3-A23.3-M84, Toronto, Ontario.
- [22] Canadian Portland Cement Association, (1985), Concrete Design Handbook, Canadian Portland Cement Association, Ottawa, Ontario.
- [23] DeSalvo, G.J., and Swanson, J.A., (1985), ANSYS, Engineering Analysis System, Users Manual, Swanson Analysis Systems, Houston, Pennsylvania.

- [24] Rankin, G.I.B., and Long, A.E., (1987), "Predicting the Punching Strength of Conventional Slab-Column Specimens", Proceedings of the Institution of Civil Engineers, Part 1, Volume 87, April 1987, pp 327-346.

Appendix A

Design of Reinforcing Steel

The design was carried out following example 5.3 of the CPCA Concrete Design Handbook [22]. References in brackets refer to Design of Concrete Structures for Buildings (CAN3-A23.3-M84).

Problem

Design the slab reinforcement layout for a typical upper story floor in an office building.

Loadings

(Based on Table 1.13 of the CPCA handbook.)

Uniformly distributed live load: 2.4 kPa

Additional dead load, assume 1.3 kPa

Dimensions

Given:

- Columns spaced 4.5 *m* on centre.
- 0.150 *m* slab thickness.
- 0.3 × 0.3 *m* column dimensions.
- $f'_c = 25 \text{ MPa}$
- $f_y = 400 \text{ MPa}$

Factored Load

$$\text{Selfweight : } 2400(0.150)(9.81)/1000 = 3.53 \times 1.25 = 4.42 \text{ kPa}$$

$$\text{Additional dead : } 1.3 \times 1.25 = 1.63 \text{ kPa}$$

$$\text{Live load : } 2.4 \times 1.5 = 3.6 \text{ kPa}$$

Total unfactored load 7.23 kPa.

Total factored load 9.65 kPa.

Preliminary Shear Capacity

Assume #10 bars to be used. (Although the nominal diameter is 11.3 mm assume 10 mm for simplicity.)

$$\text{Therefore: } d = h - \text{bar} - \text{cover}$$

$$d = 150 - 10 - 20 = 120 \text{ mm}$$

$$c + d = 300 + 120 = 420 \text{ mm}$$

$$\begin{aligned} V_f &= w_f(l^2 - (c + d)^2) \\ &= 9.65(4.5^2 - 0.420^2) = 193.7 \text{ kN} \end{aligned}$$

$$\begin{aligned} V_r &= 0.4\phi_c\sqrt{f'_c}b_0d \\ &= 0.4(0.6)\sqrt{25}(4)(420)120 = 241 \text{ kN} \end{aligned}$$

$$\frac{V_r}{V_f} = 1.24$$

Preliminary shear check okay.

Design Moments

Column strip widths: $2(l_1/4) = 2.250 \text{ m}$ (13.2.1)

Middle strips: Remainder of strip.

Solution Using the Direct Design Method

Limitations (13.6.1)

All limitations satisfied.

Moments at critical sections: (13.6.2 & 13.6.3)

$$\begin{aligned}
 M_0 &= \frac{(w_f \times 10^{-3}) l_2 l_n^2}{8} \text{ N} \cdot \text{mm} & (13.3) \\
 &= \frac{(9.65 \times 10^{-3}) 4500 (4200)^2}{8} \\
 &= 95.8 \times 10^6 \text{ N} \cdot \text{mm}
 \end{aligned}$$

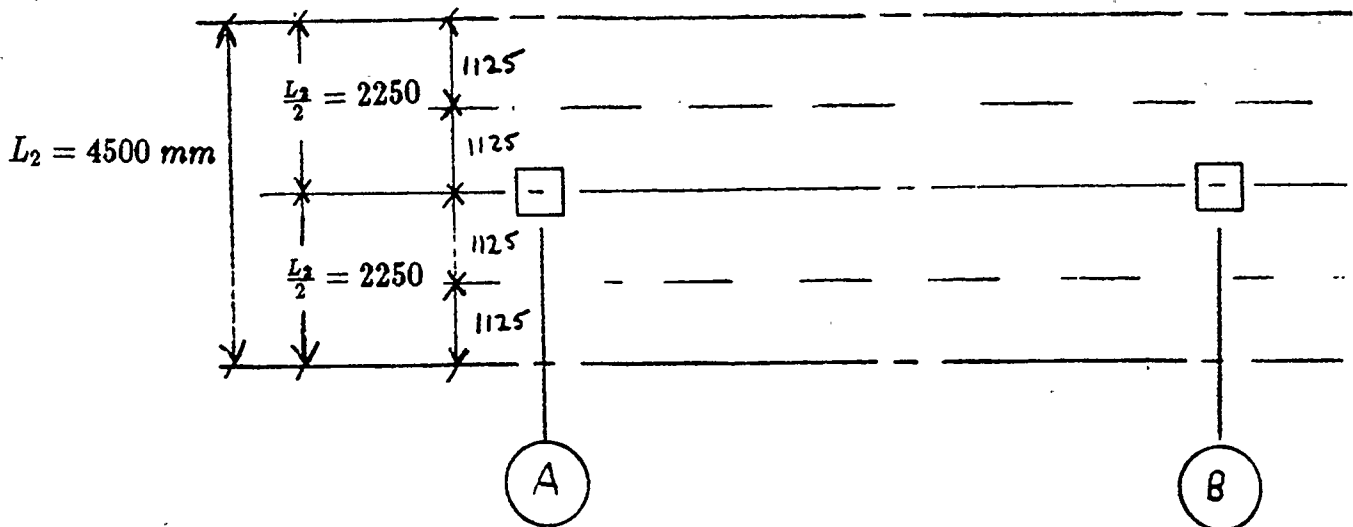


Figure A.1: Column and Middle Strips

	A		B		
$l_n (c = 300)$		4200			mm
M_0 (Eq. 13.3)		95.8			$\times 10^6 N \cdot mm$
% M_0 (13.6.3)	65	35	65		
M_{Des}	62.3	33.5	62.3		$\times 10^6 N \cdot mm$

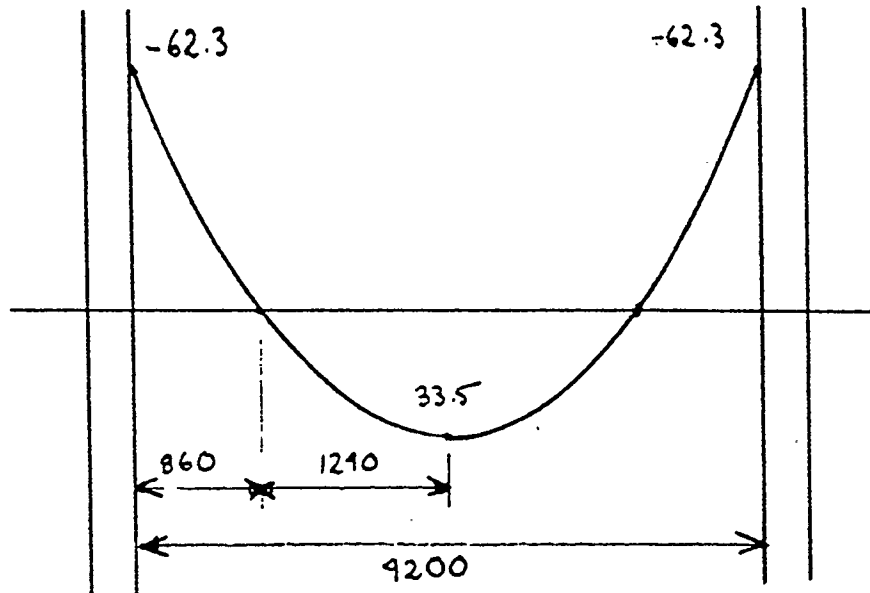


Figure A.2: Moments at Critical Sections

$$\beta_a = \frac{w_d}{w_l} \quad (\text{unfactored})$$

$$= \frac{3.53 + 1.3}{2.4} = 2.013 > 2.0 \quad (13.6.10)$$

No modification for pattern loading.

Column design moments at interior supports. (13.6.9, Eq. 13-4)

$$M_f = 0.07((w_{df} + 0.5w_{lf})l_2l_n^2 - w'_{df}l_2'(l'_n)^2)$$

$$= 0.07(0.5)(3.6)(4500)(4200)^2 = 10.0 \times 10^6 N \cdot mm$$

Choose Reinforcement

Assume #10 bars

$$d = 120 \text{ mm}$$

% of design moment that goes into column strip:

at interior supports, (13.6.4.1) 75%

at midspan, (13.6.4.4) 60%

At Interior Supports

$$M_f = 62.3(0.75) = 46.7 \times 10^6 \text{ N} \cdot \text{mm}$$

$$\text{Assume: } d - \frac{a}{2} = 0.9d = 108 \text{ mm}$$

$$A_s \approx \frac{M_f}{\phi_s f_y (d - \frac{a}{2})} = \frac{46.7}{0.85(400)(108)} = 1272 \text{ mm}^2$$

Try 14 #10 bars, $A_s = 1400 \text{ mm}^2$

$$\begin{aligned} M_r &= \phi_s f_y A_s \left(d - \frac{\phi_s f_y A_s}{\phi_c f_c' 1.7b} \right) \\ &= 0.85(400)(1400) \left(120 - \frac{0.85(400)(1400)}{0.6(25)(2250)(1.7)} \right) = 53.2 \times 10^6 \text{ N} \cdot \text{mm} \\ &> 46.7 \times 10^6 \text{ N} \cdot \text{mm} \end{aligned}$$

Use 14 #10 bars.

Interior Supports, Middle Strips

$$M_f = 0.25(62.3) = 15.6 \times 10^6 \text{ N} \cdot \text{mm}$$

$$A_s \approx \frac{15.6}{0.85(400)(108)} = 425 \text{ mm}^2$$

Try 6 #10 bars, $A_s = 600 \text{ mm}^2$

$$M_r = 0.85(400)(600)\left(120 - \frac{0.85(400)(600)}{0.6(25)(2250)1.7}\right)$$

$$= 23.7 \times 10^6 \text{ N} \cdot \text{mm} > 15.6$$

Check Spacing: $s = \frac{2250}{6} = 375 \text{ mm} > 2h = 300 \text{ mm}$, no good.

Need to use at least 8 #10 bars. $A_s = 800 \text{ mm}^2$

Positive Moment Reinforcement

Maximum spacing of 300 mm governs for both the column and middle strips.

Use #10 bars spaced at 300 mm.

Shear Moment Transfer

Because of symmetry the moments are balanced.

$$M_1 = M_2 = M_f = 0.07[0.5(3.6)(4800)(4500)^2] = 10.0 \times 10^6 \text{ N} \cdot \text{mm}$$

$$d_v = 120 \text{ mm}$$

$$k = \frac{1}{b_o d} = \frac{1}{4(300 + 120)(120)} = 4.96 \times 10^{-6}$$

$$\gamma_v = 1 - \frac{1}{1 + \frac{2}{3}\sqrt{\frac{420}{420}}} = 0.4$$

$$c' = \frac{c_1 + d}{2} = \frac{420}{2} = 210 \text{ mm}$$

$$J = \frac{(c_1 + d)d^3}{6} + \frac{(c_1 + d)^3 d}{6} + \frac{(c_1 + d)^2 (c_2 + d)d}{2}$$

$$= \frac{420(120)^3 + (420)^3(120) + 120(420)^3(3)}{6} = 6.048 \times 10^9$$

$$k_1 = \frac{\gamma_v c'}{J} = \frac{0.4(210)}{6.048 \times 10^9} = 13.9 \times 10^{-9}$$

$$V_f = w_f[(Total\ area) - (area\ within\ critical\ section)]$$

$$V_f = 9.65[4.5^2 - (300 + 120)^2] = 193700\ N$$

$$\begin{aligned} v_f &= V_f k + M_f k_1 = 193700(4.96 \times 10^{-6}) + 10.0 \times 10^6(13.9 \times 10^{-9}) \\ &= 1.10\ MPa \end{aligned}$$

$$v_r = 0.4\phi_c\lambda\sqrt{f'_c} = 0.4(0.6)\sqrt{25} = 1.2\ MPa > 1.10$$

Moment Transferred by Flexure (13.3.3)

$$\gamma_f = 0.6 \quad (c_1 = c_2)$$

$$\text{Moment transferred by flexure} = 0.6(10.0) = 6 \times 10^6\ N \cdot mm$$

$$\text{Effective transfer width} = c_2 + 3h = 300 + 450 = 750\ mm$$

$$A_s = \frac{6 \times 10^6}{0.85(400)(120)} = 148\ mm^2$$

$$(A_s)_{provided} = \frac{750}{2250}(1400) = 466\ mm^2$$

Space bars uniformly in the column strips.

N.B. The computer model assumes perfect bond between the steel and the concrete. Thus no development length is added in this case, all bars are cut off at some appropriate place. Because of symmetry, the steel in both the x and y directions is the same. The layout is shown in Figure A.2. The positive steel is placed between $x = 1200\ mm$ and $x = 2250\ mm$. The design called for the positive steel to begin at about 1050 mm. This error allowed for some flexural cracking to occur in the bottom of the slab, but only at the higher load levels. For the range considered (4.7 kPa to 11.9 kPa) no cracking occurred.

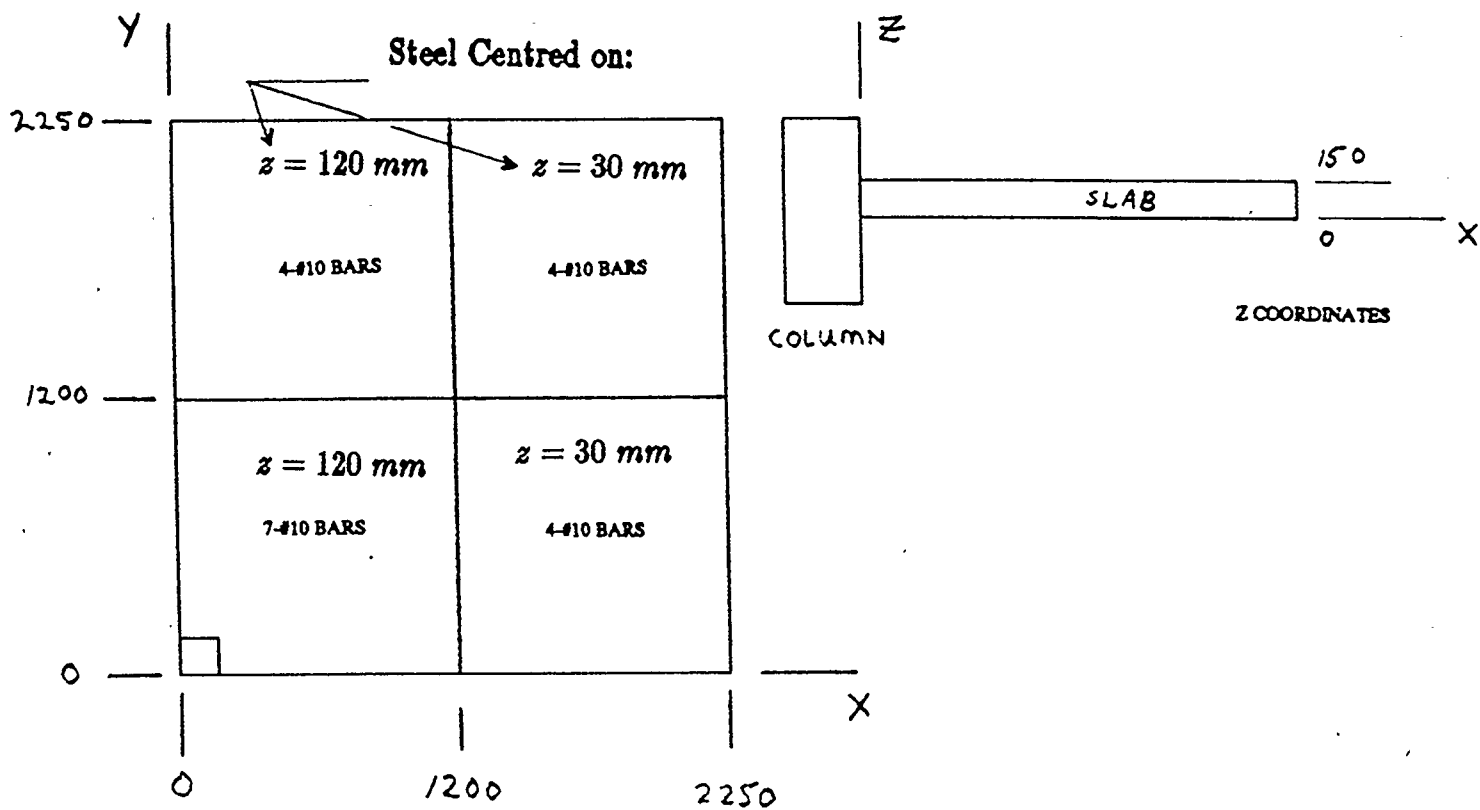


Figure A.3: Quarter Panel Reinforcing Steel, x Direction Only

Appendix B

Tables and Figures for Prediction Equations

SLAB	Hole patterns square - centreline - symmetrical												
	Series	f'c	bo	b'	b	d	rho	fy	s	c			
		MPa	in	mm	in	in	mm	%	ksi	MPa	mm	mm	
Radial Line		Reduction Method											
H3	Moe	23.7	41.0	1,041	30.0	40.0	114	1.15	47.5	328	1,829	254	
H6	Moe	28.4	26.0	660	20.0	40.0	114	1.15	47.5	328	1,829	254	
S-122-0-0-1	A-1	28.5	16.4	417	12.0	16.0	46	1.15	52.0	359	737	102	
	-2	A-1	27.0	16.4	417	12.0	16.0	46	1.15	52.0	359	737	102
S-124-0-0-1	A-1	28.0	10.4	264	8.0	16.0	46	1.15	52.0	359	737	102	
	-2	A-1	30.5	10.4	264	8.0	16.0	46	1.15	52.0	359	737	102
S-122-0-0-1	B	29.8	16.4	417	12.0	16.0	46	2.53	63.2	436	737	102	
S-124-0-0-1	B	30.2	10.4	264	8.0	16.0	46	2.53	53.9	372	737	102	
S-122-0-0-1	A-2	29.8	16.4	417	12.0	16.0	39	1.34	36.4	251	737	102	
S-124-0-0-1	A-2	29.3	10.4	264	8.0	16.0	39	1.34	36.4	251	737	102	

60 Degree Cone		Reduction Method											
H3	Moe	23.7	46.0	1,168	30.0	40.0	114	1.15	47.5	328	1,829	254	
H6	Moe	28.4	36.0	914	20.0	40.0	114	1.15	47.5	328	1,829	254	
S-122-0-0-1	A-1	28.5	18.4	467	12.0	16.0	46	1.15	52.0	359	737	102	
	-2	A-1	27.0	18.4	467	12.0	16.0	46	1.15	52.0	359	737	102
S-124-0-0-1	A-1	28.0	14.4	366	8.0	16.0	46	1.15	52.0	359	737	102	
	-2	A-1	30.5	14.4	366	8.0	16.0	46	1.15	52.0	359	737	102
S-122-0-0-1	B	29.8	18.4	467	12.0	16.0	46	2.53	63.2	436	737	102	
S-124-0-0-1	B	30.2	14.4	366	8.0	16.0	46	2.53	53.9	372	737	102	
S-122-0-0-1	A-2	29.8	18.4	467	12.0	16.0	39	1.34	36.4	251	737	102	
S-124-0-0-1	A-2	29.3	14.4	366	8.0	16.0	39	1.34	36.4	251	737	102	

90 Degree Cone		Reduction Method											
H3	Moe	23.7	46.0	1,168	30.0	40.0	114	1.15	47.5	328	1,829	254	
H6	Moe	28.4	36.0	914	20.0	40.0	114	1.15	47.5	328	1,829	254	
S-122-0-0-1	A-1	28.5	18.4	467	12.0	16.0	46	1.15	52.0	359	737	102	
	-2	A-1	27.0	18.4	467	12.0	16.0	46	1.15	52.0	359	737	102
S-124-0-0-1	A-1	28.0	14.4	366	8.0	16.0	46	1.15	52.0	359	737	102	
	-2	A-1	30.5	14.4	366	8.0	16.0	46	1.15	52.0	359	737	102
S-122-0-0-1	B	29.8	18.4	467	12.0	16.0	46	2.53	63.2	436	737	102	
S-124-0-0-1	B	30.2	14.4	366	8.0	16.0	46	2.53	53.9	372	737	102	
S-122-0-0-1	A-2	29.8	18.4	467	12.0	16.0	39	1.34	36.4	251	737	102	
S-124-0-0-1	A-2	29.3	14.4	366	8.0	16.0	39	1.34	36.4	251	737	102	

Table B.1: Centreline - Symmetric Holes, Input Data

square - centreline - symmetrical
 SLAB ky1 kb Mb Mbal kt1 kt

kN m/m kN m/m

Radial Line

H3	7.91	5.09	44.3	74.4	5.83	5.83
H6	7.91	5.09	45.1	59.6	5.27	5.27
S-122-0-0-1	7.91	5.08	8.0	14.6	6.00	6.00
-2	7.91	5.08	7.9	13.8	5.91	5.91
S-124-0-0-1	7.91	5.08	8.0	9.6	5.00	5.08
-2	7.91	5.08	8.0	10.4	5.22	5.22
S-122-0-0-1	7.91	5.08	18.2	15.3	3.74	5.08
S-124-0-0-1	7.91	5.08	16.2	10.3	2.41	5.08
S-122-0-0-1	7.91	5.08	4.8	11.0	6.39	6.39
S-124-0-0-1	7.91	5.08	4.8	7.2	5.59	5.59

60 Degree Co

H3	7.91	5.09	44.3	74.4	5.83	5.83
H6	7.91	5.09	45.1	59.6	5.27	5.27
S-122-0-0-1	7.91	5.08	8.0	14.6	6.00	6.00
-2	7.91	5.08	7.9	13.8	5.91	5.91
S-124-0-0-1	7.91	5.08	8.0	9.6	5.00	5.08
-2	7.91	5.08	8.0	10.4	5.22	5.22
S-122-0-0-1	7.91	5.08	18.2	15.3	3.74	5.08
S-124-0-0-1	7.91	5.08	16.2	10.3	2.41	5.08
S-122-0-0-1	7.91	5.08	4.8	11.0	6.39	6.39
S-124-0-0-1	7.91	5.08	4.8	7.2	5.59	5.59

90 Degree Co

H3	7.91	5.09	44.3	74.4	5.83	5.83
H6	7.91	5.09	45.1	59.6	5.27	5.27
S-122-0-0-1	7.91	5.08	8.0	14.6	6.00	6.00
-2	7.91	5.08	7.9	13.8	5.91	5.91
S-124-0-0-1	7.91	5.08	8.0	9.6	5.00	5.08
-2	7.91	5.08	8.0	10.4	5.22	5.22
S-122-0-0-1	7.91	5.08	18.2	15.3	3.74	5.08
S-124-0-0-1	7.91	5.08	16.2	10.3	2.41	5.08
S-122-0-0-1	7.91	5.08	4.8	11.0	6.39	6.39
S-124-0-0-1	7.91	5.08	4.8	7.2	5.59	5.59

Table B.2: Centreline - Symmetric Holes, Constants

SLAB	square - centreline - symmetrical					Pu	Pu/Pp
	Pvf1	Pvf2	Pvf	Pvs	Pp		
	kN	kN	kN	kN	kN		
Radial Line							
H3	258.77	329.3	258.8	248.1	248.1	325.0	1.31
H6	237.90	263.7	237.9	172.5	172.5	246.0	1.43
S-122-0-0-1	47.88	64.5	47.9	44.0	44.0	59.6	1.36
-2	46.88	61.1	46.9	42.8	42.8	53.8	1.26
S-124-0-0-1	40.46	42.2	40.5	27.6	27.6	40.0	1.45
-2	41.89	46.0	41.9	28.8	28.8	45.8	1.59
S-122-0-0-1	92.60	67.4	67.4	54.7	54.7	75.3	1.38
S-124-0-0-1	82.47	45.6	45.6	35.0	35.0	67.4	1.93
S-122-0-0-1	30.51	48.5	30.5	39.6	30.5	44.5	1.46
S-124-0-0-1	26.68	31.8	26.7	24.9	24.9	40.9	1.64
Average							1.48
Std. Dev.							0.19
Variance							0.03
60 Degree Co							
H3	258.77	329.3	258.8	278.4	258.8	325.0	1.26
H6	237.90	263.7	237.9	238.8	237.9	246.0	1.03
S-122-0-0-1	47.88	64.5	47.9	49.3	47.9	59.6	1.24
-2	46.88	61.1	46.9	48.0	46.9	53.8	1.15
S-124-0-0-1	40.46	42.2	40.5	38.3	38.3	40.0	1.05
-2	41.89	46.0	41.9	39.9	39.9	45.8	1.15
S-122-0-0-1	92.60	67.4	67.4	61.4	61.4	75.3	1.23
S-124-0-0-1	82.47	45.6	45.6	48.4	45.6	67.4	1.48
S-122-0-0-1	30.51	48.5	30.5	44.4	30.5	44.5	1.46
S-124-0-0-1	26.68	31.8	26.7	34.5	26.7	40.9	1.53
Average							1.26
Std. Dev.							0.17
Variance							0.03
90 Degree Co							
H3	258.77	329.3	258.8	278.4	258.8	325.0	1.26
H6	237.90	263.7	237.9	238.8	237.9	246.0	1.03
S-122-0-0-1	47.88	64.5	47.9	49.3	47.9	59.6	1.24
-2	46.88	61.1	46.9	48.0	46.9	53.8	1.15
S-124-0-0-1	40.46	42.2	40.5	38.3	38.3	40.0	1.05
-2	41.89	46.0	41.9	39.9	39.9	45.8	1.15
S-122-0-0-1	92.60	67.4	67.4	61.4	61.4	75.3	1.23
S-124-0-0-1	82.47	45.6	45.6	48.4	45.6	67.4	1.48
S-122-0-0-1	30.51	48.5	30.5	44.4	30.5	44.5	1.46
S-124-0-0-1	26.68	31.8	26.7	34.5	26.7	40.9	1.53
Average							1.26
Std. Dev.							0.17
Variance							0.03

Table B.3: Centreline - Symmetric Holes, Predicted Values

SLAB	Hole patterns square - centreline - nonsymmetrical												
	Series	f'c	f'c	bo	b'	b	d	rho	fy	s	c		
		psi	MPa	in	mm	in	in	mm	%	ksi	MPa	mm	mm
Radial Line	Reduction Method												
H2	Moe	3620	25.0	48.5	1,232	35.0	40.0	114	1.15	50.0	345	1,829	254
H4	Moe	3730	25.7	41.0	1,041	30.0	40.0	114	1.15	52.0	359	1,829	254
H5	Moe	3620	25.0	33.5	851	25.0	40.0	114	1.15	51.0	352	1,829	254
H9	Moe	3490	24.1	50.7	1,288	36.2	40.0	114	1.15	50.0	345	1,829	254
H10	Moe	3620	25.0	51.9	1,318	37.2	40.0	114	1.15	50.0	345	1,829	254
H11	Moe	3780	26.1	52.6	1,336	37.7	40.0	114	1.15	50.0	345	1,829	254
H14	Moe	3800	26.2	48.5	1,232	35.0	40.0	114	1.15	40.0	276	1,829	254
H15	Moe	3390	23.4	48.5	1,232	35.0	40.0	114	1.15	45.0	310	1,829	254
S-121-0-0-1	A-1	4140	28.5	19.4	493	14.0	16.0	46	1.15	52.0	359	737	102
-2	A-1	3920	27.0	19.4	493	14.0	16.0	46	1.15	52.0	359	737	102
S-122-0-0-1a	A-1	4070	28.1	16.4	417	12.0	16.0	46	1.15	52.0	359	737	102
-2a	A-1	3770	26.0	16.4	417	12.0	16.0	46	1.15	52.0	359	737	102
S-123-0-0-1	A-1	4060	28.0	13.4	340	10.0	16.0	46	1.15	52.0	359	737	102
-2	A-1	4420	30.5	13.4	340	10.0	16.0	46	1.15	52.0	359	737	102
S-121-1-0.9-	A-1	4090	28.2	21.2	538	14.6	16.0	46	1.15	52.0	359	737	102
-2-1.8-	A-1	4260	29.4	21.7	551	15.0	16.0	46	1.15	52.0	359	737	102
-3-2.7-	A-1	4910	33.9	21.9	556	15.1	16.0	46	1.15	52.0	359	737	102
-4-3.6-	A-1	4910	33.9	22.2	564	15.3	16.0	46	1.15	52.0	359	737	102
-5-4.5-	A-1	4540	31.3	22.3	566	15.4	16.0	46	1.15	52.0	359	737	102
-6-5.4-	A-1	4220	29.1	22.5	572	15.5	16.0	46	1.15	52.0	359	737	102
S-121-0-0-1	B	4550	31.4	19.4	493	14.0	16.0	46	2.53	53.3	367	737	102
-2	B	4240	29.2	19.4	493	14.0	16.0	46	2.53	54.3	374	737	102
S-122-0-0-1a	B	4380	30.2	16.4	417	12.0	16.0	46	2.53	51.9	358	737	102
S-123-0-0-1	B	4240	29.2	13.4	340	10.0	16.0	46	2.53	54.1	373	737	102
S-121-0-0-1	A-2	4160	28.7	19.4	493	14.0	16.0	39	1.34	36.4	251	737	102
S-122-0-0-1a	A-2	3770	26.0	16.4	417	12.0	16.0	39	1.34	52.0	359	737	102
S-123-0-0-1	A-2	4250	29.3	13.4	340	10.0	16.0	39	1.34	52.0	359	737	102
S-121-1-0.9-	A-2	3740	25.8	21.2	538	14.6	16.0	39	1.34	52.0	359	737	102
-2-1.8-	A-2	3740	25.8	21.7	551	15.0	16.0	39	1.34	52.0	359	737	102
-3-2.7-	A-2	4250	29.3	21.9	556	15.1	16.0	39	1.34	52.0	359	737	102
-3-2.7-	A-2	4310	29.7	21.9	556	15.1	16.0	39	1.34	52.0	359	737	102
-3-2.7-	A-2	3910	27.0	21.9	556	15.1	16.0	39	1.34	52.0	359	737	102
-4-3.6-	A-2	4250	29.3	22.2	564	15.3	16.0	39	1.34	52.0	359	737	102
-5-4.5-	A-2	4980	34.3	22.3	566	15.4	16.0	39	1.34	52.0	359	737	102
-6-5.4-	A-2	4980	34.3	22.5	572	15.5	16.0	39	1.34	52.0	359	737	102

Table B.4: Centreline - Nonsymmetric Holes, Input Data, Radial Line Method

square - centreline - nonsymmetrical
 SLAB ky1 kb Mb Mbal kt1 kt

kN m/m kN m/m

Radial Line

H2	7.91	5.09	46.7	91.7	6.14	6.14
H4	7.91	5.09	48.5	81.0	5.82	5.82
H5	7.91	5.09	47.5	65.5	5.38	5.38
H9	7.91	5.09	46.5	91.4	6.14	6.14
H10	7.91	5.09	46.7	97.4	6.24	6.24
H11	7.91	5.09	46.9	103.1	6.33	6.33
H14	7.91	5.09	38.3	96.2	6.53	6.53
H15	7.91	5.09	42.2	85.8	6.20	6.20
S-121-0-0-1	7.91	5.08	8.0	17.1	6.28	6.28
-2	7.91	5.08	7.9	16.2	6.19	6.19
S-122-0-0-1a	7.91	5.08	8.0	14.4	5.97	5.97
-2a	7.91	5.08	7.9	13.3	5.84	5.84
S-123-0-0-1	7.91	5.08	8.0	12.0	5.58	5.58
-2	7.91	5.08	8.0	13.0	5.75	5.75
S-121-1-0.9-	7.91	5.08	8.0	17.6	6.33	6.33
-2-1.8-	7.91	5.08	8.0	18.8	6.42	6.42
-3-2.7-	7.91	5.08	8.1	21.8	6.61	6.61
-4-3.6-	7.91	5.08	8.1	22.1	6.63	6.63
-5-4.5-	7.91	5.08	8.0	20.6	6.54	6.54
-6-5.4-	7.91	5.08	8.0	19.3	6.46	6.46
S-121-0-0-1	7.91	5.08	16.2	18.8	4.89	5.08
-2	7.91	5.08	16.2	17.5	4.67	5.08
S-122-0-0-1a	7.91	5.08	15.8	15.5	4.35	5.08
S-123-0-0-1	7.91	5.08	16.2	12.5	3.39	5.08
S-121-0-0-1	7.91	5.08	4.8	12.3	6.56	6.56
S-122-0-0-1a	7.91	5.08	6.5	9.6	5.53	5.53
S-123-0-0-1	7.91	5.08	6.6	9.0	5.35	5.35
S-121-1-0.9-	7.91	5.08	6.5	11.6	5.94	5.94
-2-1.8-	7.91	5.08	6.5	11.9	6.00	6.00
-3-2.7-	7.91	5.08	6.6	13.6	6.21	6.21
-3-2.7-	7.91	5.08	6.6	13.8	6.23	6.23
-3-2.7-	7.91	5.08	6.5	12.5	6.08	6.08
-4-3.6-	7.91	5.08	6.6	13.8	6.23	6.23
-5-4.5-	7.91	5.08	6.7	16.2	6.47	6.47
-6-5.4-	7.91	5.08	6.7	16.3	6.48	6.48

Table B.5: Centreline - Nonsymmetric Holes, Constants, Radial Line Method

SLAB	square - centreline - nonsymmetrical						Fu	Fu/Pp
	Fvf1	Fvf2	Fvf	Fvs	Fp			
	kN	kN	kN	kN	kN	kN		
Radial Line								
H2	286.52	405.5	286.5	301.5	286.5	329.2	1.15	
H4	282.47	358.1	282.5	258.7	258.7	289.6	1.12	
H5	255.72	289.6	255.7	208.3	208.3	249.5	1.20	
H9	285.50	404.3	285.5	309.5	285.5	347.4	1.22	
H10	291.43	431.0	291.4	322.7	291.4	351.4	1.21	
H11	296.70	456.1	296.7	334.2	296.7	356.7	1.20	
H14	249.77	425.7	249.8	308.9	249.8	252.6	1.01	
H15	261.54	379.7	261.5	291.8	261.5	344.7	1.32	
S-121-0-0-1	50.09	75.4	50.1	52.0	50.1	64.5	1.29	
-2	49.17	71.4	49.2	50.6	49.2	56.9	1.16	
S-122-0-0-1a	47.60	63.5	47.6	43.6	43.6	41.4	0.95	
-2a	46.15	58.8	46.1	42.0	42.0	53.4	1.27	
S-123-0-0-1	44.46	52.8	44.5	35.6	35.6	44.9	1.26	
-2	46.20	57.5	46.2	37.1	37.1	51.6	1.39	
S-121-1-0.9-	50.43	77.7	50.4	56.5	50.4	61.4	1.22	
-2-1.8-	51.40	83.1	51.4	59.1	51.4	60.0	1.17	
-3-2.7-	53.33	96.4	53.6	64.0	53.6	69.8	1.30	
-4-3.6-	53.69	97.7	53.7	64.9	53.7	69.4	1.29	
-5-4.5-	52.65	90.9	52.7	62.6	52.7	64.9	1.23	
-6-5.4-	51.64	85.1	51.6	60.9	51.6	63.6	1.23	
S-121-0-0-1	82.44	82.8	82.4	66.4	66.4	71.2	1.07	
-2	82.32	77.2	77.2	64.1	64.1	78.7	1.23	
S-122-0-0-1a	80.08	68.3	68.3	55.1	55.1	73.8	1.34	
S-123-0-0-1	82.09	55.1	55.1	44.3	44.3	72.1	1.63	
S-121-0-0-1	31.23	54.4	31.2	46.0	31.2	51.2	1.64	
S-122-0-0-1a	36.03	42.3	36.0	37.0	36.0	43.6	1.21	
S-123-0-0-1	35.29	39.7	35.3	32.1	32.1	43.6	1.36	
S-121-1-0.9-	38.66	51.0	38.7	47.6	38.7	50.7	1.31	
-2-1.8-	39.00	52.4	39.0	48.7	39.0	52.5	1.35	
-3-2.7-	41.00	60.0	41.0	52.4	41.0	46.7	1.14	
-3-2.7-	41.20	60.8	41.2	52.8	41.2	58.7	1.43	
-3-2.7-	39.77	55.2	39.8	50.3	39.8	50.3	1.26	
-4-3.6-	41.15	60.8	41.1	53.2	41.1	55.6	1.35	
-5-4.5-	43.35	71.7	43.4	57.8	43.4	58.3	1.34	
-6-5.4-	43.41	72.2	43.4	58.3	43.4	59.2	1.36	
Average							1.26	
Variance							0.02	

Table B.6: Centreline - Nonsymmetric Holes, Predicted Values, Radial Line Method

SLAB	Hole patterns square - centreline - nonsymmetrical												
	Series	f'c	f'c	bo	b'	b	d	rho	fy	s	c		
		psi	MPa	in	mm	in	in	mm	%	ksi	MPa	mm	mm
60 Degree Cone Reduction Method													
H2	Moe	3620	25.0	51.0	1,295	35.0	40.0	114	1.15	50.0	345	1,829	254
H4	Moe	3730	25.7	46.0	1,168	30.0	40.0	114	1.15	52.0	359	1,829	254
H5	Moe	3620	25.0	41.0	1,041	25.0	40.0	114	1.15	51.0	352	1,829	254
H9	Moe	3490	24.1	51.0	1,295	37.2	40.0	114	1.15	50.0	345	1,829	254
H10	Moe	3620	25.0	52.9	1,344	39.5	40.0	114	1.15	50.0	345	1,829	254
H11	Moe	3780	26.1	55.2	1,402	40.0	40.0	114	1.15	50.0	345	1,829	254
H14	Moe	3800	26.2	51.0	1,295	35.0	40.0	114	1.15	40.0	276	1,829	254
H15	Moe	3390	23.4	51.0	1,295	35.0	40.0	114	1.15	45.0	310	1,829	254
S-121-0-0-1	A-1	4140	28.5	20.4	518	14.0	16.0	46	1.15	52.0	359	737	102
-2	A-1	3920	27.0	20.4	518	14.0	16.0	46	1.15	52.0	359	737	102
S-122-0-0-1a	A-1	4070	28.1	18.4	467	12.0	16.0	46	1.15	52.0	359	737	102
-2a	A-1	3770	26.0	18.4	467	12.0	16.0	46	1.15	52.0	359	737	102
S-123-0-0-1	A-1	4060	28.0	16.4	417	10.0	16.0	46	1.15	52.0	359	737	102
-2	A-1	4420	30.5	16.4	417	10.0	16.0	46	1.15	52.0	359	737	102
S-121-1-0.9-	A-1	4090	28.2	21.2	538	15.0	16.0	46	1.15	52.0	359	737	102
-2-1.8-	A-1	4260	29.4	22.2	564	16.0	16.0	46	1.15	52.0	359	737	102
-3-2.7-	A-1	4910	33.9	23.2	589	16.0	16.0	46	1.15	52.0	359	737	102
-4-3.6-	A-1	4910	33.9	23.2	589	16.0	16.0	46	1.15	52.0	359	737	102
-5-4.5-	A-1	4540	31.3	23.2	589	16.0	16.0	46	1.15	52.0	359	737	102
-6-5.4-	A-1	4220	29.1	23.2	589	16.0	16.0	46	1.15	52.0	359	737	102
S-121-0-0-1	B	4550	31.4	20.4	518	14.0	16.0	46	2.53	53.3	367	737	102
-2	B	4240	29.2	20.4	518	14.0	16.0	46	2.53	54.3	374	737	102
S-122-0-0-1a	B	4380	30.2	18.4	467	12.0	16.0	46	2.53	51.9	358	737	102
S-123-0-0-1	B	4240	29.2	16.4	417	10.0	16.0	46	2.53	54.1	373	737	102
S-121-0-0-1	A-2	4160	28.7	20.4	518	14.0	16.0	39	1.34	36.4	251	737	102
S-122-0-0-1a	A-2	3770	26.0	18.4	467	12.0	16.0	39	1.34	52.0	359	737	102
S-123-0-0-1	A-2	4250	29.3	16.4	417	10.0	16.0	39	1.34	52.0	359	737	102
S-121-1-0.9-	A-2	3740	25.8	21.2	538	15.0	16.0	39	1.34	52.0	359	737	102
-2-1.8-	A-2	3740	25.8	22.2	564	16.0	16.0	39	1.34	52.0	359	737	102
-3-2.7-	A-2	4250	29.3	23.2	589	16.0	16.0	39	1.34	52.0	359	737	102
-3-2.7-	A-2	4310	29.7	23.2	589	16.0	16.0	39	1.34	52.0	359	737	102
-3-2.7-	A-2	3910	27.0	23.2	589	16.0	16.0	39	1.34	52.0	359	737	102
-4-3.6-	A-2	4250	29.3	23.2	589	16.0	16.0	39	1.34	52.0	359	737	102
-5-4.5-	A-2	4980	34.3	23.2	589	16.0	16.0	39	1.34	52.0	359	737	102
-6-5.4-	A-2	4980	34.3	23.2	589	16.0	16.0	39	1.34	52.0	359	737	102

Table B.7: Centreline - Nonsymmetric Holes, Input Data, 60 Degree Method

SLAB	square		- centreline		- nonsymmetrical	
	ky1	kb	Mb	Mbal	kt1	kt
			kN m/m	kN m/m		

60 Degree Co

H2	7.91	5.09	46.7	91.7	6.14	6.14
H4	7.91	5.09	48.5	81.0	5.82	5.82
H5	7.91	5.09	47.5	65.5	5.38	5.38
H9	7.91	5.09	46.5	93.9	6.19	6.19
H10	7.91	5.09	46.7	103.4	6.34	6.34
H11	7.91	5.09	46.9	109.4	6.42	6.42
H14	7.91	5.09	38.3	96.2	6.53	6.53
H15	7.91	5.09	42.2	85.6	6.20	6.20
S-121-0-0-1	7.91	5.08	8.0	17.1	6.28	6.28
-2	7.91	5.08	7.9	16.2	6.19	6.19
S-122-0-0-1a	7.91	5.08	8.0	14.4	5.97	5.97
-2a	7.91	5.08	7.9	13.3	5.84	5.84
S-123-0-0-1	7.91	5.08	8.0	12.0	5.58	5.58
-2	7.91	5.08	8.0	13.0	5.75	5.75
S-121-1-0.9-	7.91	5.08	8.0	18.1	6.37	6.37
-2-1.8-	7.91	5.08	8.0	20.1	6.52	6.52
-3-2.7-	7.91	5.08	8.1	23.1	6.69	6.69
-4-3.6-	7.91	5.08	8.1	23.1	6.69	6.69
-5-4.5-	7.91	5.08	8.0	21.4	6.60	6.60
-6-5.4-	7.91	5.08	8.0	19.9	6.50	6.50
S-121-0-0-1	7.91	5.08	16.2	18.8	4.89	5.08
-2	7.91	5.08	16.2	17.5	4.67	5.08
S-122-0-0-1a	7.91	5.08	15.8	15.5	4.35	5.08
S-123-0-0-1	7.91	5.08	16.2	12.3	3.39	5.08
S-121-0-0-1	7.91	5.08	4.8	12.3	6.56	6.56
S-122-0-0-1a	7.91	5.08	6.5	9.6	5.53	5.53
S-123-0-0-1	7.91	5.08	6.6	9.0	5.35	5.35
S-121-1-0.9-	7.91	5.08	6.5	11.9	6.00	6.00
-2-1.8-	7.91	5.08	6.5	12.7	6.12	6.12
-3-2.7-	7.91	5.08	6.6	14.4	6.31	6.31
-3-2.7-	7.91	5.08	6.6	14.6	6.33	6.33
-3-2.7-	7.91	5.08	6.5	13.2	6.18	6.18
-4-3.6-	7.91	5.08	6.6	14.4	6.31	6.31
-5-4.5-	7.91	5.08	6.7	16.9	6.52	6.52
-6-5.4-	7.91	5.08	6.7	16.9	6.52	6.52

Table B.8: Centreline - Nonsymmetric Holes, Constants, 60 Degree Method

SLAB	square - centreline - nonsymmetrical						Pu	Pu/Pp
	Pvf1	Pvf2	Pvf	Pvs	Pp	Pu		
	kN	kN	kN	kN	kN	kN		
60 Degree Co								
H2	286.52	405.5	286.5	317.1	286.5	329.2	1.15	
H4	282.47	358.1	282.5	290.3	282.5	289.6	1.03	
H5	255.72	289.6	255.7	254.9	254.9	249.5	0.98	
H9	287.72	415.5	287.7	311.3	287.7	347.4	1.21	
H10	295.98	457.6	296.0	328.9	296.0	351.4	1.19	
H11	300.98	483.9	301.0	350.7	301.0	356.7	1.19	
H14	249.77	425.7	249.8	324.9	249.8	252.6	1.01	
H15	261.54	379.7	261.5	306.8	261.5	344.7	1.32	
S-121-0-0-1	50.09	75.4	50.1	54.7	50.1	64.5	1.29	
-2	49.17	71.4	49.2	53.3	49.2	56.9	1.16	
S-122-0-0-1a	47.60	63.5	47.6	48.9	47.6	41.4	0.87	
-2a	46.15	58.8	46.1	47.1	46.1	53.4	1.16	
S-123-0-0-1	44.46	52.8	44.5	43.6	43.6	44.9	1.03	
-2	46.20	57.5	46.2	45.5	45.5	51.6	1.13	
S-121-1-0.9-	50.76	79.8	50.8	56.5	50.8	61.4	1.21	
-2-1.8-	52.14	88.6	52.1	60.4	52.1	60.0	1.15	
-3-2.7-	54.14	102.2	54.1	67.8	54.1	69.8	1.29	
-4-3.6-	54.14	102.2	54.1	67.8	54.1	69.4	1.28	
-5-4.5-	53.07	94.5	53.1	65.2	53.1	64.9	1.22	
-6-5.4-	52.00	87.8	52.0	62.8	52.0	63.6	1.22	
S-121-0-0-1	82.44	82.8	82.4	69.9	69.9	71.2	1.02	
-2	82.32	77.2	77.2	67.5	67.5	78.7	1.17	
S-122-0-0-1a	80.08	68.3	68.3	61.8	61.8	73.8	1.19	
S-123-0-0-1	82.09	55.1	55.1	54.2	54.2	72.1	1.33	
S-121-0-0-1	31.23	54.4	31.2	48.3	31.2	51.2	1.64	
S-122-0-0-1a	36.03	42.3	36.0	41.5	36.0	43.6	1.21	
S-123-0-0-1	35.29	39.7	35.3	39.3	35.3	43.6	1.24	
S-121-1-0.9-	39.00	52.4	39.0	47.6	39.0	50.7	1.30	
-2-1.8-	39.78	55.9	39.8	49.9	39.8	52.5	1.32	
-3-2.7-	41.63	63.6	41.6	55.5	41.6	46.7	1.12	
-3-2.7-	41.82	64.5	41.8	55.9	41.8	58.7	1.40	
-3-2.7-	40.44	58.5	40.4	53.3	40.4	50.3	1.24	
-4-3.6-	41.63	63.6	41.6	55.5	41.6	55.6	1.34	
-5-4.5-	43.71	74.5	43.7	60.1	43.7	58.3	1.33	
-6-5.4-	43.71	74.5	43.7	60.1	43.7	59.2	1.35	
Average							1.21	
Variance							0.02	

Table B.9: Centreline - Nonsymmetric Holes, Predicted Values, 60 Degree Method

SLAB	Hole patterns square - centreline - nonsymmetrical												
	Series	f'c	f'c	bo	b'	b	d	rho	fy	s	c		
		psi	MPa	in	mm	in	in	mm	%	ksi	MPa	mm	mm
90 Degree Cone Reduction Method													
H2	Moe	3620	25.0	51.0	1,295	35.0	40.0	114	1.15	50.0	345	1,829	254
H4	Moe	3730	25.7	46.0	1,168	30.0	40.0	114	1.15	52.0	359	1,829	254
H5	Moe	3620	25.0	41.0	1,041	25.0	40.0	114	1.15	51.0	352	1,829	254
H9	Moe	3490	24.1	51.0	1,295	38.8	40.0	114	1.15	50.0	345	1,829	254
H10	Moe	3620	25.0	54.9	1,394	40.0	40.0	114	1.15	50.0	345	1,829	254
H11	Moe	3780	26.1	56.0	1,422	40.0	40.0	114	1.15	50.0	345	1,829	254
H14	Moe	3800	26.2	51.0	1,295	35.0	40.0	114	1.15	40.0	276	1,829	254
H15	Moe	3390	23.4	51.0	1,295	35.0	40.0	114	1.15	45.0	310	1,829	254
S-121-0-0-1	A-1	4140	28.5	20.4	518	14.0	16.0	46	1.15	52.0	359	737	102
-2	A-1	3920	27.0	20.4	518	14.0	16.0	46	1.15	52.0	359	737	102
S-122-0-0-1a	A-1	4070	28.1	18.4	467	12.0	16.0	46	1.15	52.0	359	737	102
-2a	A-1	3770	26.0	18.4	467	12.0	16.0	46	1.15	52.0	359	737	102
S-123-0-0-1	A-1	4060	28.0	16.4	417	10.0	16.0	46	1.15	52.0	359	737	102
-2	A-1	4420	30.5	16.4	417	10.0	16.0	46	1.15	52.0	359	737	102
S-121-1-0.9-	A-1	4090	28.2	21.2	538	15.8	16.0	46	1.15	52.0	359	737	102
-2-1.8-	A-1	4260	29.4	22.9	582	16.0	16.0	46	1.15	52.0	359	737	102
-3-2.7-	A-1	4910	33.9	23.2	589	16.0	16.0	46	1.15	52.0	359	737	102
-4-3.6-	A-1	4910	33.9	23.2	589	16.0	16.0	46	1.15	52.0	359	737	102
-5-4.5-	A-1	4540	31.3	23.2	589	16.0	16.0	46	1.15	52.0	359	737	102
-6-5.4-	A-1	4220	29.1	23.2	589	16.0	16.0	46	1.15	52.0	359	737	102
S-121-0-0-1	B	4550	31.4	20.4	518	14.0	16.0	46	2.53	53.3	367	737	102
-2	B	4240	29.2	20.4	518	14.0	16.0	46	2.53	54.3	374	737	102
S-122-0-0-1a	B	4380	30.2	18.4	467	12.0	16.0	46	2.53	51.9	358	737	102
S-123-0-0-1	B	4240	29.2	16.4	417	10.0	16.0	46	2.53	54.1	373	737	102
S-121-0-0-1	A-2	4160	28.7	20.4	518	14.0	16.0	39	1.34	36.4	291	737	102
S-122-0-0-1a	A-2	3770	26.0	18.4	467	12.0	16.0	39	1.34	52.0	359	737	102
S-123-0-0-1	A-2	4250	29.3	16.4	417	10.0	16.0	39	1.34	52.0	359	737	102
S-121-1-0.9-	A-2	3740	25.8	21.2	538	15.8	16.0	39	1.34	52.0	359	737	102
-2-1.8-	A-2	3740	25.8	22.9	582	16.0	16.0	39	1.34	52.0	359	737	102
-3-2.7-	A-2	4250	29.3	23.2	589	16.0	16.0	39	1.34	52.0	359	737	102
-3-2.7-	A-2	4310	29.7	23.2	589	16.0	16.0	39	1.34	52.0	359	737	102
-3-2.7-	A-2	3910	27.0	23.2	589	16.0	16.0	39	1.34	52.0	359	737	102
-4-3.6-	A-2	4250	29.3	23.2	589	16.0	16.0	39	1.34	52.0	359	737	102
-5-4.5-	A-2	4980	34.3	23.2	589	16.0	16.0	39	1.34	52.0	359	737	102
-6-5.4-	A-2	4980	34.3	23.2	589	16.0	16.0	39	1.34	52.0	359	737	102

Table B.10: Centreline - Nonsymmetric Holes, Input Data, 90 Degree Method

SLAB	square - centreline		- nonsymmetrical			
	ky1	kb	Mb	Mbal	kt1	kt
			kN m/m	kN m/m		

90 Degree Co

H2	7.91	5.09	46.7	91.7	6.14	6.14
H4	7.91	5.09	48.5	81.0	5.82	5.82
H5	7.91	5.09	47.5	65.5	5.38	5.38
H9	7.91	5.09	46.5	98.0	6.26	6.26
H10	7.91	5.09	46.7	104.8	6.36	6.36
H11	7.91	5.09	46.9	109.4	6.42	6.42
H14	7.91	5.09	38.3	96.2	6.53	6.53
H15	7.91	5.09	42.2	85.8	6.20	6.20
S-121-0-0-1	7.91	5.08	8.0	17.1	6.28	6.28
-2	7.91	5.08	7.9	16.2	6.19	6.19
S-122-0-0-1a	7.91	5.08	8.0	14.4	5.97	5.97
-2a	7.91	5.08	7.9	13.3	5.84	5.84
S-123-0-0-1	7.91	5.08	8.0	12.0	5.58	5.58
-2	7.91	5.08	8.0	13.0	5.75	5.75
S-121-1-0.9-	7.91	5.08	8.0	19.0	6.45	6.45
-2-1.8-	7.91	5.08	8.0	20.1	6.52	6.52
-3-2.7-	7.91	5.08	8.1	23.1	6.69	6.69
-4-3.6-	7.91	5.08	8.1	23.1	6.69	6.69
-5-4.5-	7.91	5.08	8.0	21.4	6.60	6.60
-6-5.4-	7.91	5.08	8.0	19.9	6.50	6.50
S-121-0-0-1	7.91	5.08	16.2	18.8	4.89	5.08
-2	7.91	5.08	16.2	17.5	4.67	5.08
S-122-0-0-1a	7.91	5.08	15.8	15.5	4.35	5.08
S-123-0-0-1	7.91	5.08	16.2	12.5	3.39	5.08
S-121-0-0-1	7.91	5.08	4.8	12.3	6.56	6.56
S-122-0-0-1a	7.91	5.08	6.5	9.6	5.53	5.53
S-123-0-0-1	7.91	5.08	6.6	9.0	5.35	5.35
S-121-1-0.9-	7.91	5.08	6.5	12.5	6.09	6.09
-2-1.8-	7.91	5.08	6.5	12.7	6.12	6.12
-3-2.7-	7.91	5.08	6.6	14.4	6.31	6.31
-3-2.7-	7.91	5.08	6.6	14.6	6.33	6.33
-3-2.7-	7.91	5.08	6.5	13.2	6.18	6.18
-4-3.6-	7.91	5.08	6.6	14.4	6.31	6.31
-5-4.5-	7.91	5.08	6.7	16.9	6.52	6.52
-6-5.4-	7.91	5.08	6.7	16.9	6.52	6.52

Table B.11: Centreline - Nonsymmetric Holes, Constants, 90 Degree Method

SLAB	square - centreline - nonsymmetrical						Pu/Pp	125
	Pvf1	Pvf2	Pvf	Fvs	Pp	Pu		
	kN	kN	kN	kN	kN	kN		
90 Degree Co								
H2	286.52	405.5	286.5	317.1	286.5	329.2	1.15	
H4	282.47	358.1	282.5	290.3	282.5	289.6	1.03	
H5	255.72	289.6	255.7	254.9	254.9	249.5	0.98	
H9	291.04	433.4	291.0	311.3	291.0	347.4	1.19	
H10	296.90	463.4	296.9	341.3	296.9	351.4	1.18	
H11	300.98	483.9	301.0	355.8	301.0	356.7	1.19	
H14	249.77	425.7	249.8	324.9	249.8	252.6	1.01	
H15	261.54	379.7	261.5	306.8	261.5	344.7	1.32	
S-121-0-0-1	50.09	75.4	50.1	54.7	50.1	64.5	1.29	
-2	49.17	71.4	49.2	53.3	49.2	56.9	1.16	
S-122-0-0-1a	47.60	63.5	47.6	48.9	47.6	41.4	0.87	
-2a	46.15	58.8	46.1	47.1	46.1	53.4	1.16	
S-123-0-0-1	44.46	52.8	44.5	43.6	43.6	44.9	1.03	
-2	46.20	57.5	46.2	45.5	45.5	51.6	1.13	
S-121-1-0.9-	51.38	84.0	51.4	56.5	51.4	61.4	1.19	
-2-1.8-	52.14	88.6	52.1	62.3	52.1	60.0	1.15	
-3-2.7-	54.14	102.2	54.1	67.8	54.1	69.8	1.29	
-4-3.6-	54.14	102.2	54.1	67.8	54.1	69.4	1.28	
-5-4.5-	53.07	94.5	53.1	65.2	53.1	64.9	1.22	
-6-5.4-	52.00	87.8	52.0	62.8	52.0	63.6	1.22	
S-121-0-0-1	82.44	82.8	82.4	69.9	69.9	71.2	1.02	
-2	82.32	77.2	77.2	67.5	67.5	78.7	1.17	
S-122-0-0-1a	80.08	68.3	68.3	61.8	61.8	73.8	1.19	
S-123-0-0-1	82.09	55.1	55.1	54.2	54.2	72.1	1.33	
S-121-0-0-1	31.23	54.4	31.2	48.3	31.2	51.2	1.64	
S-122-0-0-1a	36.03	42.3	36.0	41.5	36.0	43.6	1.21	
S-123-0-0-1	35.29	39.7	35.3	39.3	35.3	43.6	1.24	
S-121-1-0.9-	39.63	55.2	39.6	47.6	39.6	50.7	1.28	
-2-1.8-	39.78	55.9	39.8	51.4	39.8	52.5	1.32	
-3-2.7-	41.63	63.6	41.6	55.5	41.6	46.7	1.12	
-3-2.7-	41.82	64.5	41.8	55.9	41.8	58.7	1.40	
-3-2.7-	40.44	58.5	40.4	53.3	40.4	50.3	1.24	
-4-3.6-	41.63	63.6	41.6	55.5	41.6	55.6	1.34	
-5-4.5-	43.71	74.5	43.7	60.1	43.7	58.3	1.33	
-6-5.4-	43.71	74.5	43.7	60.1	43.7	59.2	1.35	
Average							1.21	
Variance							0.02	

Table B.12: Centreline - Nonsymmetric Holes, Predicted Values, 90 Degree Method

SLAB	Hole Pattern: Square - Corner - Symmetrical											
	Series	f'c	bo	b'	b	d	rho	fy	s	c		
		MPa	in	mm	in	in	mm	%	ksi	MPa	mm	mm
Radial Line	Reduction Method											
H12	Moe	27.8	26.0	660	20.0	40.0	114	1.15	47.5	328	1,829	254
H13	Moe	24.6	16.0	406	12.5	40.0	114	1.15	47.5	328	1,829	254
S-222-0-0-1	B	30.7	16.4	417	12.0	16.0	46	2.53	66.3	457	737	102
S-224-0-0-1	B	33.8	10.4	264	8.0	16.0	46	2.53	65.0	448	737	102
S-242-9-0-1	B	32.8	14.4	366	10.5	16.0	46	2.53	67.1	463	737	102
-2	B	29.6	14.4	366	10.5	16.0	46	2.53	67.1	463	737	102
S-244-9-0-1	B	24.8	6.4	163	5.0	16.0	46	2.53	52.3	361	737	102
-2	B	33.8	6.4	163	5.0	16.0	46	2.53	64.1	442	737	102
S-224-0-0-1	A-1	28.3	10.4	264	8.0	16.0	46	1.15	52.0	359	737	102
S-242-9-0-1	A-1	28.1	14.4	366	10.5	16.0	46	1.15	52.0	359	737	102
-17-	A-1	29.9	14.4	366	10.5	16.0	46	1.15	52.0	359	737	102
-18-	A-1	26.5	14.4	366	10.5	16.0	46	1.15	52.0	359	737	102
S-244-9-0-1	A-1	31.0	6.4	163	5.0	16.0	46	1.15	52.0	359	737	102
-11-	A-1	28.9	6.4	163	5.0	16.0	46	1.15	52.0	359	737	102
-10-	A-1	28.9	6.4	163	5.0	16.0	46	1.15	52.0	359	737	102
-23-	A-1	29.9	6.4	163	5.0	16.0	46	1.15	52.0	359	737	102
-24-	A-1	29.3	6.4	163	5.0	16.0	46	1.15	52.0	359	737	102
S-224-0-0-1	A-2	28.2	10.4	264	8.0	16.0	39	1.34	52.0	359	737	102
S-242-9-0-1	A-2	28.2	14.4	366	10.5	16.0	39	1.34	52.0	359	737	102
S-244-9-0-1	A-2	34.8	6.4	163	5.0	16.0	39	1.34	52.0	359	737	102
-2	A-2	32.2	6.4	163	5.0	16.0	39	1.34	52.0	359	737	102
-3	A-2	30.1	6.4	163	5.0	16.0	39	1.34	52.0	359	737	102
-4	A-2	29.2	6.4	163	5.0	16.0	39	1.34	52.0	359	737	102
-10-0-1	A-2	29.2	6.4	163	5.0	16.0	39	1.34	52.0	359	737	102
-11-0-1	A-2	29.7	6.4	163	5.0	16.0	39	1.34	52.0	359	737	102

Table B.13: Corner - Symmetric Holes, Input Data, Radial Line Method

square - corner - symmetrical
 SLAB kyl kb Mb Mbal kt1 kt

kN m/m kN m/m

Radial Line

H12	7.91	5.09	45.0	58.3	5.22	5.22
H13	7.91	5.09	44.5	32.2	3.09	5.09
S-222-0-0-1	7.91	5.08	19.0	15.7	3.68	5.08
S-224-0-0-1	7.91	5.08	19.2	11.5	2.09	5.08
S-242-9-0-1	7.91	5.08	19.5	14.7	3.26	5.08
-2	7.91	5.08	19.0	13.3	2.91	5.08
S-244-9-0-1	7.91	5.08	15.1	5.3	-2.05	5.08
-2	7.91	5.08	19.0	7.2	-1.31	5.08
S-224-0-0-1	7.91	5.08	8.0	9.7	5.03	5.08
S-242-9-0-1	7.91	5.08	8.0	12.6	5.70	5.70
-17-	7.91	5.08	8.0	13.4	5.82	5.82
-18-	7.91	5.08	7.9	11.9	5.58	5.58
S-244-9-0-1	7.91	5.08	8.0	6.6	3.67	5.08
-11-	7.91	5.08	8.0	6.2	3.39	5.08
-10-	7.91	5.08	8.0	6.2	3.39	5.08
-23-	7.91	5.08	8.0	6.4	3.52	5.08
-24-	7.91	5.08	8.0	6.3	3.44	5.08
S-224-0-0-1	7.91	5.08	6.6	6.9	4.59	5.08
S-242-9-0-1	7.91	5.08	6.6	9.1	5.38	5.38
S-244-9-0-1	7.91	5.08	6.7	5.3	3.52	5.08
-2	7.91	5.08	6.7	4.9	3.20	5.08
-3	7.91	5.08	6.6	4.6	2.90	5.08
-4	7.91	5.08	6.6	4.5	2.77	5.08
-10-0-1	7.91	5.08	6.6	4.5	2.77	5.08
-11-0-1	7.91	5.08	6.6	4.6	2.84	5.08

Table B.14: Corner - Symmetric Holes, Constants, Radial Line Method

SLAB	square - corner - symmetrical				Pp	Pu	Pu/Pp
	Pvf1	Pvf2	Pvf	Pvs			
	kN	kN	kN	kN			
Radial Line							
H12	235.02	258.0	235.0	170.6	170.6	269.0	1.58
H13	226.47	142.4	142.4	98.7	98.7	201.0	2.04
S-222-0-0-1	96.64	69.4	69.4	55.6	55.6	80.3	1.45
S-224-0-0-1	97.71	51.0	51.0	37.0	37.0	70.6	1.91
S-242-9-0-1	99.25	64.9	64.9	50.4	50.4	65.8	1.31
-2	96.41	58.6	58.6	47.9	47.9	65.5	1.37
S-244-9-0-1	76.77	23.4	23.4	19.5	19.5	56.3	2.89
-2	96.69	31.9	31.9	22.7	22.7	59.8	2.63
S-224-0-0-1	40.50	42.7	40.5	27.8	27.8	44.9	1.62
S-242-9-0-1	45.42	55.6	45.4	38.3	38.3	48.5	1.27
-17-	46.65	59.2	46.7	39.5	39.5	46.3	1.17
-18-	44.21	52.5	44.2	37.2	37.2	49.8	1.34
S-244-9-0-1	40.83	29.2	29.2	17.9	17.9	40.9	2.29
-11-	40.58	27.3	27.3	17.3	17.3	42.3	2.45
-10-	40.58	27.3	27.3	17.3	17.3	46.3	2.68
-23-	40.70	28.2	28.2	17.6	17.6	42.7	2.43
-24-	40.63	27.6	27.6	17.4	17.4	44.5	2.56
S-224-0-0-1	33.38	30.6	30.6	24.4	24.4	44.5	1.82
S-242-9-0-1	35.38	40.1	35.4	33.8	33.8	40.5	1.20
S-244-9-0-1	34.09	23.6	23.6	16.7	16.7	32.5	1.95
-2	33.84	21.8	21.8	16.1	16.1	53.8	3.35
-3	33.61	20.4	20.4	15.5	15.5	43.6	2.81
-4	33.51	19.8	19.8	15.3	15.3	40.9	2.67
-10-0-1	33.51	19.8	19.8	15.3	15.3	39.1	2.56
-11-0-1	33.57	20.1	20.1	15.4	15.4	40.0	2.59
Average							2.06
Std. Dev.							0.62
Variance							0.39

Table B.15: Corner - Symmetric Holes, Predicted Values, Radial Line Method

SLAB	Hole Pattern: Square - Corner - Symmetrical											
	Series	f'c	bo	b'	b	d	rho	fy	s	c		
		MPa	in	mm	in	in	mm	%	ksi	MPa	mm	mm
60 Degree Cone Reduction Method												
H12	Moe	27.8	33.3	846	30.0	40.0	114	1.15	47.5	328	1,829	254
H13	Moe	24.6	21.0	533	17.5	40.0	114	1.15	47.5	328	1,829	254
S-222-0-0-1	B	30.7	17.9	455	14.0	16.0	46	2.53	66.3	457	737	102
S-224-0-0-1	B	33.8	13.4	340	12.0	16.0	46	2.53	65.0	448	737	102
S-242-9-0-1	B	32.8	15.4	391	11.5	16.0	46	2.53	67.1	463	737	102
-2	B	29.6	15.4	391	11.5	16.0	46	2.53	67.1	463	737	102
S-244-9-0-1	B	24.8	8.4	213	7.0	16.0	46	2.53	52.3	361	737	102
-2	B	33.8	8.4	213	7.0	16.0	46	2.53	64.1	442	737	102
S-224-0-0-1	A-1	28.3	13.4	340	12.0	16.0	46	1.15	52.0	359	737	102
S-242-9-0-1	A-1	28.1	15.4	391	11.5	16.0	46	1.15	52.0	359	737	102
-17-	A-1	29.9	15.4	391	11.5	16.0	46	1.15	52.0	359	737	102
-18-	A-1	26.5	15.4	391	11.5	16.0	46	1.15	52.0	359	737	102
S-244-9-0-1	A-1	31.0	8.4	213	7.0	16.0	46	1.15	52.0	359	737	102
-11-	A-1	28.9	8.4	213	7.0	16.0	46	1.15	52.0	359	737	102
-10-	A-1	28.9	8.4	213	7.0	16.0	46	1.15	52.0	359	737	102
-23-	A-1	29.9	8.4	213	7.0	16.0	46	1.15	52.0	359	737	102
-24-	A-1	29.3	8.4	213	7.0	16.0	46	1.15	52.0	359	737	102
S-224-0-0-1	A-2	28.2	13.4	340	12.0	16.0	39	1.34	52.0	359	737	102
S-242-9-0-1	A-2	28.2	15.4	391	11.5	16.0	39	1.34	52.0	359	737	102
S-244-9-0-1	A-2	34.8	8.4	213	7.0	16.0	39	1.34	52.0	359	737	102
-2	A-2	32.2	8.4	213	7.0	16.0	39	1.34	52.0	359	737	102
-3	A-2	30.1	8.4	213	7.0	16.0	39	1.34	52.0	359	737	102
-4	A-2	29.2	8.4	213	7.0	16.0	39	1.34	52.0	359	737	102
-10-0-1	A-2	29.2	8.4	213	7.0	16.0	39	1.34	52.0	359	737	102
-11-0-1	A-2	29.7	8.4	213	7.0	16.0	39	1.34	52.0	359	737	102

Table B.16: Corner - Symmetric Holes, Input Data, 60 Degree Method

square - corner - symmetrical
 SLAB ky1 kb Mb Mbal kt1 kt

kN m/m kN m/m

60 Degree Cone

H12	7.91	5.09	45.0	87.5	6.12	6.12
H13	7.91	5.09	44.5	45.1	4.47	5.09
S-222-0-0-1	7.91	5.08	19.0	18.3	4.29	5.08
S-224-0-0-1	7.91	5.08	19.2	17.3	4.03	5.08
S-242-9-0-1	7.91	5.08	19.5	16.1	3.66	5.08
-2	7.91	5.08	19.0	14.5	3.34	5.08
S-244-9-0-1	7.91	5.08	15.1	7.4	0.79	5.08
-2	7.91	5.08	19.0	10.1	1.32	5.08
S-224-0-0-1	7.91	5.08	8.0	14.5	5.99	5.99
S-242-9-0-1	7.91	5.08	8.0	13.8	5.89	5.89
-17-	7.91	5.08	8.0	14.7	6.00	6.00
-18-	7.91	5.08	7.9	13.0	5.78	5.78
S-244-9-0-1	7.91	5.08	8.0	9.5	4.88	5.08
-11-	7.91	5.08	8.0	8.6	4.68	5.08
-10-	7.91	5.08	8.0	8.6	4.68	5.08
-23-	7.91	5.08	8.0	8.9	4.78	5.08
-24-	7.91	5.08	8.0	8.8	4.72	5.08
S-224-0-0-1	7.91	5.08	6.6	10.4	5.70	5.70
S-242-9-0-1	7.91	5.08	6.6	10.0	5.60	5.60
S-244-9-0-1	7.91	5.08	6.7	7.5	4.77	5.08
-2	7.91	5.08	6.7	6.9	4.55	5.08
-3	7.91	5.08	6.6	6.5	4.33	5.08
-4	7.91	5.08	6.6	6.3	4.24	5.08
-10-0-1	7.91	5.08	6.6	6.3	4.24	5.08
-11-0-1	7.91	5.08	6.6	6.4	4.29	5.08

Table B.17: Corner - Symmetric Holes, Constants, 60 Degree Method

SLAB	square - corner - symmetrical						Fu	Fu/Pp
	Pvf1	Pvf2	Pvf	Pvs	Pp			
	kN	kN	kN	kN	kN	kN		
60 Degree Cone								
H12	275.48	387.0	275.5	218.4	218.4	269.0	1.23	
H13	226.47	199.4	199.4	129.5	129.5	201.0	1.55	
S-222-0-0-1	96.64	81.0	81.0	60.6	60.6	80.3	1.32	
S-224-0-0-1	97.71	76.5	76.5	47.6	47.6	70.6	1.48	
S-242-9-0-1	99.25	71.0	71.0	53.9	53.9	65.8	1.22	
-2	96.41	64.2	64.2	51.2	51.2	65.5	1.28	
S-244-9-0-1	76.77	32.8	32.8	25.6	25.6	56.3	2.20	
-2	96.69	44.6	44.6	29.9	29.9	59.8	2.00	
S-224-0-0-1	47.76	64.1	47.8	35.8	35.8	44.9	1.25	
S-242-9-0-1	46.96	60.9	47.0	41.0	41.0	48.5	1.18	
-17-	48.11	64.9	48.1	42.3	42.3	46.3	1.09	
-18-	45.82	57.5	45.8	39.8	39.8	49.8	1.25	
S-244-9-0-1	40.83	40.9	40.8	23.5	23.5	40.9	1.74	
-11-	40.58	38.2	38.2	22.7	22.7	42.3	1.87	
-10-	40.58	38.2	38.2	22.7	22.7	46.3	2.04	
-23-	40.70	39.5	39.5	23.1	23.1	42.7	1.85	
-24-	40.63	38.7	38.7	22.8	22.8	44.5	1.95	
S-224-0-0-1	37.46	45.9	37.5	31.5	31.5	44.5	1.41	
S-242-9-0-1	36.83	44.0	36.8	36.2	36.2	40.5	1.12	
S-244-9-0-1	34.09	33.0	33.0	21.9	21.9	32.5	1.48	
-2	33.84	30.6	30.6	21.1	21.1	53.8	2.55	
-3	33.61	28.6	28.6	20.4	20.4	43.6	2.14	
-4	33.51	27.7	27.7	20.1	20.1	40.9	2.04	
-10-0-1	33.51	27.7	27.7	20.1	20.1	39.1	1.95	
-11-0-1	33.57	28.2	28.2	20.2	20.2	40.0	1.98	
Average							1.65	
Std. Dev.							0.40	
Variance							0.16	

Table B.18: Corner - Symmetric Holes, Predicted Values, 60 Degree Method

SLAB	Hole Pattern: Square - Corner - Symmetrical											
	Series	f'c	bo		b'	b	d	rho	fy	s	c	
		MPa	in	mm	in	in	mm	%	ksi	MPa	mm	
90 Degree Cone		Reduction Method										
H12	Moe	27.8	40.0	1,016	30.0	40.0	114	1.15	47.5	328	1,829	254
H13	Moe	24.6	40.0	1,016	17.5	40.0	114	1.15	47.5	328	1,829	254
S-222-0-0-1	B	30.7	19.6	498	14.0	16.0	46	2.53	66.3	457	737	102
S-224-0-0-1	B	33.8	16.0	406	12.0	16.0	46	2.53	65.0	448	737	102
S-242-9-0-1	B	32.8	19.6	498	11.5	16.0	46	2.53	67.1	463	737	102
-2	B	29.6	19.6	498	11.5	16.0	46	2.53	67.1	463	737	102
S-244-9-0-1	B	24.8	16.0	406	7.0	16.0	46	2.53	52.3	361	737	102
-2	B	33.8	16.0	406	7.0	16.0	46	2.53	64.1	442	737	102
S-224-0-0-1	A-1	28.3	16.0	406	12.0	16.0	46	1.15	52.0	359	737	102
S-242-9-0-1	A-1	28.1	19.6	498	11.5	16.0	46	1.15	52.0	359	737	102
-17-	A-1	29.9	19.6	498	11.5	16.0	46	1.15	52.0	359	737	102
-18-	A-1	26.5	19.6	498	11.5	16.0	46	1.15	52.0	359	737	102
S-244-9-0-1	A-1	31.0	16.0	406	7.0	16.0	46	1.15	52.0	359	737	102
-11-	A-1	28.9	16.0	406	7.0	16.0	46	1.15	52.0	359	737	102
-10-	A-1	28.9	16.0	406	7.0	16.0	46	1.15	52.0	359	737	102
-23-	A-1	29.9	16.0	406	7.0	16.0	46	1.15	52.0	359	737	102
-24-	A-1	29.3	16.0	406	7.0	16.0	46	1.15	52.0	359	737	102
S-224-0-0-1	A-2	28.2	16.0	406	12.0	16.0	39	1.34	52.0	359	737	102
S-242-9-0-1	A-2	28.2	19.6	498	11.5	16.0	39	1.34	52.0	359	737	102
S-244-9-0-1	A-2	34.8	16.0	406	7.0	16.0	39	1.34	52.0	359	737	102
-2	A-2	32.2	16.0	406	7.0	16.0	39	1.34	52.0	359	737	102
-3	A-2	30.1	16.0	406	7.0	16.0	39	1.34	52.0	359	737	102
-4	A-2	29.2	16.0	406	7.0	16.0	39	1.34	52.0	359	737	102
-10-0-1	A-2	29.2	16.0	406	7.0	16.0	39	1.34	52.0	359	737	102
-11-0-1	A-2	29.7	16.0	406	7.0	16.0	39	1.34	52.0	359	737	102

Table B.19: Corner - Symmetric Holes, Input Data, 90 Degree Method

square - corner - symmetrical
 SLAB ky1 kb Mb Mbal kt1 kt
 kN m/m kN m/m

90 Degree Cone

SLAB	ky1	kb	Mb	Mbal	kt1	kt
H12	7.91	5.09	45.0	87.5	6.12	6.12
H13	7.91	5.09	44.5	45.1	4.47	5.09
S-222-0-0-1	7.91	5.08	19.0	18.3	4.29	5.08
S-224-0-0-1	7.91	5.08	19.2	17.3	4.03	5.08
S-242-9-0-1	7.91	5.08	19.5	16.1	3.66	5.08
-2	7.91	5.08	19.0	14.5	3.34	5.08
S-244-9-0-1	7.91	5.08	15.1	7.4	0.79	5.08
-2	7.91	5.08	19.0	10.1	1.32	5.08
S-224-0-0-1	7.91	5.08	8.0	14.5	5.99	5.99
S-242-9-0-1	7.91	5.08	8.0	13.8	5.89	5.89
-17-	7.91	5.08	8.0	14.7	6.00	6.00
-18-	7.91	5.08	7.9	13.0	5.78	5.78
S-244-9-0-1	7.91	5.08	8.0	9.3	4.88	5.08
-11-	7.91	5.08	8.0	8.6	4.68	5.08
-10-	7.91	5.08	8.0	8.6	4.68	5.08
-23-	7.91	5.08	8.0	8.9	4.78	5.08
-24-	7.91	5.08	8.0	8.8	4.72	5.08
S-224-0-0-1	7.91	5.08	6.6	10.4	5.70	5.70
S-242-9-0-1	7.91	5.08	6.6	10.0	5.60	5.60
S-244-9-0-1	7.91	5.08	6.7	7.5	4.77	5.08
-2	7.91	5.08	6.7	6.9	4.55	5.08
-3	7.91	5.08	6.6	6.5	4.33	5.08
-4	7.91	5.08	6.6	6.3	4.24	5.08
-10-0-1	7.91	5.08	6.6	6.3	4.24	5.08
-11-0-1	7.91	5.08	6.6	6.4	4.29	5.08

Table B.20: Corner - Symmetric Holes, Constants, 90 Degree Method

SLAB	square - corner - symmetrical					Fu	Fu/Pp
	Pvf1	Pvf2	Pvf	Pvs	Pp		
	kN	kN	kN	kN	kN		
90 Degree Cone							
H12	275.48	387.0	275.5	262.4	262.4	269.0	1.03
H13	226.47	199.4	199.4	246.6	199.4	201.0	1.01
S-222-0-0-1	96.64	81.0	81.0	66.4	66.4	80.3	1.21
S-224-0-0-1	97.71	76.5	76.5	56.9	56.9	70.6	1.24
S-242-9-0-1	99.25	71.0	71.0	68.6	68.6	65.8	0.96
-2	96.41	64.2	64.2	65.2	64.2	65.5	1.02
S-244-9-0-1	76.77	32.8	32.8	48.7	32.8	56.3	1.72
-2	96.69	44.6	44.6	56.9	44.6	59.8	1.34
S-224-0-0-1	47.76	64.1	47.8	42.7	42.7	44.9	1.05
S-242-9-0-1	46.96	60.9	47.0	52.2	47.0	48.5	1.03
-17-	48.11	64.9	48.1	53.8	48.1	46.3	0.96
-18-	45.82	57.5	45.8	50.7	45.8	49.8	1.09
S-244-9-0-1	40.83	40.9	40.8	44.7	40.8	40.9	1.00
-11-	40.58	38.2	38.2	43.2	38.2	42.3	1.11
-10-	40.58	38.2	38.2	43.2	38.2	46.3	1.21
-23-	40.70	39.5	39.5	43.9	39.5	42.7	1.08
-24-	40.63	38.7	38.7	43.5	38.7	44.5	1.15
S-224-0-0-1	37.46	45.9	37.5	37.6	37.5	44.5	1.19
S-242-9-0-1	36.83	44.0	36.8	46.0	36.8	40.5	1.10
S-244-9-0-1	34.09	33.0	33.0	41.7	33.0	32.5	0.98
-2	33.84	30.6	30.6	40.2	30.6	53.8	1.76
-3	33.61	28.6	28.6	38.8	28.6	43.6	1.53
-4	33.51	27.7	27.7	38.2	27.7	40.9	1.48
-10-0-1	33.51	27.7	27.7	38.2	27.7	39.1	1.41
-11-0-1	33.57	28.2	28.2	38.6	28.2	40.0	1.42
Average							1.20
Std. Dev.							0.23
Variance							0.05

Table B.21: Corner - Symmetric Holes, Predicted Values, 90 Degree Method

SLAB	Hole Pattern: Square - Corner - Nonsymmetrical											
	Series	f'c	bo	b'	b	d	rho	fy	s	c		
		MPa	in	mm	in	in	mm	%	ksi	MPa	mm	mm
Radial Line	Reduction Method											
S-221-0-0-1	A-1	28.2	19.4	493	14.0	16.0	46	1.15	52.0	359	737	102
S-241-9-0-1	A-1	27.9	18.4	467	13.2	16.0	46	1.15	52.0	359	737	102
-15-	A-1	27.9	18.4	467	13.2	16.0	46	1.15	52.0	359	737	102
-16-	A-1	27.9	18.4	467	13.2	16.0	46	1.15	52.0	359	737	102
S-242-9-0-1a	A-1	31.1	14.4	366	10.5	16.0	46	1.15	52.0	359	737	102
-19-	A-1	26.5	14.4	366	10.5	16.0	46	1.15	52.0	359	737	102
-20-	A-1	28.3	14.4	366	10.5	16.0	46	1.15	52.0	359	737	102
S-243-9-0-1	A-1	28.3	10.4	264	7.8	16.0	46	1.15	52.0	359	737	102
-21-	A-1	27.8	10.4	264	7.8	16.0	46	1.15	52.0	359	737	102
-22-	A-1	27.8	10.4	264	7.8	16.0	46	1.15	52.0	359	737	102
S-221-0-0-1	B	34.6	19.4	493	14.0	16.0	46	2.53	66.4	458	737	102
S-222-0-0-1a	B	34.6	16.4	417	12.0	16.0	46	2.53	67.2	463	737	102
S-233-0-0-1	B	30.6	13.4	340	10.0	16.0	46	2.53	65.8	454	737	102
S-241-9-0-1	B	29.8	18.4	467	13.2	16.0	46	2.53	67.1	463	737	102
S-242-9-0-1a	B	32.8	14.4	366	10.5	16.0	46	2.53	64.3	443	737	102
S-243-9-0-1	B	24.8	10.4	264	7.8	16.0	46	2.53	63.2	436	737	102
S-221-0-0-1	A-2	31.5	19.4	493	14.0	16.0	46	1.34	52.0	359	737	102
-2	A-2	27.8	19.4	493	14.0	16.0	39	1.34	52.0	359	737	102
S-241-9-0-1	A-2	28.2	18.4	467	13.2	16.0	39	1.34	52.0	359	737	102
S-242-9-0-1a	A-2	27.2	14.4	366	10.5	16.0	39	1.34	52.0	359	737	102
S-243-9-0-1	A-2	27.2	10.4	264	7.8	16.0	39	1.34	52.0	359	737	102

Table B.22: Corner - Nonsymmetric Holes, Input Data, Radial Line Method

SLAB

square - corner - nonsymmetrical
ky1 kb Mb Mbal kt1 kt

136

kN m/m kN m/m

Radial Line

SLAB	ky1	kb	Mb	Mbal	kt1	kt
S-221-0-0-1	7.91	5.08	8.0	16.9	6.26	6.26
S-241-9-0-1	7.91	5.08	8.0	15.7	6.14	6.14
-15-	7.91	5.08	8.0	15.7	6.14	6.14
-16-	7.91	5.08	8.0	15.7	6.14	6.14
S-242-9-0-1a	7.91	5.08	8.0	13.9	5.89	5.89
-19-	7.91	5.08	7.9	11.9	5.58	5.58
-20-	7.91	5.08	8.0	12.7	5.71	5.71
S-243-9-0-1	7.91	5.08	8.0	9.4	4.95	5.08
-21-	7.91	5.08	8.0	9.3	4.91	5.08
-22-	7.91	5.08	8.0	9.3	4.91	5.08
S-221-0-0-1	7.91	5.08	19.7	20.7	4.59	5.08
S-222-0-0-1a	7.91	5.08	19.8	17.7	4.00	5.08
S-233-0-0-1	7.91	5.08	18.9	13.1	2.85	5.08
S-241-9-0-1	7.91	5.08	19.0	16.8	3.95	5.08
S-242-9-0-1a	7.91	5.08	18.9	14.7	3.41	5.08
S-243-9-0-1	7.91	5.08	17.2	8.3	0.63	5.08
S-221-0-0-1	7.91	5.08	9.3	18.8	6.19	6.19
-2	7.91	5.08	6.6	11.9	5.99	5.99
S-241-9-0-1	7.91	5.08	6.6	11.4	5.90	5.90
S-242-9-0-1a	7.91	5.08	6.5	8.8	5.30	5.30
S-243-9-0-1	7.91	5.08	6.5	6.5	4.40	5.08

Table B.23: Corner - Nonsymmetric Holes, Constants, Radial Line Method

SLAB	square - corner - nonsymmetrical					Fu	Fu/Pp
	Pvf1	Pvf2	Pvf	Pvs	Pp		
	kN	kN	kN	kN	kN		
137							
Radial Line							
S-221-0-0-1	49.88	74.5	49.9	51.7	49.9	57.4	1.15
S-241-9-0-1	48.90	69.5	48.9	48.8	48.8	48.5	0.99
-15-	48.90	69.5	48.9	48.8	48.8	48.5	0.99
-16-	48.90	69.5	48.9	48.8	48.8	47.6	0.98
S-242-9-0-1a	47.41	61.6	47.4	40.3	40.3	49.4	1.22
-19-	44.21	52.5	44.2	37.2	37.2	47.1	1.27
-20-	45.57	56.0	45.6	38.5	38.5	48.0	1.25
S-243-9-0-1	40.50	41.6	40.5	27.8	27.8	45.8	1.65
-21-	40.43	40.9	40.4	27.5	27.5	47.1	1.71
-22-	40.43	40.9	40.4	27.5	27.5	51.6	1.87
S-221-0-0-1	99.88	91.4	91.4	69.8	69.8	89.4	1.28
S-222-0-0-1a	100.78	78.3	78.3	59.0	59.0	85.2	1.44
S-233-0-0-1	96.04	57.7	57.7	45.3	45.3	64.1	1.41
S-241-9-0-1	96.63	74.2	74.2	61.4	61.4	71.0	1.16
S-242-9-0-1a	96.21	65.0	65.0	50.4	50.4	72.7	1.44
S-243-9-0-1	87.39	36.5	36.5	31.7	31.7	56.5	1.78
S-221-0-0-1	57.30	83.2	57.3	56.8	56.8	42.7	0.75
-2	39.31	52.8	39.3	45.2	39.3	48.9	1.24
S-241-9-0-1	38.78	50.5	38.8	43.2	38.8	47.6	1.23
S-242-9-0-1a	34.70	38.7	34.7	33.2	33.2	38.7	1.16
S-243-9-0-1	33.24	28.8	28.8	24.0	24.0	38.7	1.61
Average							1.31
Variance							0.08

Table B.24: Corner - Nonsymmetric Holes, Predicted Values, Radial Line Method

SLAB	Hole Pattern: Square - Corner - Nonsymmetrical											
	Series	f'c	bo	b'	b	d	rho	fy	s	c		
		MPa	in	mm	in	in	mm	%	ksi	MPa	mm	mm
60 Degree Cone												
Reduction Method												
S-221-0-0-1	A-1	28.2	20.2	513	15.0	16.0	46	1.15	52.0	359	737	102
S-241-9-0-1	A-1	27.9	18.9	480	13.8	16.0	46	1.15	52.0	359	737	102
-15-	A-1	27.9	18.9	480	13.8	16.0	46	1.15	52.0	359	737	102
-16-	A-1	27.9	18.9	480	13.8	16.0	46	1.15	52.0	359	737	102
S-242-9-0-1a	A-1	31.1	15.4	391	11.5	16.0	46	1.15	52.0	359	737	102
-19-	A-1	26.5	15.4	391	11.5	16.0	46	1.15	52.0	359	737	102
-20-	A-1	28.3	15.4	391	11.5	16.0	46	1.15	52.0	359	737	102
S-243-9-0-1	A-1	28.3	11.9	302	9.3	16.0	46	1.15	52.0	359	737	102
-21-	A-1	27.8	11.9	302	9.3	16.0	46	1.15	52.0	359	737	102
-22-	A-1	27.8	11.9	302	9.3	16.0	46	1.15	52.0	359	737	102
S-221-0-0-1	B	34.6	20.2	513	15.0	16.0	46	2.53	66.4	458	737	102
S-222-0-0-1a	B	34.6	17.9	455	14.0	16.0	46	2.53	67.2	463	737	102
S-233-0-0-1	B	30.6	15.6	396	13.0	16.0	46	2.53	65.8	454	737	102
S-241-9-0-1	B	29.8	18.9	480	13.8	16.0	46	2.53	67.1	463	737	102
S-242-9-0-1a	B	32.8	15.4	391	11.5	16.0	46	2.53	64.3	443	737	102
S-243-9-0-1	B	24.8	11.9	302	9.3	16.0	46	2.53	63.2	436	737	102
S-221-0-0-1	A-2	31.5	20.2	513	15.0	16.0	46	1.34	52.0	359	737	102
-2	A-2	27.8	20.2	513	15.0	16.0	39	1.34	52.0	359	737	102
S-241-9-0-1	A-2	28.2	18.9	480	13.8	16.0	39	1.34	52.0	359	737	102
S-242-9-0-1a	A-2	27.2	15.4	391	11.5	16.0	39	1.34	52.0	359	737	102
S-243-9-0-1	A-2	27.2	11.9	302	9.3	16.0	39	1.34	52.0	359	737	102

Table B.25: Corner - Nonsymmetric Holes, Input Data, 60 Degree Method

SLAB	square - corner - nonsymmetrical					
	ky1	kb	Mb	Mbal	kt1	kt
			kN m/m		kN m/m	

60 Degree Cone

S-221-0-0-1	7.91	5.08	8.0	18.1	6.37	6.37
S-241-9-0-1	7.91	5.08	8.0	16.4	6.22	6.22
-15-	7.91	5.08	8.0	16.4	6.22	6.22
-16-	7.91	5.08	8.0	16.4	6.22	6.22
S-242-9-0-1a	7.91	5.08	8.0	15.3	6.07	6.07
-19-	7.91	5.08	7.9	13.0	5.78	5.78
-20-	7.91	5.08	8.0	13.9	5.91	5.91
S-243-9-0-1	7.91	5.08	8.0	11.2	5.43	5.43
-21-	7.91	5.08	8.0	11.0	5.39	5.39
-22-	7.91	5.08	8.0	11.0	5.39	5.39
S-221-0-0-1	7.91	5.08	19.7	22.2	4.81	5.08
S-222-0-0-1a	7.91	5.08	19.8	20.7	4.56	5.08
S-233-0-0-1	7.91	5.08	18.9	17.0	4.02	5.08
S-241-9-0-1	7.91	5.08	19.0	17.6	4.12	5.08
S-242-9-0-1a	7.91	5.08	18.9	16.1	3.80	5.08
S-243-9-0-1	7.91	5.08	17.2	9.9	1.81	5.08
S-221-0-0-1	7.91	5.08	9.3	20.2	6.31	6.31
-2	7.91	5.08	6.6	12.8	6.12	6.12
S-241-9-0-1	7.91	5.08	6.6	11.9	5.99	5.99
S-242-9-0-1a	7.91	5.08	6.5	9.6	5.53	5.53
S-243-9-0-1	7.91	5.08	6.5	7.8	4.96	5.08

Table B.26: Corner - Nonsymmetric Holes, Constants, 60 Degree Method

SLAB	square - corner - nonsymmetrical					Fu	Fu/Pp
	Pvf1	Pvf2	Pvf	Pvs	Po		
	kN	kN	kN	kN	kN	kN	140
60 Degree Cone							
S-221-0-0-1	50.76	79.8	50.8	53.9	50.8	57.4	1.13
S-241-9-0-1	49.51	72.6	49.5	50.1	49.5	48.5	0.98
-15-	49.51	72.6	49.5	50.1	49.5	48.5	0.98
-16-	49.51	72.6	49.5	50.1	49.5	47.6	0.96
S-242-9-0-1a	48.82	67.5	48.8	43.1	43.1	49.4	1.14
-19-	45.82	57.5	45.8	39.8	39.8	47.1	1.18
-20-	47.09	61.4	47.1	41.1	41.1	48.0	1.17
S-243-9-0-1	43.31	49.6	43.3	31.8	31.8	45.8	1.44
-21-	42.92	48.8	42.9	31.5	31.5	47.1	1.50
-22-	42.92	48.8	42.9	31.5	31.5	51.6	1.64
S-221-0-0-1	99.38	97.9	97.9	72.7	72.7	89.4	1.23
S-222-0-0-1a	100.78	91.4	91.4	64.4	64.4	85.2	1.32
S-233-0-0-1	96.04	75.0	75.0	52.8	52.8	64.1	1.21
S-241-9-0-1	96.63	77.6	77.6	63.1	63.1	71.0	1.13
S-242-9-0-1a	96.21	71.1	71.1	53.9	53.9	72.7	1.35
S-243-9-0-1	87.39	43.5	43.5	36.2	36.2	56.5	1.56
S-221-0-0-1	58.35	89.1	58.4	59.1	58.4	42.7	0.73
-2	40.15	56.5	40.2	47.1	40.2	48.9	1.22
S-241-9-0-1	39.35	52.8	39.4	44.4	39.4	47.6	1.21
S-242-9-0-1a	36.19	42.4	36.2	35.5	35.5	38.7	1.09
S-243-9-0-1	33.24	34.3	33.2	27.5	27.5	38.7	1.41
							Average
							Variance
							1.22
							0.04

Table B.27: Corner - Nonsymmetric Holes, Predicted Values, 60 Degree Method

SLAB	Hole Pattern: Square - Corner - Nonsymmetrical											
	Series	f'c	bo	b'	b	d	rho	fy	e	c		
		MPa	in	mm	in	in	mm	%	ksi	MPa	mm	mm
90 Degree Cone		Reduction Method										
S-221-0-0-1	A-1	28.2	20.6	523	16.0	16.0	46	1.15	52.0	359	737	102
S-241-9-0-1	A-1	27.9	20.6	523	16.0	16.0	46	1.15	52.0	359	737	102
-15-	A-1	27.9	20.6	523	16.0	16.0	46	1.15	52.0	359	737	102
-16-	A-1	27.9	20.6	523	16.0	16.0	46	1.15	52.0	359	737	102
S-242-9-0-1a	A-1	31.1	19.6	498	16.0	16.0	46	1.15	52.0	359	737	102
-19-	A-1	26.5	19.6	498	16.0	16.0	46	1.15	52.0	359	737	102
-20-	A-1	28.3	19.6	498	16.0	16.0	46	1.15	52.0	359	737	102
S-243-9-0-1	A-1	28.3	17.2	437	16.0	16.0	46	1.15	52.0	359	737	102
-21-	A-1	27.8	17.2	437	16.0	16.0	46	1.15	52.0	359	737	102
-22-	A-1	27.8	17.2	437	16.0	16.0	46	1.15	52.0	359	737	102
S-221-0-0-1	B	34.6	20.6	523	16.0	16.0	46	2.53	66.4	458	737	102
S-222-0-0-1a	B	34.6	19.6	498	16.0	16.0	46	2.53	67.2	463	737	102
S-233-0-0-1	B	30.6	17.2	437	16.0	16.0	46	2.53	65.8	454	737	102
S-241-9-0-1	B	29.8	20.6	523	16.0	16.0	46	2.53	67.1	463	737	102
S-242-9-0-1a	B	32.8	19.6	498	16.0	16.0	46	2.53	64.3	443	737	102
S-243-9-0-1	B	24.8	17.2	437	16.0	16.0	46	2.53	63.2	436	737	102
S-221-0-0-1	A-2	31.5	20.6	523	16.0	16.0	46	1.34	52.0	359	737	102
-2	A-2	27.8	20.6	523	16.0	16.0	39	1.34	52.0	359	737	102
S-241-9-0-1	A-2	28.2	20.6	523	16.0	16.0	39	1.34	52.0	359	737	102
S-242-9-0-1a	A-2	27.2	19.6	498	16.0	16.0	39	1.34	52.0	359	737	102
S-243-9-0-1	A-2	27.2	17.2	437	16.0	16.0	39	1.34	52.0	359	737	102

Table B.28: Corner - Nonsymmetric Holes, Input Data, 90 Degree Method

SLAB	square - corner - nonsymmetrical					Pu	Pu/Pp
	Pvf1	Pvf2	Pvf	Pvs	Pp		
	kN	kN	kN	kN	kN		
							143
90 Degree Cone							
S-221-0-0-1	51.53	85.1	51.5	54.9	51.5	57.4	1.11
S-241-9-0-1	51.37	84.2	51.4	54.6	51.4	48.5	0.94
-15-	51.37	84.2	51.4	54.6	51.4	48.5	0.94
-16-	51.37	84.2	51.4	54.6	51.4	47.6	0.93
S-242-9-0-1a	52.97	93.9	53.0	54.9	53.0	49.4	0.93
-19-	50.56	80.0	50.6	50.7	50.6	47.1	0.93
-20-	51.58	85.4	51.6	52.4	51.6	48.0	0.93
S-243-9-0-1	51.58	85.4	51.6	45.9	45.9	45.8	1.00
-21-	51.31	83.9	51.3	45.5	45.5	47.1	1.04
-22-	51.31	83.9	51.3	45.5	45.5	51.6	1.13
S-221-0-0-1	99.88	104.4	99.9	74.1	74.1	89.4	1.21
S-222-0-0-1a	100.78	104.4	100.8	70.5	70.5	85.2	1.21
S-233-0-0-1	96.04	92.3	92.3	58.2	58.2	64.1	1.10
S-241-9-0-1	96.63	89.9	89.9	68.8	68.8	71.0	1.03
S-242-9-0-1a	96.21	99.0	96.2	68.6	68.6	72.7	1.06
S-243-9-0-1	87.39	74.8	74.8	52.4	52.4	56.5	1.08
S-221-0-0-1	59.28	95.1	59.3	60.3	59.3	42.7	0.72
-2	40.89	60.3	40.9	48.0	40.9	48.9	1.20
S-241-9-0-1	41.09	61.2	41.1	48.4	41.1	47.6	1.16
S-242-9-0-1a	40.57	59.0	40.6	45.2	40.6	38.7	0.95
S-243-9-0-1	40.57	59.0	40.6	39.7	39.7	38.7	0.98
			Average				1.03
			Variance				0.01

Table B.30: Corner - Nonsymmetric Holes, Predicted Values, 90 Degree Method

SLAB	Code Equation							144	
	Hole patterns square - centreline - symmetrical								
	Serie	f'c	bo	d	Pp	Pu	Pu/Pp		
	MPa	in	mm	mm	kN	kN			
Radial Line		Reduction Method							
H3	Moe	23.7	41.0	1,041	114	230.9	325.0	1.41	
H6	Moe	28.4	26.0	660	114	160.5	246.0	1.53	
S-122-0-0-1	A-1	28.5	16.4	417	46	40.9	59.6	1.46	
	-2	A-1	27.0	16.4	417	46	39.8	53.8	1.35
S-124-0-0-1	A-1	28.0	10.4	264	46	25.7	40.0	1.56	
	-2	A-1	30.5	10.4	264	46	26.8	45.8	1.71
S-122-0-0-1	B	29.8	16.4	417	46	41.8	75.3	1.80	
S-124-0-0-1	B	30.2	10.4	264	46	26.7	67.4	2.52	
S-122-0-0-1	A-2	29.8	16.4	417	39	35.5	44.5	1.25	
S-124-0-0-1	A-2	29.3	10.4	264	39	22.3	40.9	1.83	
Average								1.64	
Variance								0.12	
60 Degree Cone		Reduction Method							
H3	Moe	23.7	46.0	1,168	114	259.1	325.0	1.25	
H6	Moe	28.4	36.0	914	114	222.2	246.0	1.11	
S-122-0-0-1	A-1	28.5	18.4	467	46	45.9	59.6	1.30	
	-2	A-1	27.0	18.4	467	46	44.7	53.8	1.20
S-124-0-0-1	A-1	28.0	14.4	366	46	35.6	40.0	1.12	
	-2	A-1	30.5	14.4	366	46	37.2	45.8	1.23
S-122-0-0-1	B	29.8	18.4	467	46	46.9	75.3	1.60	
S-124-0-0-1	B	30.2	14.4	366	46	37.0	67.4	1.82	
S-122-0-0-1	A-2	29.8	18.4	467	39	39.8	44.5	1.12	
S-124-0-0-1	A-2	29.3	14.4	366	39	30.9	40.9	1.32	
Average								1.31	
Variance								0.05	
90 Degree Cone		Reduction Method							
H3	Moe	23.7	46.0	1,168	114	259.1	325.0	1.25	
H6	Moe	28.4	36.0	914	114	222.2	246.0	1.11	
S-122-0-0-1	A-1	28.5	18.4	467	46	45.9	59.6	1.30	
	-2	A-1	27.0	18.4	467	46	44.7	53.8	1.20
S-124-0-0-1	A-1	28.0	14.4	366	46	35.6	40.0	1.12	
	-2	A-1	30.5	14.4	366	46	37.2	45.8	1.23
S-122-0-0-1	B	29.8	18.4	467	46	46.9	75.3	1.60	
S-124-0-0-1	B	30.2	14.4	366	46	37.0	67.4	1.82	
S-122-0-0-1	A-2	29.8	18.4	467	39	39.8	44.5	1.12	
S-124-0-0-1	A-2	29.3	14.4	366	39	30.9	40.9	1.32	
Average								1.31	
Variance								0.05	

Table B.31: Centreline - Symmetric Holes, Input Data

SLAB	Code Equation								
	Hole patterns square - centreline - nonsymmetrical								
	Series	f'c	f'c	bo	d	Pp	Pu	Pu/Pp	
	FSI	MPa	in	mm	mm	kN	kN	145	
Radial Line		Reduction Method							
H2	Moe	3620	25.0	48.5	1,232	114	280.6	329.2	1.17
H4	Moe	3730	25.7	41.0	1,041	114	240.8	289.6	1.20
H5	Moe	3620	25.0	33.5	851	114	193.8	249.5	1.29
H9	Moe	3490	24.1	50.7	1,288	114	288.1	347.4	1.21
H10	Moe	3620	25.0	51.9	1,318	114	300.3	351.4	1.17
H11	Moe	3780	26.1	52.6	1,336	114	311.0	356.7	1.15
H14	Moe	3800	26.2	48.5	1,232	114	287.5	252.6	0.88
H15	Moe	3390	23.4	48.5	1,232	114	271.6	344.7	1.27
S-121-0-0-1	A-1	4140	28.5	19.4	493	46	48.4	64.5	1.33
-2	A-1	3920	27.0	19.4	493	46	47.1	56.9	1.21
S-122-0-0-1a	A-1	4070	28.1	16.4	417	46	40.6	41.4	1.02
-2a	A-1	3770	26.0	16.4	417	46	39.1	53.4	1.37
S-123-0-0-1	A-1	4060	28.0	13.4	340	46	33.1	44.9	1.36
-2	A-1	4420	30.5	13.4	340	46	34.6	51.6	1.49
S-121-1-0.9-	A-1	4090	28.2	21.2	538	46	52.6	61.4	1.17
-2-1.8-	A-1	4260	29.4	21.7	551	46	55.0	60.0	1.09
-3-2.7-	A-1	4910	33.9	21.9	556	46	59.6	69.8	1.17
-4-3.6-	A-1	4910	33.9	22.2	564	46	60.4	69.4	1.15
-5-4.5-	A-1	4540	31.3	22.3	566	46	58.3	64.9	1.11
-6-5.4-	A-1	4220	29.1	22.5	572	46	56.7	63.6	1.12
S-121-0-0-1	B	4550	31.4	19.4	493	46	50.8	71.2	1.40
-2	B	4240	29.2	19.4	493	46	49.0	78.7	1.61
S-122-0-0-1a	B	4380	30.2	16.4	417	46	42.1	73.8	1.75
S-123-0-0-1	B	4240	29.2	13.4	340	46	33.9	72.1	2.13
S-121-0-0-1	A-2	4160	28.7	19.4	493	39	41.2	51.2	1.24
S-122-0-0-1a	A-2	3770	26.0	16.4	417	39	33.1	43.6	1.32
S-123-0-0-1	A-2	4250	29.3	13.4	340	39	28.7	43.6	1.52
S-121-1-0.9-	A-2	3740	25.8	21.2	538	39	42.7	50.7	1.19
-2-1.8-	A-2	3740	25.8	21.7	551	39	43.7	52.5	1.20
-3-2.7-	A-2	4250	29.3	21.9	556	39	47.0	46.7	0.99
-3-2.7-	A-2	4310	29.7	21.9	556	39	47.3	58.7	1.24
-3-2.7-	A-2	3910	27.0	21.9	556	39	45.1	50.3	1.12
-4-3.6-	A-2	4250	29.3	22.2	564	39	47.6	55.6	1.17
-5-4.5-	A-2	4980	34.3	22.3	566	39	51.8	58.3	1.13
-6-5.4-	A-2	4980	34.3	22.5	572	39	52.2	59.2	1.13
Average								1.26	
Variance								0.05	

Table B.32: Centreline - Nonsymmetric Holes, Input Data, Radial Line Method

SLAB	Code Equation								
	Hole patterns square - centreline - nonsymmetrical								
	Series	f'c	f'c	bo	d	Pp	Pu	Pu/Pp	146
	PSI	MPa	in	mm	mm	kN	kN		
60 Degree Cone Reduction Method									
H2	Moe	3620	25.0	51.0	1,295	114	295.1	329.2	1.12
H4	Moe	3730	25.7	46.0	1,168	114	270.2	289.6	1.07
H5	Moe	3620	25.0	41.0	1,041	114	237.2	249.5	1.05
H9	Moe	3490	24.1	51.0	1,295	114	289.8	347.4	1.20
H10	Moe	3620	25.0	52.9	1,344	114	306.1	351.4	1.15
H11	Moe	3780	26.1	55.2	1,402	114	326.4	356.7	1.09
H14	Moe	3800	26.2	51.0	1,295	114	302.4	252.6	0.84
H15	Moe	3390	23.4	51.0	1,295	114	285.6	344.7	1.21
S-121-0-0-1	A-1	4140	28.5	20.4	518	46	50.9	64.5	1.27
-2	A-1	3920	27.0	20.4	518	46	49.6	56.9	1.15
S-122-0-0-1a	A-1	4070	28.1	18.4	467	46	45.6	41.4	0.91
-2a	A-1	3770	26.0	18.4	467	46	43.8	53.4	1.22
S-123-0-0-1	A-1	4060	28.0	16.4	417	46	40.6	44.9	1.11
-2	A-1	4420	30.5	16.4	417	46	42.3	51.6	1.22
S-121-1-0.9-	A-1	4090	28.2	21.2	538	46	52.6	61.4	1.17
-2-1.8-	A-1	4260	29.4	22.2	564	46	56.2	60.0	1.07
-3-2.7-	A-1	4910	33.9	23.2	589	46	63.1	69.8	1.11
-4-3.6-	A-1	4910	33.9	23.2	589	46	63.1	69.4	1.10
-5-4.5-	A-1	4540	31.3	23.2	589	46	60.7	64.9	1.07
-6-5.4-	A-1	4220	29.1	23.2	589	46	58.5	63.6	1.09
S-121-0-0-1	B	4550	31.4	20.4	518	46	53.4	71.2	1.33
-2	B	4240	29.2	20.4	518	46	51.5	78.7	1.53
S-122-0-0-1a	B	4380	30.2	18.4	467	46	47.3	73.8	1.56
S-123-0-0-1	B	4240	29.2	16.4	417	46	41.4	72.1	1.74
S-121-0-0-1	A-2	4160	28.7	20.4	518	39	43.3	51.2	1.18
S-122-0-0-1a	A-2	3770	26.0	18.4	467	39	37.2	43.6	1.17
S-123-0-0-1	A-2	4250	29.3	16.4	417	39	35.2	43.6	1.24
S-121-1-0.9-	A-2	3740	25.8	21.2	538	39	42.7	50.7	1.19
-2-1.8-	A-2	3740	25.8	22.2	564	39	44.7	52.5	1.18
-3-2.7-	A-2	4250	29.3	23.2	589	39	49.8	46.7	0.94
-3-2.7-	A-2	4310	29.7	23.2	589	39	50.1	58.7	1.17
-3-2.7-	A-2	3910	27.0	23.2	589	39	47.7	50.3	1.05
-4-3.6-	A-2	4250	29.3	23.2	589	39	49.8	55.6	1.12
-5-4.5-	A-2	4980	34.3	23.2	589	39	53.9	58.3	1.08
-6-5.4-	A-2	4980	34.3	23.2	589	39	53.9	59.2	1.10
Average									1.16
Variance									0.03

Table B.33: Centreline - Nonsymmetric Holes, Input Data, 60 Degree Method

SLAB	Hole patterns square - centreline - nonsymmetrical									
	Series	f'c	f'c	bo	d	Fp	Fu	Fu/Pp	147	
		PSI	MPa	in	mm	mm	kN	kN		
90 Degree Cone		Reduction Method								
H2	Moe	3620	25.0	51.0	1,295	114	295.1	329.2	1.12	
H4	Moe	3730	25.7	46.0	1,168	114	270.2	289.6	1.07	
H5	Moe	3620	25.0	41.0	1,041	114	237.2	249.5	1.05	
H9	Moe	3490	24.1	51.0	1,295	114	289.8	347.4	1.20	
H10	Moe	3620	25.0	54.9	1,394	114	317.7	351.4	1.11	
H11	Moe	3780	26.1	56.0	1,422	114	331.1	356.7	1.08	
H14	Moe	3800	26.2	51.0	1,295	114	302.4	252.6	0.84	
H15	Moe	3390	23.4	51.0	1,295	114	285.6	344.7	1.21	
S-121-0-0-1	A-1	4140	28.5	20.4	518	46	50.9	64.5	1.27	
	-2	A-1	3920	27.0	20.4	518	46	49.6	56.9	1.15
S-122-0-0-1a	A-1	4070	28.1	18.4	467	46	45.6	41.4	0.91	
	-2a	A-1	3770	26.0	18.4	467	46	43.8	53.4	1.22
S-123-0-0-1	A-1	4060	28.0	16.4	417	46	40.6	44.9	1.11	
	-2	A-1	4420	30.5	16.4	417	46	42.3	51.6	1.22
S-121-1-0.9-	A-1	4090	28.2	21.2	538	46	52.6	61.4	1.17	
	-2-1.8-	A-1	4260	29.4	22.9	582	46	58.0	60.0	1.04
	-3-2.7-	A-1	4910	33.9	23.2	589	46	63.1	69.8	1.11
	-4-3.6-	A-1	4910	33.9	23.2	589	46	63.1	69.4	1.10
	-5-4.5-	A-1	4540	31.3	23.2	589	46	60.7	64.9	1.07
	-6-5.4-	A-1	4220	29.1	23.2	589	46	58.5	63.6	1.09
S-121-0-0-1	B	4550	31.4	20.4	518	46	53.4	71.2	1.33	
	-2	B	4240	29.2	20.4	518	46	51.5	78.7	1.53
S-122-0-0-1a	B	4380	30.2	18.4	467	46	47.3	73.8	1.56	
S-123-0-0-1	B	4240	29.2	16.4	417	46	41.4	72.1	1.74	
S-121-0-0-1	A-2	4160	28.7	20.4	518	39	43.3	51.2	1.18	
S-122-0-0-1a	A-2	3770	26.0	18.4	467	39	37.2	43.6	1.17	
S-123-0-0-1	A-2	4250	29.3	16.4	417	39	35.2	43.6	1.24	
S-121-1-0.9-	A-2	3740	25.8	21.2	538	39	42.7	50.7	1.19	
	-2-1.8-	A-2	3740	25.8	22.9	582	39	46.1	52.5	1.14
	-3-2.7-	A-2	4250	29.3	23.2	589	39	49.8	46.7	0.94
	-3-2.7-	A-2	4310	29.7	23.2	589	39	50.1	58.7	1.17
	-3-2.7-	A-2	3910	27.0	23.2	589	39	47.7	50.3	1.05
	-4-3.6-	A-2	4250	29.3	23.2	589	39	49.8	55.6	1.12
	-5-4.5-	A-2	4980	34.3	23.2	589	39	53.9	58.3	1.08
	-6-5.4-	A-2	4980	34.3	23.2	589	39	53.9	59.2	1.10
Average								1.16		
Variance								0.03		

Table B.34: Centreline - Nonsymmetric Holes, Input Data, 90 Degree Method

SLAB	Series	f'c	bo	d	Fp	Pu	Pu/Pp	
		MPa	in	mm	mm	kN	kN	
Radial Line	Reduction Method							
H12	Moe	27.8	26.0	660	114	158.8	269.0	1.69
H13	Moe	24.6	16.0	406	114	91.8	201.0	2.19
S-222-0-0-1	B	30.7	16.4	417	46	42.5	80.3	1.89
S-224-0-0-1	B	33.8	10.4	264	46	28.2	70.6	2.50
S-242-9-0-1	B	32.8	14.4	366	46	38.5	65.8	1.71
-2	B	29.6	14.4	366	46	36.6	65.5	1.79
S-244-9-0-1	B	24.8	6.4	163	46	14.9	56.3	3.78
-2	B	33.8	6.4	163	46	17.4	59.8	3.44
S-224-0-0-1	A-1	28.3	10.4	264	46	25.9	44.9	1.74
S-242-9-0-1	A-1	28.1	14.4	366	46	35.7	48.5	1.36
-17-	A-1	29.9	14.4	366	46	36.8	46.3	1.26
-18-	A-1	26.5	14.4	366	46	34.6	49.8	1.44
S-244-9-0-1	A-1	31.0	6.4	163	46	16.7	40.9	2.46
-11-	A-1	28.9	6.4	163	46	16.1	42.3	2.63
-10-	A-1	28.9	6.4	163	46	16.1	46.3	2.88
-23-	A-1	29.9	6.4	163	46	16.4	42.7	2.61
-24-	A-1	29.3	6.4	163	46	16.2	44.5	2.75
S-224-0-0-1	A-2	28.2	10.4	264	39	21.9	44.5	2.03
S-242-9-0-1	A-2	28.2	14.4	366	39	30.3	40.5	1.34
S-244-9-0-1	A-2	34.8	6.4	163	39	15.0	32.5	2.17
-2	A-2	32.2	6.4	163	39	14.4	53.8	3.74
-3	A-2	30.1	6.4	163	39	13.9	43.6	3.13
-4	A-2	29.2	6.4	163	39	13.7	40.9	2.98
-10-0-1	A-2	29.2	6.4	163	39	13.7	39.1	2.85
-11-0-1	A-2	29.7	6.4	163	39	13.8	40.0	2.89
Average							2.37	
Variance							0.53	

Table B.35: Corner - Symmetric Holes, Input Data, Radial Line Method

Code equation								
Hole Pattern: Square - Corner - Symmetrical								
SLAB	Series	f'c	bo	d	Pp	Fu	Fu/Pp	
		MPa	in	mm	mm	kN	kN	149
60 Degree Cone		Reduction Method						
H12	Moe	27.8	33.3	846	114	203.3	269.0	1.32
H13	Moe	24.6	21.0	533	114	120.5	201.0	1.67
S-222-0-0-1	B	30.7	17.9	455	46	46.3	80.3	1.73
S-224-0-0-1	B	33.8	13.4	340	46	36.4	70.6	1.94
S-242-9-0-1	B	32.8	15.4	391	46	41.2	65.8	1.60
-2	B	29.6	15.4	391	46	39.1	65.5	1.67
S-244-9-0-1	B	24.8	8.4	213	46	19.6	56.3	2.88
-2	B	33.8	8.4	213	46	22.8	59.8	2.62
S-224-0-0-1	A-1	28.3	13.4	340	46	33.3	44.9	1.35
S-242-9-0-1	A-1	28.1	15.4	391	46	38.2	48.5	1.27
-17-	A-1	29.9	15.4	391	46	39.4	46.3	1.18
-18-	A-1	26.5	15.4	391	46	37.1	49.8	1.34
S-244-9-0-1	A-1	31.0	8.4	213	46	21.9	40.9	1.87
-11-	A-1	28.9	8.4	213	46	21.1	42.3	2.00
-10-	A-1	28.9	8.4	213	46	21.1	46.3	2.19
-23-	A-1	29.9	8.4	213	46	21.5	42.7	1.99
-24-	A-1	29.3	8.4	213	46	21.3	44.5	2.09
S-224-0-0-1	A-2	28.2	13.4	340	39	28.2	44.5	1.58
S-242-9-0-1	A-2	28.2	15.4	391	39	32.4	40.5	1.25
S-244-9-0-1	A-2	34.8	8.4	213	39	19.6	32.5	1.66
-2	A-2	32.2	8.4	213	39	18.9	53.8	2.85
-3	A-2	30.1	8.4	213	39	18.3	43.6	2.39
-4	A-2	29.2	8.4	213	39	18.0	40.9	2.27
-10-0-1	A-2	29.2	8.4	213	39	18.0	39.1	2.17
-11-0-1	A-2	29.7	8.4	213	39	18.1	40.0	2.21
Average							1.88	
Variance							0.23	

Table B.36: Corner - Symmetric Holes, Input Data, 60 Degree Method

SLAB	Code Equation							150
	Hole Pattern: Square - Corner - Symmetrical							
	Series	f'c	bo	d	Fp	Fu	Fu/Fp	
	MPa	in	mm	mm	kN	kN		
90 Degree Cone		Reduction Method						
H12	Moe	27.8	40.0	1,016	114	244.2	269.0	1.10
H13	Moe	24.6	40.0	1,016	114	229.6	201.0	0.88
S-222-0-0-1	B	30.7	19.6	498	46	50.7	80.3	1.58
S-224-0-0-1	B	33.8	16.0	406	46	43.5	70.6	1.62
S-242-9-0-1	B	32.8	19.6	498	46	52.4	65.8	1.26
-2	B	29.6	19.6	498	46	49.8	65.5	1.31
S-244-9-0-1	B	24.8	16.0	406	46	37.3	56.3	1.51
-2	B	33.8	16.0	406	46	43.5	59.8	1.37
S-224-0-0-1	A-1	28.3	16.0	406	46	39.8	44.9	1.13
S-242-9-0-1	A-1	28.1	19.6	498	46	48.6	48.5	1.00
-17-	A-1	29.9	19.6	498	46	50.1	46.3	0.92
-18-	A-1	26.5	19.6	498	46	47.2	49.8	1.06
S-244-9-0-1	A-1	31.0	16.0	406	46	41.6	40.9	0.98
-11-	A-1	28.9	16.0	406	46	40.2	42.3	1.05
-10-	A-1	28.9	16.0	406	46	40.2	46.3	1.15
-23-	A-1	29.9	16.0	406	46	40.9	42.7	1.04
-24-	A-1	29.3	16.0	406	46	40.5	44.5	1.10
S-224-0-0-1	A-2	28.2	16.0	406	39	33.7	44.5	1.32
S-242-9-0-1	A-2	28.2	19.6	498	39	41.2	40.5	0.98
S-244-9-0-1	A-2	34.8	16.0	406	39	37.4	32.5	0.87
-2	A-2	32.2	16.0	406	39	36.0	53.8	1.50
-3	A-2	30.1	16.0	406	39	34.8	43.6	1.25
-4	A-2	29.2	16.0	406	39	34.3	40.9	1.19
-10-0-1	A-2	29.2	16.0	406	39	34.3	39.1	1.14
-11-0-1	A-2	29.7	16.0	406	39	34.6	40.0	1.16
Average								1.18
Variance								0.04

Table B.37: Corner - Symmetric Holes, Input Data, 90 Degree Method

SLAB	Code Equation							151
	Hole Pattern: Square - Corner - Nonsymmetrical							
	Series	f'c	bo	d	Pp	Pu	Pu/Po	
	MPa	in	mm	mm	kN	kN		
Radial Line	Reduction Method							
S-221-0-0-1	A-1	28.2	19.4	493	46	48.1	57.4	1.19
S-241-9-0-1	A-1	27.9	18.4	467	46	45.4	48.5	1.07
-15-	A-1	27.9	18.4	467	46	45.4	48.5	1.07
-16-	A-1	27.9	18.4	467	46	45.4	47.6	1.05
S-242-9-0-1a	A-1	31.1	14.4	366	46	37.5	49.4	1.32
-19-	A-1	26.5	14.4	366	46	34.6	47.1	1.36
-20-	A-1	28.3	14.4	366	46	35.8	48.0	1.34
S-243-9-0-1	A-1	28.3	10.4	264	46	25.9	45.8	1.77
-21-	A-1	27.8	10.4	264	46	25.6	47.1	1.84
-22-	A-1	27.8	10.4	264	46	25.6	51.6	2.01
S-221-0-0-1	B	34.6	19.4	493	46	53.3	89.4	1.68
S-222-0-0-1a	B	34.6	16.4	417	46	45.1	85.2	1.89
S-233-0-0-1	B	30.6	13.4	340	46	34.6	64.1	1.85
S-241-9-0-1	B	29.8	18.4	467	46	46.9	71.0	1.51
S-242-9-0-1a	B	32.8	14.4	366	46	38.5	72.7	1.89
S-243-9-0-1	B	24.8	10.4	264	46	24.2	56.5	2.33
S-221-0-0-1	A-2	31.5	19.4	493	46	50.9	42.7	0.84
-2	A-2	27.8	19.4	493	39	40.5	48.9	1.21
S-241-9-0-1	A-2	28.2	18.4	467	39	38.7	47.6	1.23
S-242-9-0-1a	A-2	27.2	14.4	366	39	29.8	38.7	1.30
S-243-9-0-1	A-2	27.2	10.4	264	39	21.5	38.7	1.80
						Average		1.50
						Variance		0.15

Table B.38: Corner - Nonsymmetric Holes, Input Data, Radial Line Method

SLAB	Code Equation							152
	Hole Pattern: Square - Corner - Nonsymmetrical							
	Series	f'c	bo	d	Fp	Fu	Fu/Pp	
	MPa	in	mm	mm	kN	kN		
60 Degree Cone	Reduction Method							
S-221-0-0-1	A-1	28.2	20.2	513	46	50.1	57.4	1.14
S-241-9-0-1	A-1	27.9	18.9	480	46	46.7	48.5	1.04
-15-	A-1	27.9	18.9	480	46	46.7	48.5	1.04
-16-	A-1	27.9	18.9	480	46	46.7	47.6	1.02
S-242-9-0-1a	A-1	31.1	15.4	391	46	40.1	49.4	1.23
-19-	A-1	26.5	15.4	391	46	37.1	47.1	1.27
-20-	A-1	28.3	15.4	391	46	38.3	48.0	1.25
S-243-9-0-1	A-1	28.3	11.9	302	46	29.6	45.8	1.55
-21-	A-1	27.8	11.9	302	46	29.3	47.1	1.61
-22-	A-1	27.8	11.9	302	46	29.3	51.6	1.76
S-221-0-0-1	B	34.6	20.2	513	46	55.5	89.4	1.61
S-222-0-0-1a	B	34.6	17.9	455	46	49.2	85.2	1.73
S-233-0-0-1	B	30.6	15.6	396	46	40.3	64.1	1.59
S-241-9-0-1	B	29.8	18.9	480	46	48.2	71.0	1.47
S-242-9-0-1a	B	32.8	15.4	391	46	41.2	72.7	1.76
S-243-9-0-1	B	24.8	11.9	302	46	27.7	56.5	2.04
S-221-0-0-1	A-2	31.5	20.2	513	46	53.0	42.7	0.81
-2	A-2	27.8	20.2	513	39	42.2	48.9	1.16
S-241-9-0-1	A-2	28.2	18.9	480	39	39.8	47.6	1.20
S-242-9-0-1a	A-2	27.2	15.4	391	39	31.8	38.7	1.22
S-243-9-0-1	A-2	27.2	11.9	302	39	24.6	38.7	1.57
						Average		1.38
						Variance		0.09

Table B.39: Corner - Nonsymmetric Holes, Input Data, 60 Degree Method

SLAB	Code Equation							153
	Hole Pattern: Square - Corner - Nonsymmetrical							
	Series	f'c	bo	d	Pp	Pu	Pu/Pp	
	MPa	in	mm	mm	kN	kN		
90 Degree Cone	Reduction Method							
S-221-0-0-1	A-1	28.2	20.6	523	46	51.1	57.4	1.12
S-241-9-0-1	A-1	27.9	20.6	523	46	50.9	48.5	0.95
-15-	A-1	27.9	20.6	523	46	50.9	48.5	0.95
-16-	A-1	27.9	20.6	523	46	50.9	47.6	0.94
S-242-9-0-1a	A-1	31.1	19.6	498	46	51.1	49.4	0.97
-19-	A-1	26.5	19.6	498	46	47.2	47.1	1.00
-20-	A-1	28.3	19.6	498	46	48.7	48.0	0.99
S-243-9-0-1	A-1	28.3	17.2	437	46	42.8	45.8	1.07
-21-	A-1	27.8	17.2	437	46	42.4	47.1	1.11
-22-	A-1	27.8	17.2	437	46	42.4	51.6	1.22
S-221-0-0-1	B	34.6	20.6	523	46	56.6	89.4	1.58
S-222-0-0-1a	B	34.6	19.6	498	46	53.9	85.2	1.58
S-233-0-0-1	B	30.6	17.2	437	46	44.5	64.1	1.44
S-241-9-0-1	B	29.8	20.6	523	46	52.6	71.0	1.35
S-242-9-0-1a	B	32.8	19.6	498	46	52.5	72.7	1.39
S-243-9-0-1	B	24.8	17.2	437	46	40.0	56.5	1.41
S-221-0-0-1	A-2	31.5	20.6	523	46	54.0	42.7	0.79
-2	A-2	27.8	20.6	523	39	43.0	48.9	1.14
S-241-9-0-1	A-2	28.2	20.6	523	39	43.3	47.6	1.10
S-242-9-0-1a	A-2	27.2	19.6	498	39	40.5	38.7	0.96
S-243-9-0-1	A-2	27.2	17.2	437	39	35.5	38.7	1.09
						Average		1.15
						Variance		0.05

Table B.40: : Corner - Nonsymmetric Holes, Input Data, 90 Degree Method

Square Holes on Column Centreline
Symmetric Hole Pattern

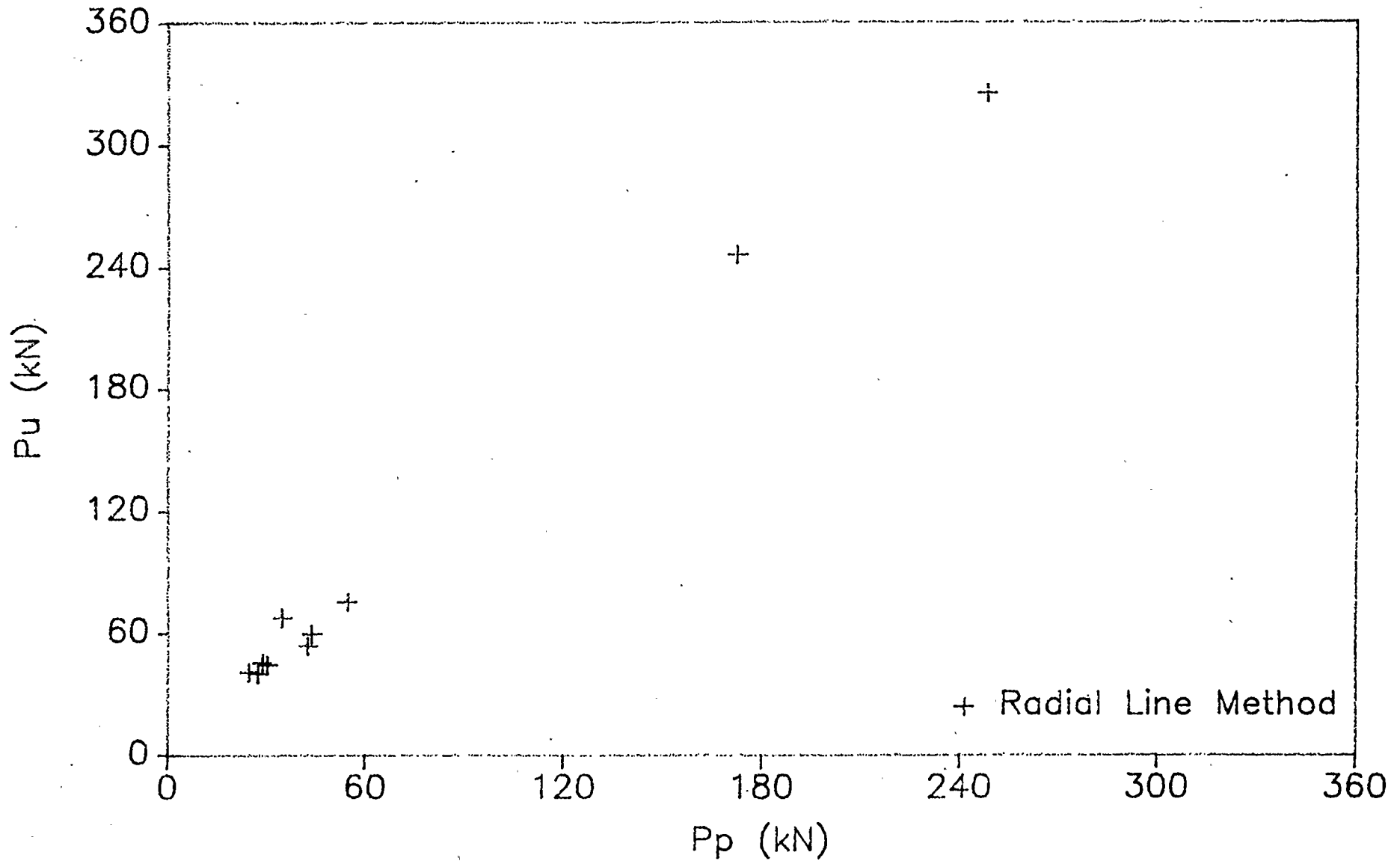


Figure B.1: Centreline - Symmetric Holes, Radial Line Method, Long's Eqn.

Square Holes on Column Centreline
Symmetric Hole Pattern

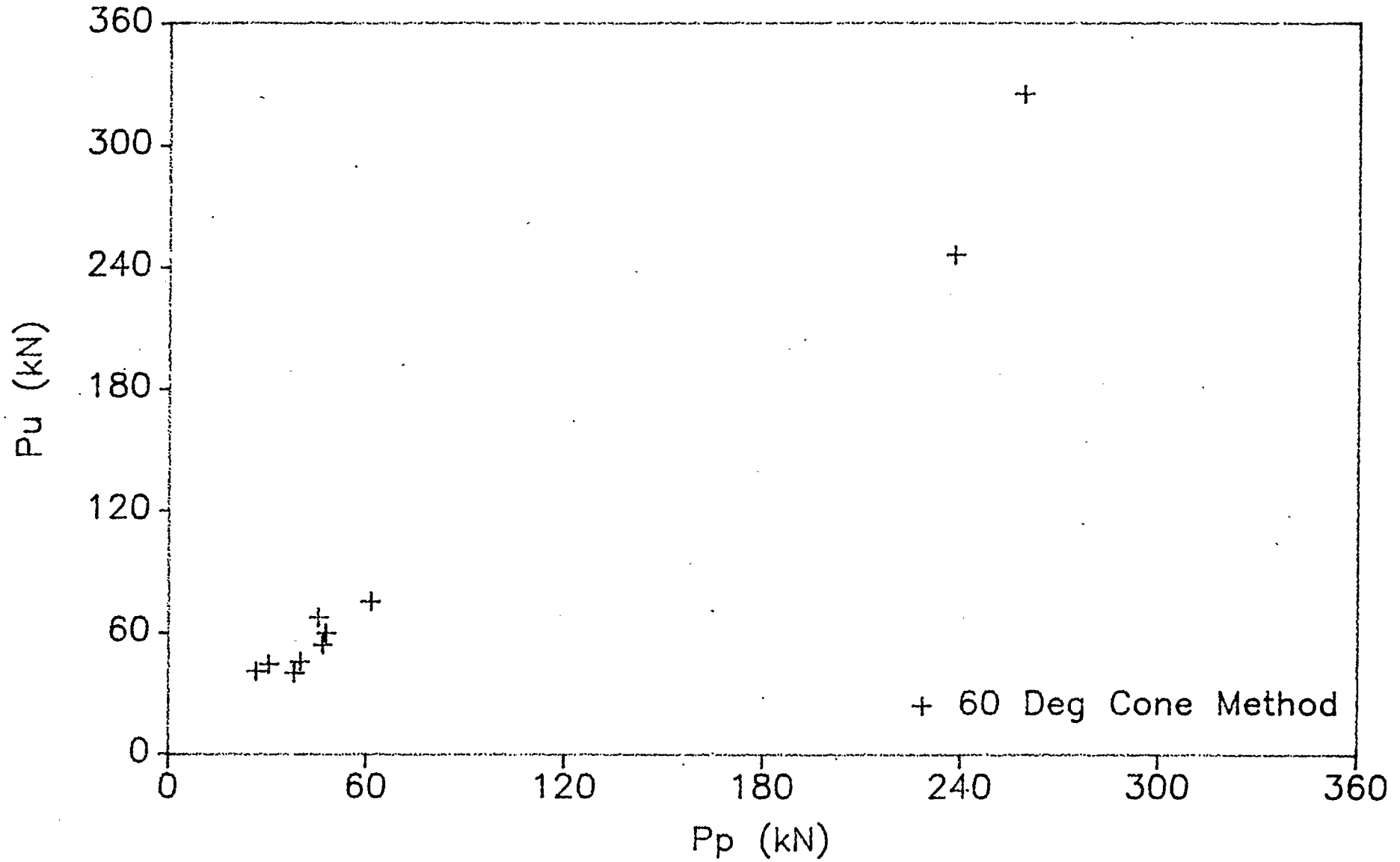


Figure B.2: Centreline - Symmetric Holes, 60 Degree Cone Method, Long's Eqn.

Square Holes on Column Centreline
Symmetric Hole Pattern

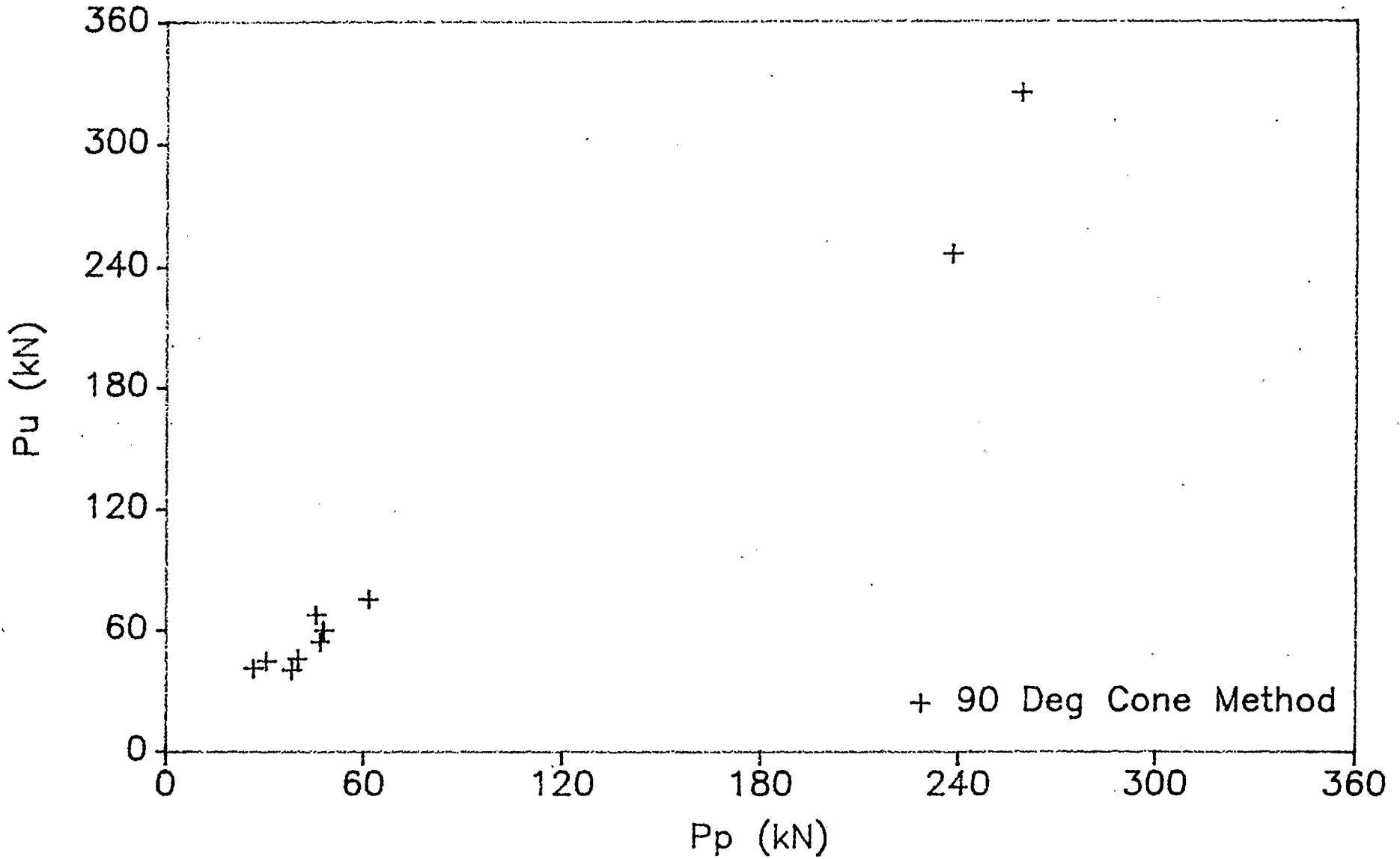


Figure B.3: Centreline - Symmetric Holes, 90 Degree Cone Method, Long's Eqn.

Square Holes on Column Centreline
Nonsymmetric Hole Pattern

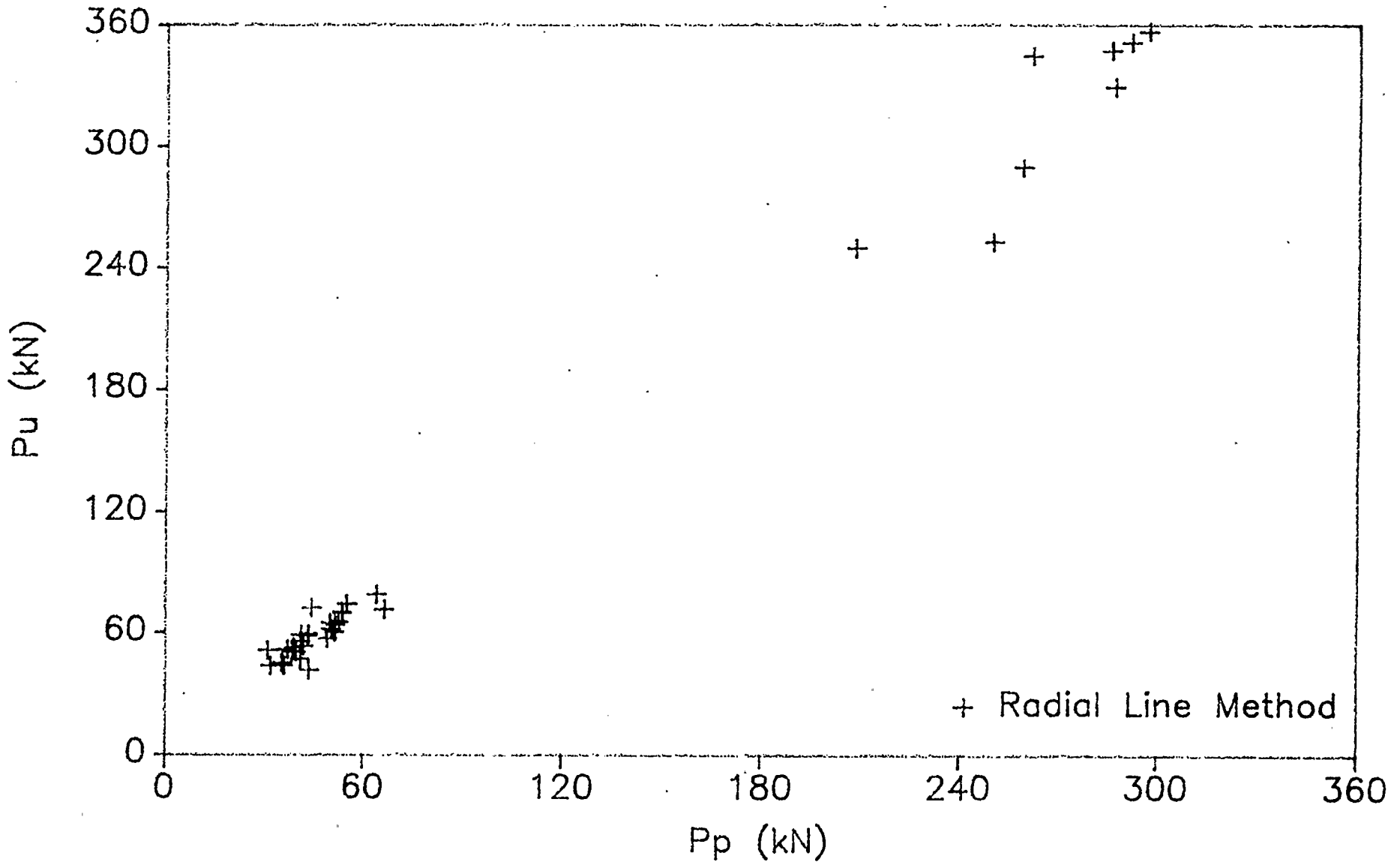


Figure B.4: Centreline - Nonsymmetric Holes, Radial Line Method, Long's Eqn.

Square Holes on Column Centreline
Nonsymmetric Hole Pattern

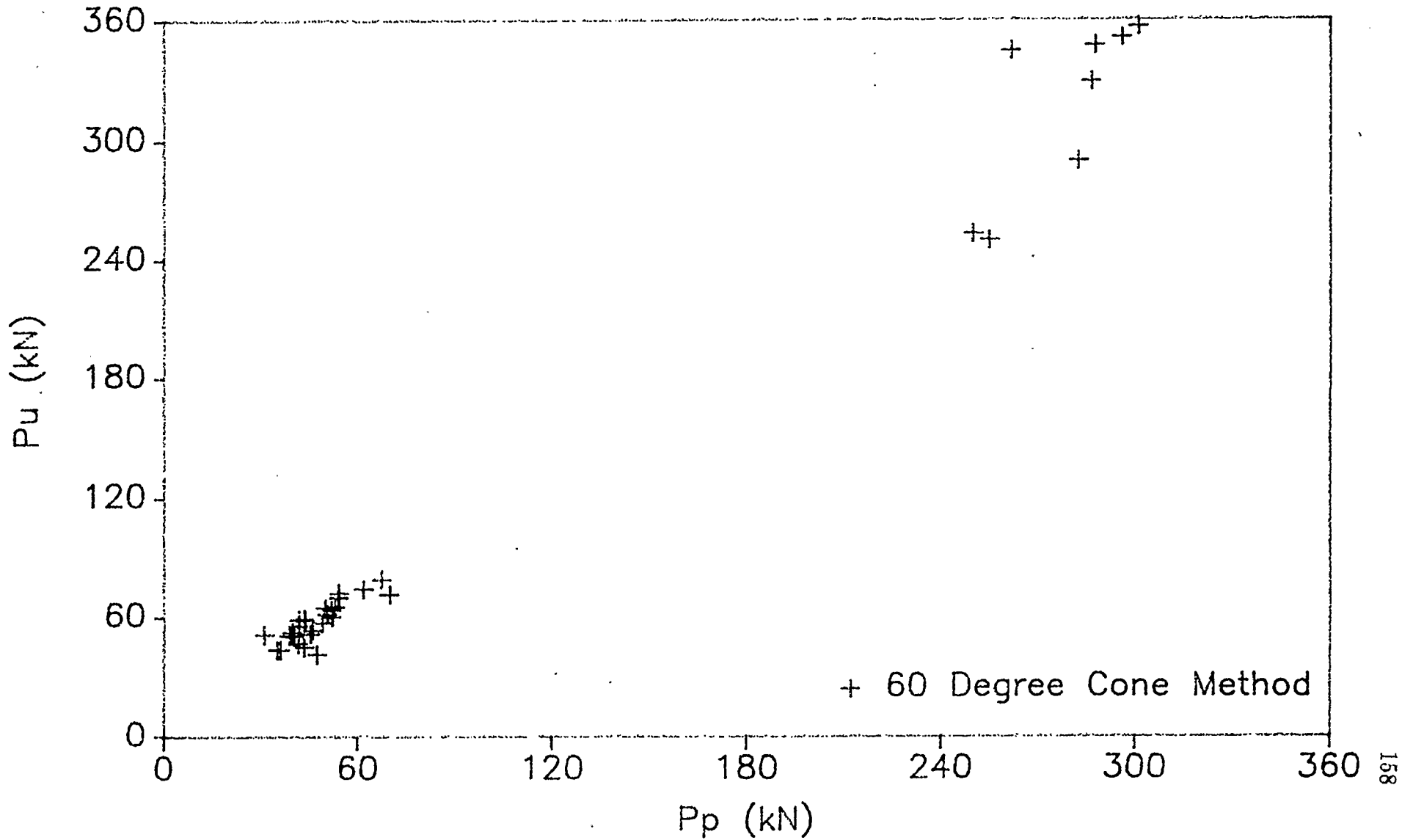


Figure B.5: Centreline - Nonsymmetric Holes, 60 Degree Cone Method, Long's Eqn.

Square Holes on Column Centreline
Nonsymmetric Hole Pattern

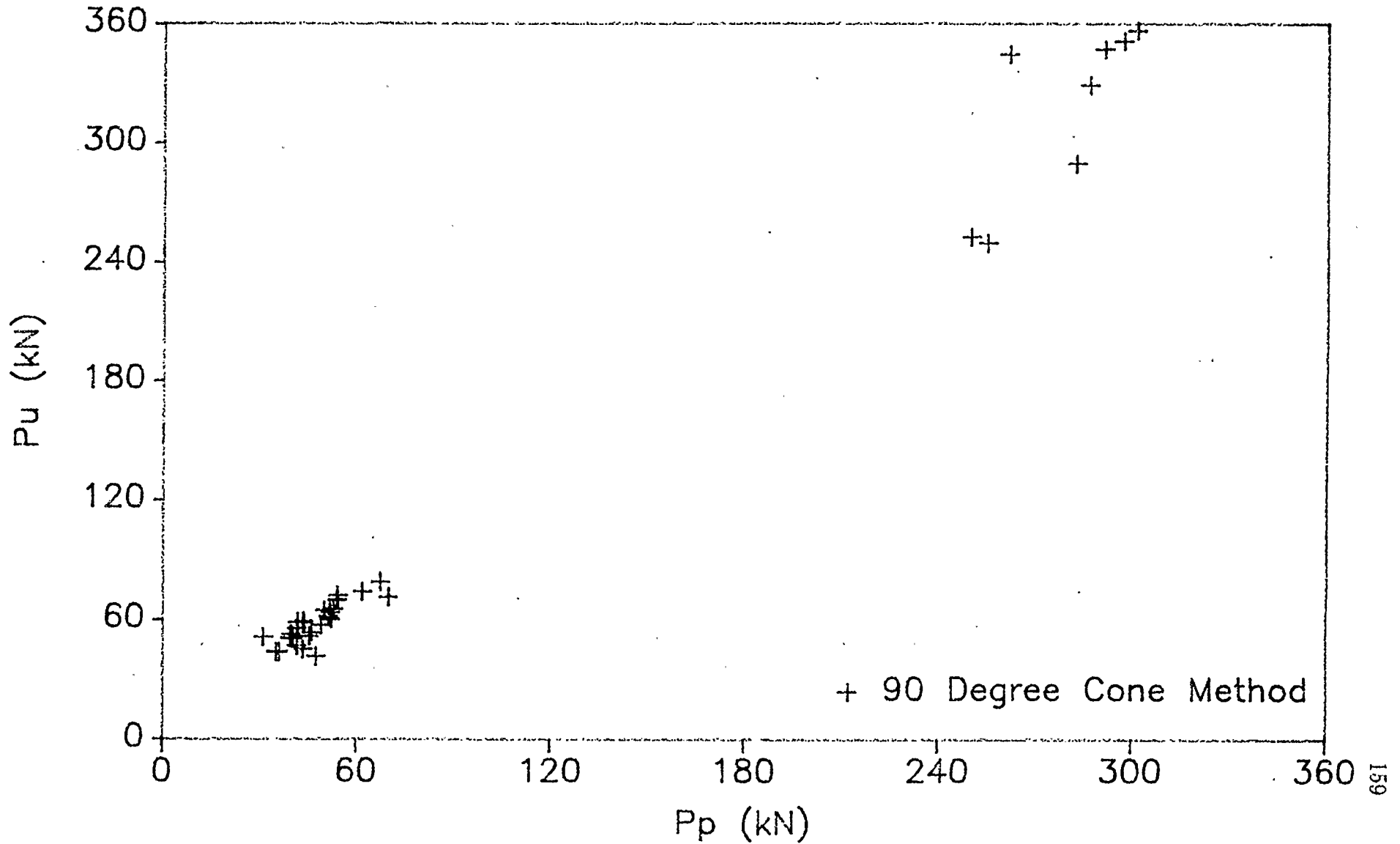


Figure B.6: Centreline - Nonsymmetric Holes, 90 Degree Cone Method, Long's
Eqn

Square Holes on Column Corners
Symmetric Hole Patterns

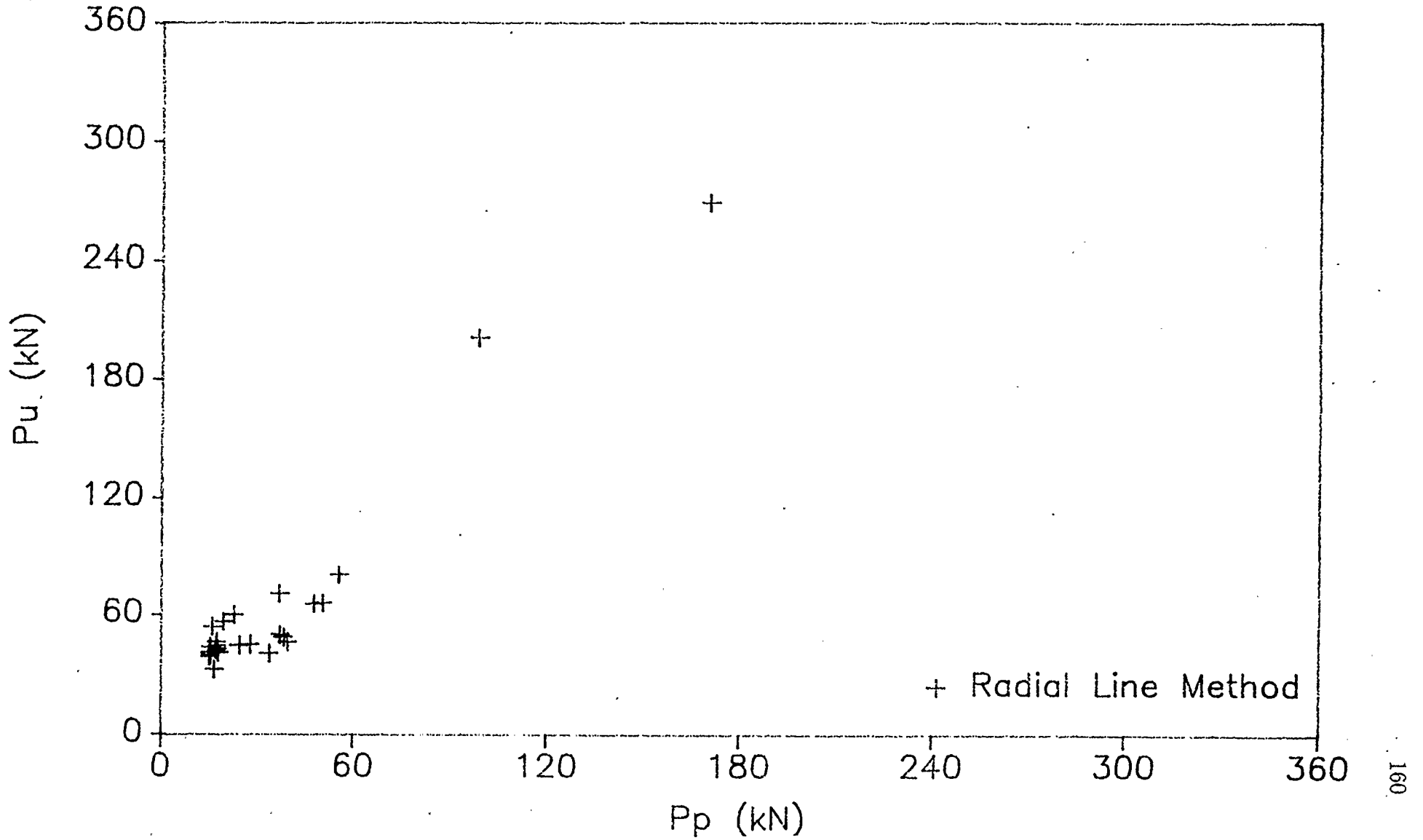


Figure B.7: Corner - Symmetric Holes, Radial Line Method, Long's Eqn.

Square Holes on Column Corners
Symmetric Hole Patterns

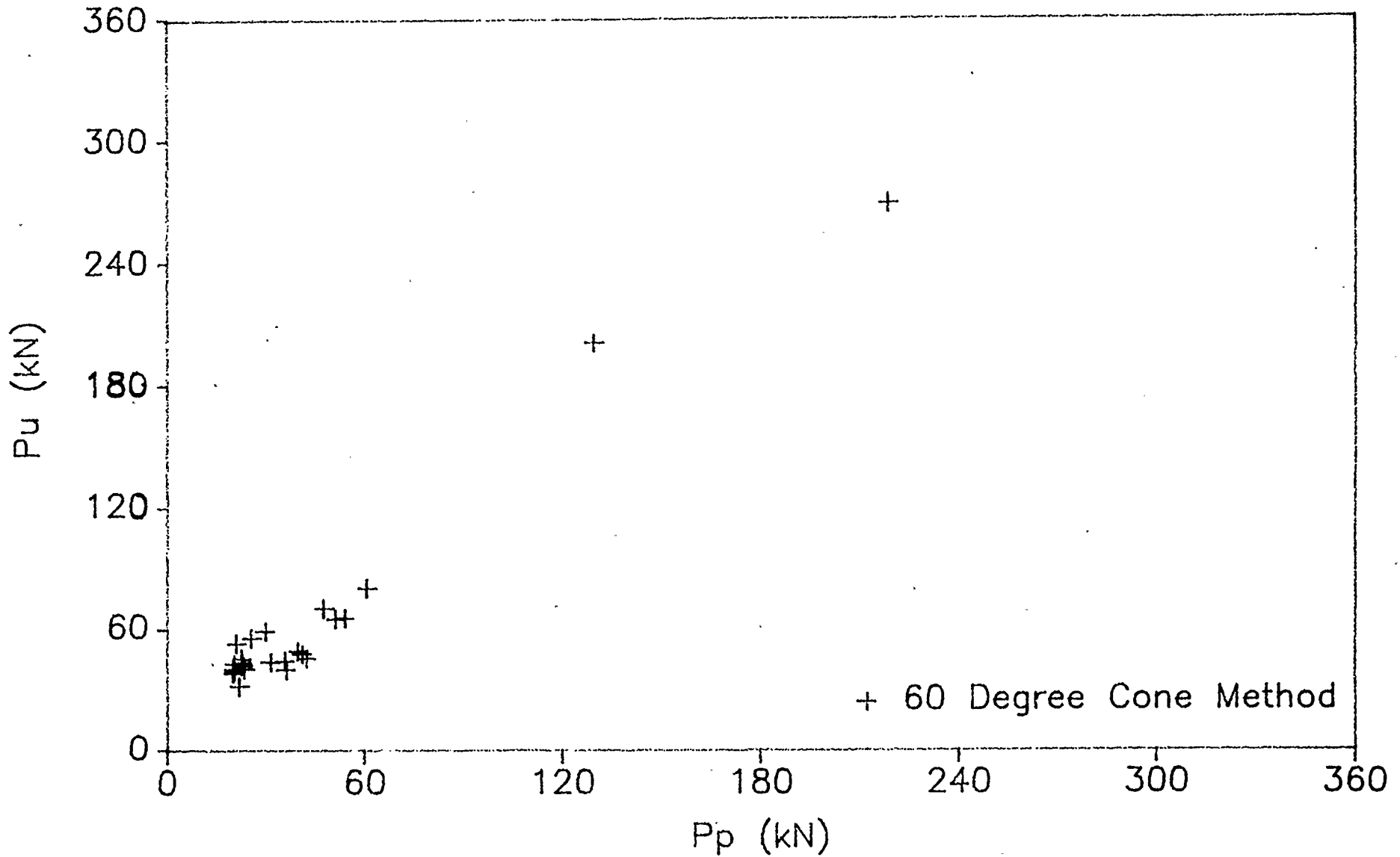


Figure B.8: Corner - Symmetric Holes, 60 Degree Cone Method, Long's Eqn.

Square Holes on Column Corners Symmetric Hole Patterns

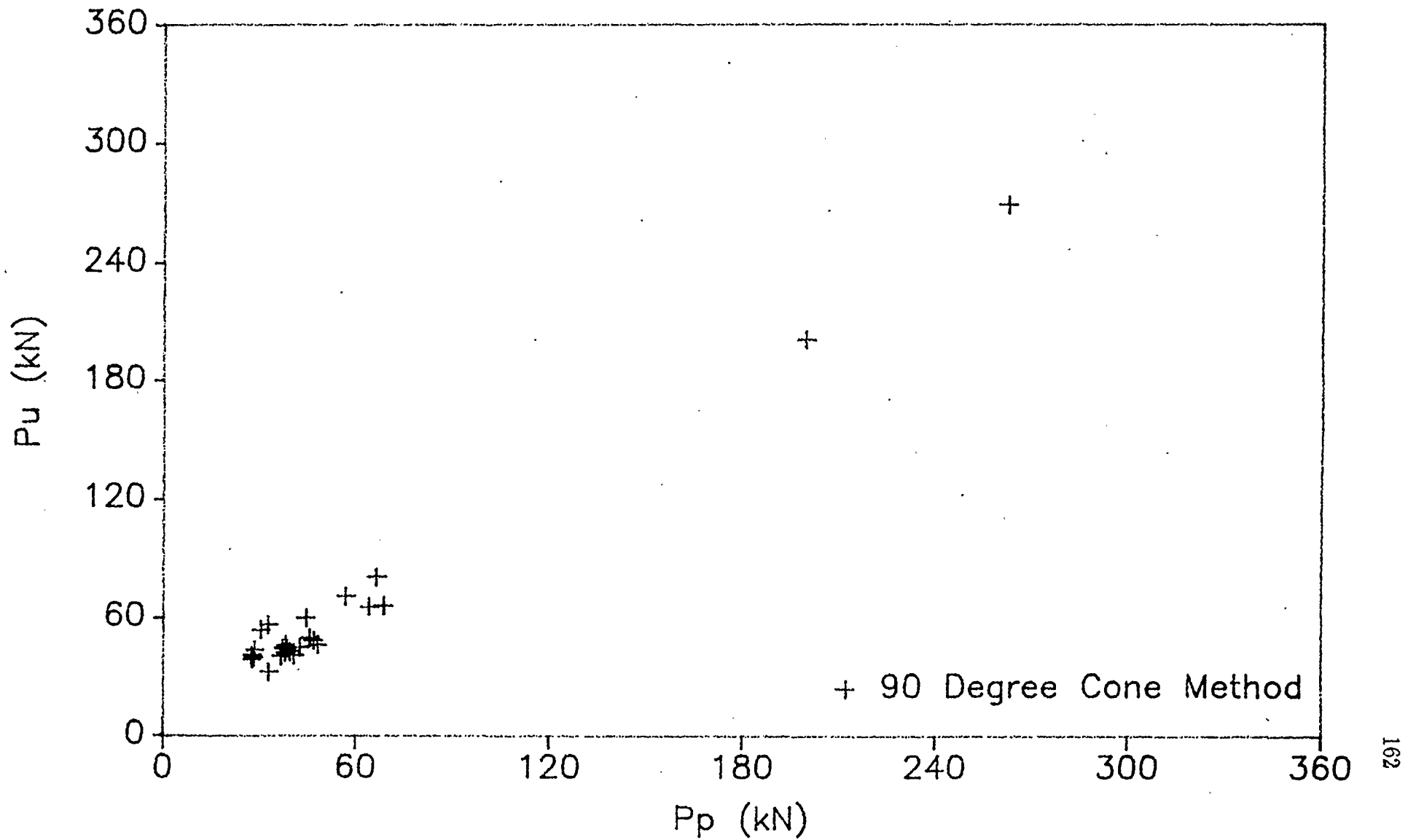


Figure B.9: Corner - Nonsymmetric Holes, 90 Degree Cone Method, Long's Eqn.

Square Holes on Column Corners Nonsymmetric Hole Patterns

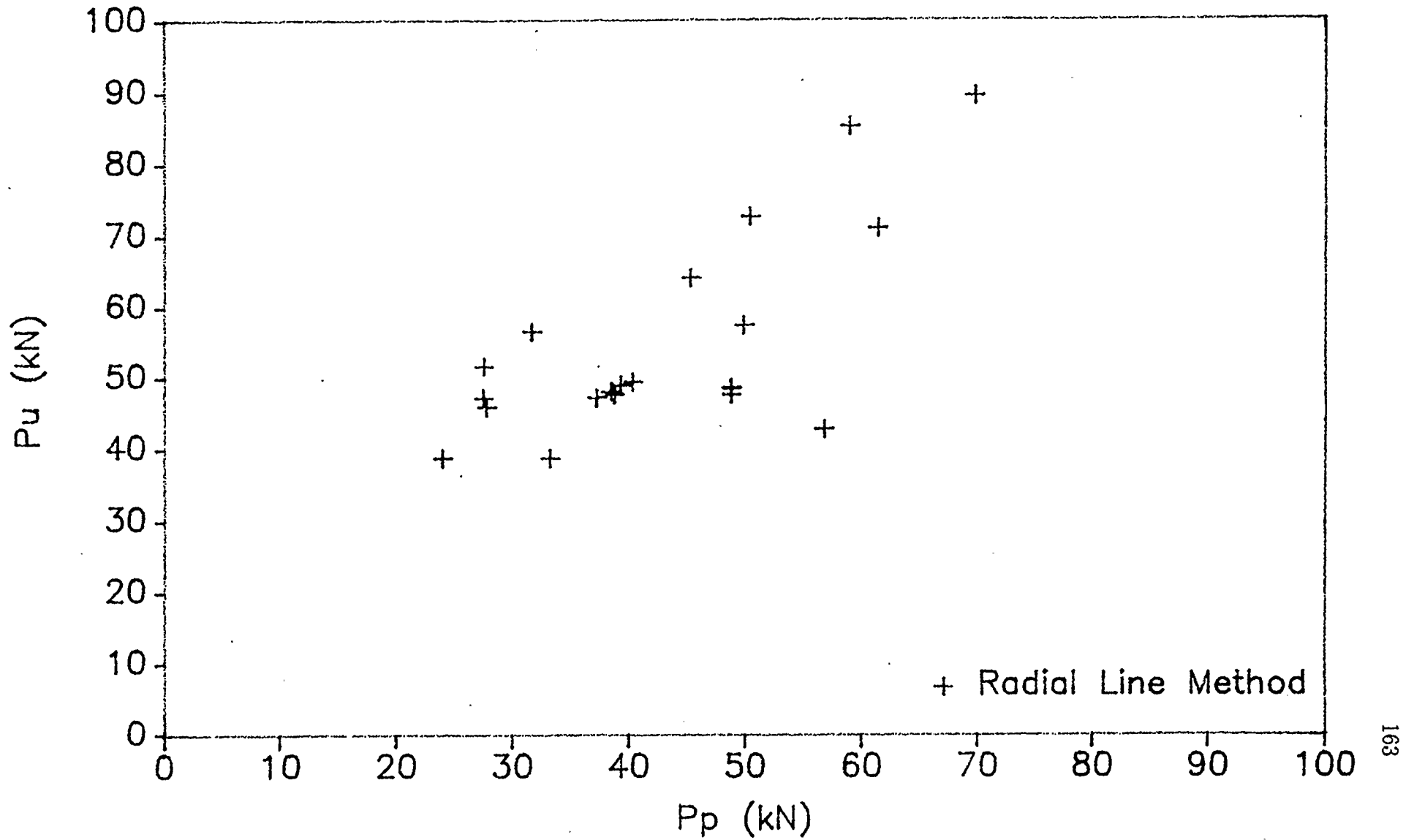


Figure B.10: Corner - Nonsymmetric Holes, Radial Line Method, Long's Eqn.

Square Holes on Column Corners
Nonsymmetric Hole Patterns

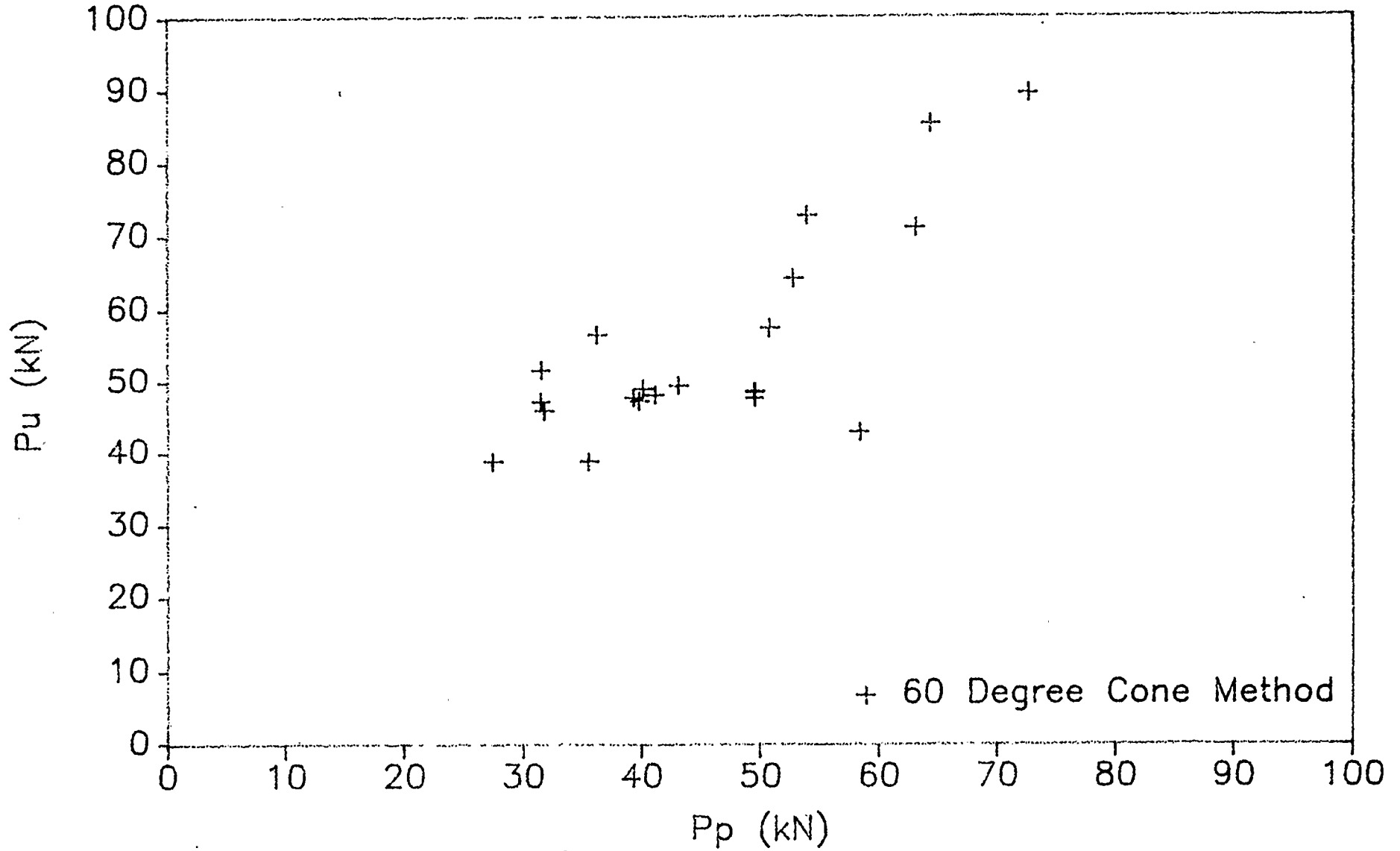


Figure B.11: Corner - Nonsymmetric Holes, 60 Degree Cone Method, Long's Eqn.

Square Holes on Column Corners Nonsymmetric Hole Patterns

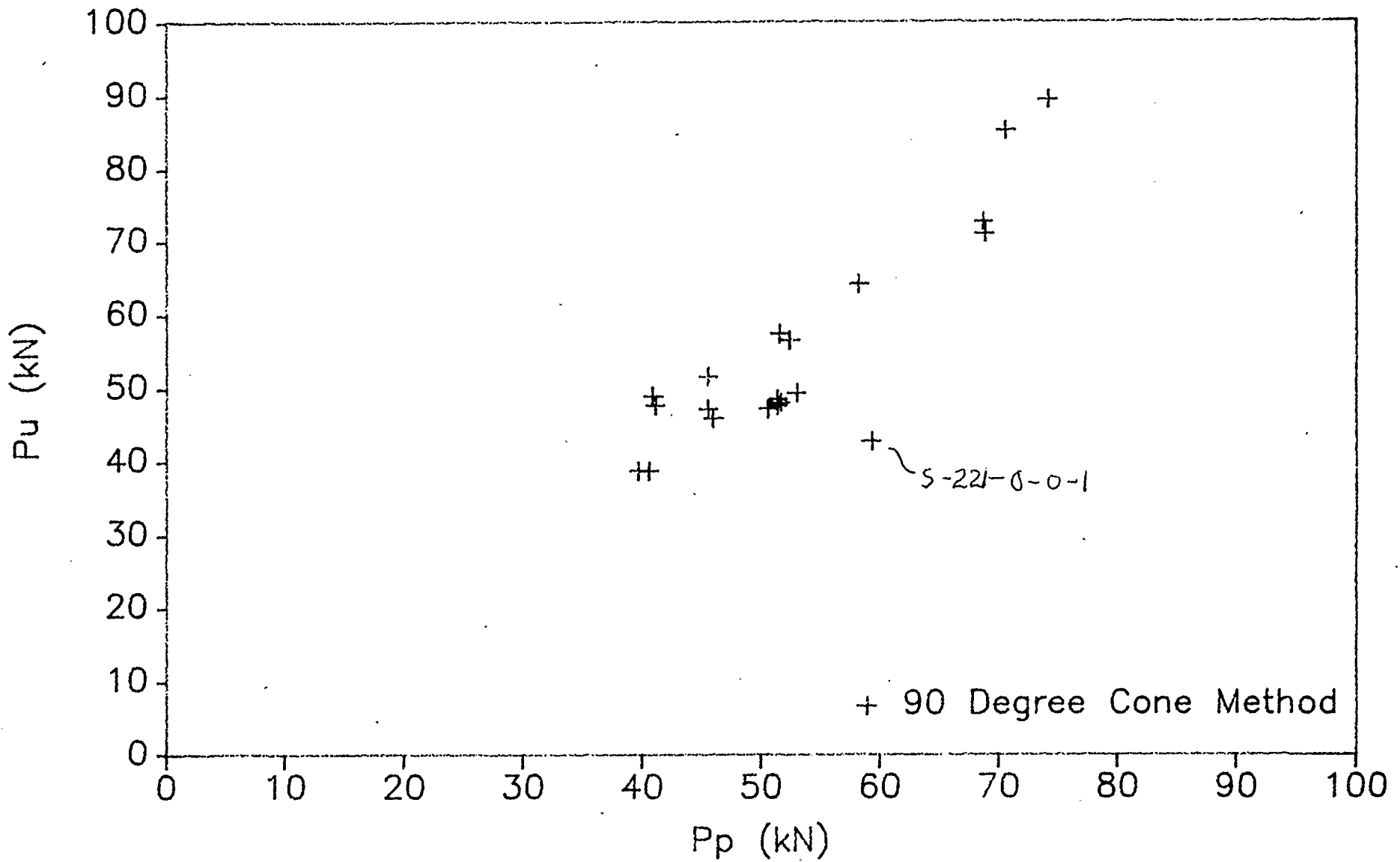


Figure B.12: Corner - Nonsymmetric Holes, 90 Degree Cone Method, Long's Eqn.



National Library of Canada

Bibliothèque nationale du Canada

Ottawa, Canada
K1A 0N4

ISBN

49

CANADIAN THESES SERVICE – SERVICE DES THÈSES CANADIENNES

PERMISSION TO MICROFILM – AUTORISATION DE MICROFILMER

• Please print or type – Écrire en lettres moulées ou dactylographier

AUTHOR – AUTEUR

Surname – Nom de famille

Given Names – Prénoms

FINNIGAN

COREY

Date of Birth – Date de naissance

10 MAY 1963

Canadian Citizen – Citoyen canadien

Yes / Oui

No / Non

Country of Birth – Lieu de naissance (pays)

CANADA

Permanent Address – Résidence fixe

361 STRATHALLAN AVE
BURLINGTON ONTARIO

THESIS – THÈSE

Title of Thesis – Titre de la thèse

EFFECTS OF HOLES ON
INTERIOR COLUMN-SLAB
CONNECTIONS

Degree for which thesis was presented
Grade pour lequel cette thèse fut présentée

MSC

Year this degree conferred
Année d'obtention de ce grade

1988

University – Université

UNIV OF CALGARY

Name of Supervisor – Nom du directeur de thèse

DR. R.E. LOOV

AUTHORIZATION – AUTORISATION

Permission is hereby granted to the NATIONAL LIBRARY OF CANADA to microfilm this thesis and to lend or sell copies of the film.

L'autorisation est, par la présente, accordée à la BIBLIOTHÈQUE NATIONALE DU CANADA de microfilmer cette thèse et de prêter ou de vendre des exemplaires du film.

The author reserves other publication rights, and neither the thesis nor extensive extracts from it may be printed or otherwise reproduced without the author's written permission.

L'auteur se réserve les autres droits de publication; ni la thèse ni de longs extraits de celle-ci ne doivent être imprimés ou autrement reproduits sans l'autorisation écrite de l'auteur.

ATTACH FORM TO THESIS – VEUILLEZ JOINDRE CE FORMULAIRE À LA THÈSE

Signature

Corey Finning

Date

Oct 21/88

RC

05/10/89